U. S. Department of Commerce
Henry A. Wallace, Secretary
National Bureau of Standards
E. U. Condon, Director

JOURNAL OF RESEARCH of the NATIONAL BUREAU OF STANDARDS

1.5

JULY 1946

VOLUME 37

NUMBER 1

UNITED STATES
GOVERNMENT PRINTING OFFICE
WASHINGTON, D. C.

Contents

RP — Page

1723. Radio proximity fuse design. Wilbur S. Hinman, Jr., and Cledo Brunetti. (Price 10 cents) 1

1724. Assembly, testing, and operation of laboratory distilling columns of high efficiency. Charles B. Willingham and Frederick D. Rossini. (Price 10 cents) 15

1725. Nickel plating on steel by chemical reduction. Abner Brenner and Grace E. Riddell. (Price 5 cents) 31

1726. Temperature coefficients for proving rings. Bruce L. Wilson, Douglas R. Tate, and George Borkowski. (Price 10 cents) 35

1727. Mutarotation and ring structure of mannuronic lactone. Horace S. Isbell and Harriet L. Frush. (Price 5 cents) 43

1728. Heats of formation and combustion of the normal alkylcyclopentanes and cyclohexanes and the increment per CH_2 group for several homologous series of hydrocarbons. Edward J. Prosen, Walter H. Johnson, and Frederick D. Rossini. (Price 5 cents) 51

1729. Preliminary description and analysis of the first spectrum of uranium. C. C. Kiess, Curtis J. Humphreys, and Donald D. Laun. (Price 10 cents) 57

With this issue the JOURNAL OF RESEARCH appears in a new typographical style and size. The increased trim size agrees in general with that of many scientific and technical magazines and recently adopted for the Bureau's TECHNICAL NEWS BULLETIN.

Improvements in the format of the JOURNAL are the double reading columns, the insertion of two-point spaces between lines of text and tabular matter, and the use of modern type for display heads.

The changes are intended to make the printed page more easily read and to improve the physical appearance of the publication.

It is hoped that the new form will meet with the approval of the readers of the JOURNAL.

Engin. Lib.

U. S. Department of Commerce
National Bureau of Standards

Research Paper **RP1723**
Volume 37, July 1946

Part of Journal of Research of the National Bureau of Standards

Radio Proximity Fuze Design

By Wilbur S. Hinman, Jr., and Cledo Brunetti

The general principles governing the design of radio proximity fuzes are presented. The paper deals primarily with fuzes for smooth-bore projectiles,* such as bombs, rockets and mortars. Illustrations and descriptions of the various fuzes in this category which were developed during World War II are given. Within security regulations, there is a reasonably detailed discussion of the performance and construction of fuze components, such as the oscillator, the amplifier, the antennas, the power supply and the safety and arming mechanisms. There is also a brief description of production practices and problems and methods of inspection and quality control.

I. Introduction

Electronic arts are generally linked to intelligence, and the radio proximity fuze follows the pattern. Intelligence might be described as the ability to adopt or change a course of action according to the circumstances of the moment to give the most effective result without external influence. This sense, which is the prime feature of the radio proximity fuze, fulfills one of the dreams of the ordnance man and provides a fuze that increases weapon effectiveness many fold. If a projectile can be made to explode at its closest approach to an airplane target, the effective size of the target is increased greatly; if a projectile can be made to explode above the ground, fragments are sprayed out over a wide area instead of being buried in the ground at the point of contact or directed harmlessly upward.

The radio proximity fuze was developed to meet these requirements. It is an extremely small transmitting station with a receiver to detect any reflections of the transmitted wave. It works on the Doeppler principle, and operates whenever the amplitude of the reflected signals exceed a predetermined value. There is the additional restriction that the velocity of approach must be such that the resulting Doeppler frequency lies in the relatively narrow frequency band for which the fuze was designed.

As certain specific details of fuze construction still fall under the heading of classified information, it is necessary to introduce some generalities in this paper in order to meet security regulations.

*Distinction is made between the application to rotating and nonrotating projectiles. The difference lies principally in factors such as power supply, arming mechanism, and physical structure. The first two considerations are dependent primarily on the conditions of acceleration and motion. The physical structure is governed by the size and contour of the projectile.

Contents

		Page
I.	Introduction	1
II.	General description	3
III.	Oscillator	4
IV.	Amplifier	4
V.	Radiation, reflection, and operating range	7
VI.	Power supply	8
VII.	Safety and arming	10
VIII.	Tubes and other components	11
IX.	Production and laboratory testing	11
X.	Field testing	12

The impact of this new application of electronics on military science and tactics is enormous. It is the counter-weapon to airplanes and robots raiding ships or cities. It is a new offensive weapon for airplanes. When used against entrenched troops or troops on the march, it provides a new order of importance for the shell, bomb, or rocket with which it is used. Some of the foremost military leaders have said that it precluded troop movement in the open. Remembering that most military tactics depend upon the movement of troops and supplies for sudden attacks and quick support of defenses, one can begin to see the importance of the application.

The work on proximity fuzes started in this country in August 1940 under Office of Scientific Research and Development auspices. In the spring of 1941, in order to press the development with maximum efficiency, the Navy assumed responsibility for the development and procurement of proximity fuzes for rotating projectiles, such as antiaircraft and artillery shells, while the Army directed the development of fuzes for nonrotating projectiles, such as bombs, rockets, and mortars. This paper deals with the Army phase of proximity fuze development. Some of these fuzes mounted on projectiles are shown in figure 1.

The existence of an effective radio fuze was one of the best-kept secrets of the war. Scientists of all countries had the basic concept, but only the United States and her Allies were able to work from the concept to practical and effective operation and production, for the radio proximity fuze is a paradox. Simple in general theory, it is extraordinarily complex in the variety of applied arts that are combined in its practical aspects.

Much of the necessary engineering and development work was devoted to meeting exacting military requirements, such as (1) the fuze must fit existing projectiles using the same fuze well as the mechanical fuzes, and it must not project more than say 5 inches beyond the well; (2) it must be capable of withstanding long storage conditions at high and low temperatures and of operating under these conditions; (3) it must not alter the ballistic characteristics of the projectile; and (4) it must meet other strict requirements relating to time of activation, safety, and performance.

The size limitations for radio proximity fuzes were fixed by military necessity. One might think that in the case of a 500- or 1,000-pound bomb, a few extra cubic inches or an extra pound or two would not be important, but bombs and bomb bays were already designed and in use. A fuze projecting so far as to prohibit loading a fuzed bomb into the bomb bay would be useless. Ballistic tables for all bombs were available, and if the radio fuze affected the trajectory and changed the bombing tables appreciably, use of the fuze would be prejudiced. For the smaller projectiles, such as the trench mortar, size and weight limitations were even more severe. One of the 81-mm mortar shells weighs approximately 8 pounds, and unless the radio fuze is light and fairly well streamlined, the range of the mortar is reduced—a severe handicap to its military effectiveness.

Other basic difficulties are readily apparent. Mortar fuzes must withstand acceleration of 10,000 *g*. In the fuzes for bombs and rockets the projectile vibrations caused by flight velocities approaching or exceeding the speed of sound required great rigidity in the design of the fuzes and their components. Some idea of the energy producing these vibrations may be had by considering conditions at terminal velocity. Air friction and turbulence prevent further acceleration and do work on the bomb, which work appears as vibration and heat. For a 1,000-pound bomb at a terminal velocity of 1,000 ft/sec, the rate of energy dissipation is 1,000,000 ft-lb/sec or 1,356 kilowatts. Taking into account the desirable requirements of low cost and small size, and with the further realization that an extraordinary degree of electronic stability is needed for satisfactory operation, it is evident that the performance requirements for these electronic devices are very strict.

These restrictions required the development of new, very small and strong components. It is fortunate that "small" and "strong" go together. Weight is proportional to the cube of the linear dimension, while the supporting area is proportional to the square of the linear dimension. Thus, dimensional reduction by a factor of 10 results in an object whose strength under acceleration is increased by 10. Resistance against centrifugal forces and bending moments is also greatly increased by a reduction in size. This is the reason that electronic components, generally considered delicate, can be constructed so as to withstand the high vibratory and accelerating forces which are developed in the various projectiles.

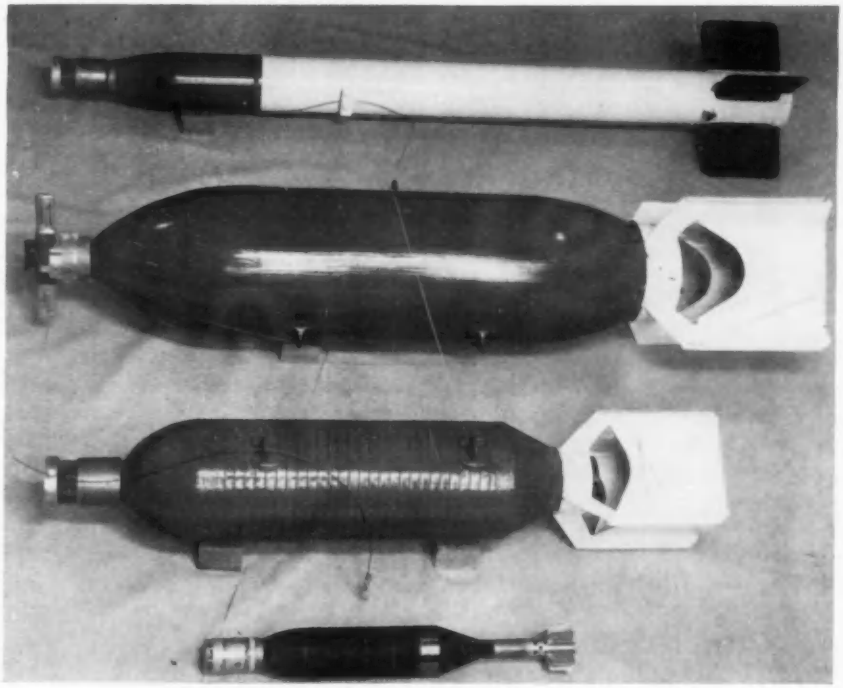

FIGURE 1.—*Radio proximity fuzes mounted on high-velocity aircraft rocket, 500- and 265-lb bombs, and 81-mm trench mortar.*

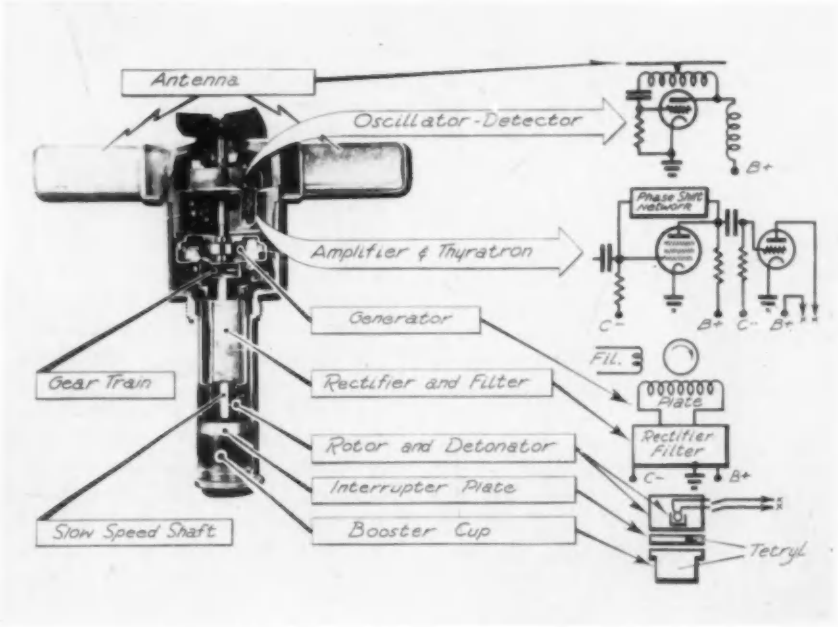

FIGURE 2.—*Cutaway of fuze and generalized fuze circuit.*

UNIV. OF MICH.

II. General Description

The radio fuze is essentially an oscillating detector. The operating signal is furnished by the combination of the wave reflected from the target with the voltage of the local oscillator. The time of travel of the radiated wave from the oscillator to the reflecting surface, or target, and back results in a phase difference between the transmitted and reflected wave. If the distance to and from the reflecting surface changes, the relative phase changes. When the oscillating detector is approaching the reflecting surface, the phase change appears as an increase in the frequency of the reflected wave, each returning wave front reaching the detector sooner than it would if the oscillating detector were stationary. Thus, the apparent distance between wave fronts is shorter and the frequency is higher.

The actual frequency of the returning wave (since it must go to, and return from, the target) is the outgoing frequency, f_1, plus 2 (relative velocity/wave length) and the "difference" beat frequency is 2 (relative velocity/wave length). The latter is the signal used to detonate the fuze when it approaches the reflecting target at a preselected velocity (hence beat frequency) and when it is close enough for the reflected wave to have sufficient amplitude.

At useful operating ranges of from 20 to 70 feet, the amplitude of the reflected wave seen by the detector is of the order of a small fraction of a volt. Amplification is necessary to make this voltage large enough to operate the detonator control circuit, usually a thyratron. A single-tube amplifier whose pass band is designed to favor the reflected signal over spurious noise or other signals, is used to increase the amplitude of the detected beat frequency to several volts, enough to cause the standard control circuits to function.

A power supply and a mechanical safety arrangement to prevent premature operation of the detonator completes the primary components of the fuze.

VT fuzes are designed to certain over-all sensitivities which, obviously, involve both oscillator and amplifier design. Greater amplifier gain may completely compensate for a weak or inefficient oscillator detector, but if a weak oscillator is used without a commensurate reduction in the noise voltage (the peak rectified noise voltage at the detector output), the signal to noise ratio is reduced.

Throughout the development and production of VT fuzes, electrical stability in the presence of severe vibration was a prime problem. Although generally called an electronic fuze, the structural and mechanical design required a great deal of attention. Improper design might cause the fuze to operate spontaneously prior to reaching the target. A large part of the engineering and development work was directed toward obtaining the best performance possible, for you cannot drop the same bomb twice. The work was directed along three general lines:

1. Improvement of circuit stability.
2. Reduction of tube microphonics.
3. Reduction of vibration introduced by unbalance in the high-speed generator.

Certain cardinal precepts were established early in the program. Shock mounting was not used because shock mounts have a low natural period with a multitude of harmonics. It was found preferable to make the parts "so rigid that there could be no relative motion." Of course, this really means that the natural resonances of all parts were placed out of the range of the signal frequencies at which the amplifier was responsive. It was accomplished by extremely solid and rugged mounting of all parts and by careful design of all components. Ideally, all parts should be made as a block so that the completed fuze would be literally as solid as a brick. This ideal condition was approached by cementing the oscillator components into cavities in a solid insulator in the form of a disk one-half inch thick, the assembly being tightly fastened to a suitable heavy metal casting. The amplifier was built on a light Bakelite or fiber chassis and set into a cavity in the heavy casting. The cavity was then filled with a potting material so that all parts were fixed in position.

The mounting of the fuze to the projectile was particularly important. For a given vibratory force, acceleration is inversely proportional to mass, and the effective mass is greatly increased if the fuze is made a rigid part of the projectile. Considering the vibration of the rotating system, a firm mounting between the fuze and the projectile did much to reduce its amplitude.

Figure 2 is a cutaway view of one of the bomb fuzes and general circuit diagrams of the primary fuze subassemblies. A more detailed discussion of each of these subassemblies follows.

III. Oscillator

The primary problems of oscillator design are sensitivity, stability, and size. Sensitivity is defined as the absolute change in detected output voltage per unit change in antenna radiation resistance. It may be represented by the equation

$$\Delta E = \frac{S \Delta R_A}{R_A},$$

where ΔV is the change in detected output voltage, S is the sensitivity, ΔR_A is the effective change in radiation resistance, and R_A is the radiation resistance, the antenna circuit being tuned to resonance. In the limit, the equation for sensitivity becomes

$$S = \frac{dE}{dR_A/R_A} = \frac{dE}{d(\log R_A)}.$$

The latter form of equation suggests a simple method of measuring the r-f sensitivity. Measurements are made of detector voltage, E, for various values of radiation resistance, R_A. The range of radiation resistance is selected to cover the values of all projectiles on which the fuze is to be used.

The next step is to plot the detector voltage against the log of the radiation resistance. The slope of this curve is dE/d (log R_A) and, therefore, is the r-f sensitivity. Note that the unit of r-f sensitivity is the volt and, again, is interpreted as the number of volts change in detector voltage per unit of change of radiation resistance.

Any oscillating detector will have appreciable r-f sensitivity for a reasonable range of radiation resistances. In a well-designed system, the oscillator is stable and the sensitivity is high for radiation resistance values varying over a large range. This is an important factor in fuze design, since it allows use of the same fuze with a variety of projectiles, small and large. Class C oscillators are generally used because this type gives high sensitivity with good stability and is largely independent of tube characteristics and radiation resistance.

In addition to considering the change in voltage in the presence of a change in radiation resistance one must consider the absolute value of detector voltage, V. For a given sensitivity, the lower we make the value of V, the lower will be the noise voltage. Any circuit which increases the sensitivity to noise ratio is to be preferred, even though the absolute signal voltage is low, for low signals are easily amplified.

Note, then, that the radio fuze does not require a detector which is sensitive in the usual sense; i. e. responsive to extremely weak signals. Efficiency is a better word; that is, we are interested in the percentage of the voltage developed by the oscillator that appears at the detector output when the oscillator approaches to a fixed distance from a given type of reflector. The higher the percentage, the more stable is the fuze.

IV. Amplifier

Fuzes have been designed to operate at distances up to 70 feet against aircraft and up to several hundred feet over ground. At these distances, the reflected signal is a small fraction of a volt. This low voltage does not provide a safe margin for controlling the gas relay (thyratron) used to detonate the fuze, and so it must be amplified to a reasonable working voltage. While this is the primary amplifier function, other considerations apply, without which satisfactory operation could not be attained.

The first of these is discrimination against microphonics and other stray noise. The Doeppler frequencies lie in a rather narrow band for any individual fuze and projectile, ($F = 2V/\lambda$). Bomb velocities, for instance, vary from about 400 to 1,000 feet per second, depending on the altitude from which the bomb is dropped, while rocket velocities of projectiles used in World War II varied from 1,000 to 1,800 feet per second. Frequencies other than the corresponding Doppler frequencies play no useful role in the radio fuze, and every effort is made to reject them through the use of band pass amplifier circuits.

The use of wind-driven alternators (described later) gives an additional reason for restricting the band width of the amplifier. Many fuzes are required to be operative in less than a second so that directly heated filaments must be used. By keeping the alternator frequency outside of the Doeppler range, the frequency cutoff of the amplifier discriminates against the hum in the a-c filament supply to such an extent that filament center tapping is not needed.

Another consideration is the class of target. There are two general types—the ground and the aerial target. The ground is considered to be a level plane, and the Doeppler frequency is proportional to the vertical component of velocity. The aerial target as represented by the airplane has a complicated reflection characteristic whose reflecting power can be roughly compared with that of a tuned half-wave dipole insofar as general characteristics are concerned. The actual reflecting power is determined by a series of field measurements.

To understand the factors affecting the optimum gain frequency characteristics of amplifiers, it is necessary to consider the directivity, or radiation characteristic of the antenna. Nearly all radio fuze antenna systems are rather highly directional. Since the same antenna is used for transmitting and receiving, the sensitivity characteristic is the square of the radiation characteristic. Projectiles approach the ground at a variety of angles and the fuze should not detonate the projectile at heights above ground which are sharply dependent on the angle of approach; a uniform burst height is desired.

Depending on the type of antenna, the gain-frequency characteristic is adjusted to give a uniform height of function for the fuze for any angle and velocity of approach to the target. The two most common antenna types are the longitudinal, employing the body of the projectile as the antenna,[1] and the transverse, employing a bar as a dipole disposed at right angles to the projectile axis (fig. 1). Longitudinal and transverse directivity envelopes, i. e., for ring-type and bar-type fuzes, respectively, mounted on bombs, are shown in figure 3. Minimum radiation occurs, of course, on the axis of the antenna in each case and maximum radiation is roughly at right angles to that axis.

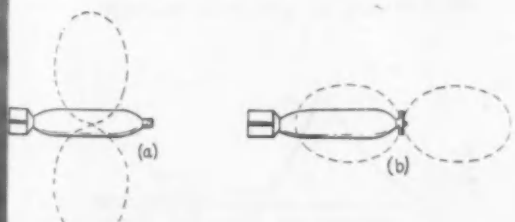

FIGURE 3.—*Radiation patterns for bomb fuzes.*

(a) Ring-type, (b) bar-type fuze.

[1] R-f energy is end-fed to the body through the antenna ring or cap of the fuze.

For the longitudinal type, it is obvious that the radiation is least for a vertical drop, and it approaches a maximum as the angle with respect to the vertical is increased. Now, as the vertical component of velocity is highest for high-altitude bomb releases, the angle with the vertical is small, the radiation is low, and the Doeppler frequency is high. For this condition, high amplifier gain compensates for the low power radiated toward the target. Conversely, for low-altitude bomb releases, the vertical velocity is low, the angle with the vertical large, and the Doeppler frequency low. Here, less amplifier gain compensates for the higher power radiated toward the target. By proper design of the amplification characteristic, the height at which the fuzed projectile functions may be held quite uniform, regardless of the altitude of release. This will be treated in more detail later.

The second type, the transverse antenna, has a substantially constant radiation toward the ground for all except extremely low altitude releases, where the angle of fall with respect to the vertical is very large. The amplifier for this type fuze has essentially constant gain over the corresponding range of Doeppler frequencies. Figure 4 shows representative gain-frequency characteristics for the two types of fuzes.

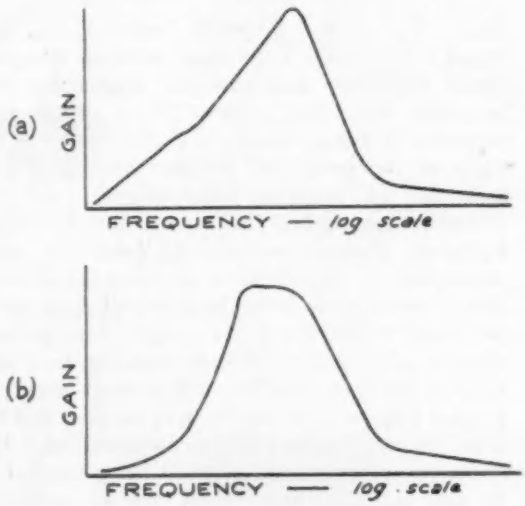

FIGURE 4.—*Typical amplifier characteristics.*

(a) Ring-type fuze, (b) bar-type fuze.

The radio fuze for aerial targets presents problems in amplifier design that differ from those of the application over ground. The requirement is that the fuze must function at the optimum point as it passes the target. The fragments of an exploding projectile have two velocities—one due to the projectile motion and the other due to the explosion. The greatest concentration of fragments is at right angles to the path of travel of the projectile axis (statically). The projectile velocity combines with the velocity generated by the explosion to cause the equatorial spray of fragments to move forward of the normal to the projectile. Thus, the optimum point for detonation is that where the line from the projectile to the target makes an angle of from 15 to 30 degrees with the normal to the trajectory.

The preferred type of antenna for aerial targets is that using longitudinal excitation, because radiation reaches the target only when the projectile commences to pass it. Consideration of the Doeppler signal pattern, commonly called the *M* wave, as a fuze passes an aerial target will show the means of using the amplifier characteristic to control the burst point (fig. 5, a). Consider a projectile approaching an aerial target from a distance. The Doeppler frequency depends on the relative velocity of the projectile and the reflecting target. For a target and a projectile traveling in the same direction,

$$F=2\frac{(V_1-V_2)}{\lambda}\cos\ \theta,$$

where V_1 is the projectile velocity, V_2 the target velocity, and θ the angle between the projectile trajectory and the line connecting the projectile and the target. Thus, when the projectile is distant from the target, $\cos\ \theta \cong 1$, while at the instant of passing the target, $\cos\ \theta=0$ (for an idealized point target). As the projectile approaches the target, the Doeppler frequency changes continuously from that corresponding to the difference of the projectile and target velocities to zero, being at all times proportional to $\cos\ \theta$. If the amplifier is peaked sharply at a frequency corresponding to some value of $\cos\ \theta$, the amplifier will be most sensitive at that frequency (or angle), and the fuze will be most likely to explode at the corresponding point on its trajectory, the exact point being influenced by the radiation pattern. A typical amplifier gain-frequency characteristic is shown in figure 5, c.

The *M* wave signal at the amplifier output is shown in figure 5, b. This is the *M* wave, of figure 5, a, modified according to the amplifier gain for the varying frequency.

Most of the amplifiers use only one tube. The high degree of selectivity is shown in figure 4. It is obtained through the use of strongly regenerative-degenerative circuits. Noise or hum voltages large enough to overload the amplifier may appear at the input, but by feeding the corresponding out-of-phase voltage back from the output, the undesired voltages are bucked out and suppressed.

Conventional resonant L-C circuits are used in combination with the feedback circuits to provide the flat-top band pass characteristic needed for the transverse-excitation type of fuze. The practice of tuning the resonant circuit to the lower limit of the desired frequency band was widely used. Other types of circuits are, of course, possible, but space limitations and circuit complexity prejudice their use.

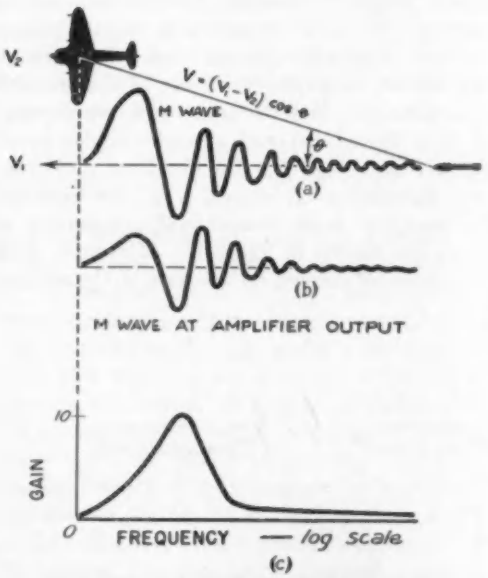

FIGURE 5.—*Reflected signal from aerial target and amplifier characteristic.*

(a) Reflected signal, (b) reflected signal altered by fuze amplifier, (c) frequency characteristic or fuze amplifier.

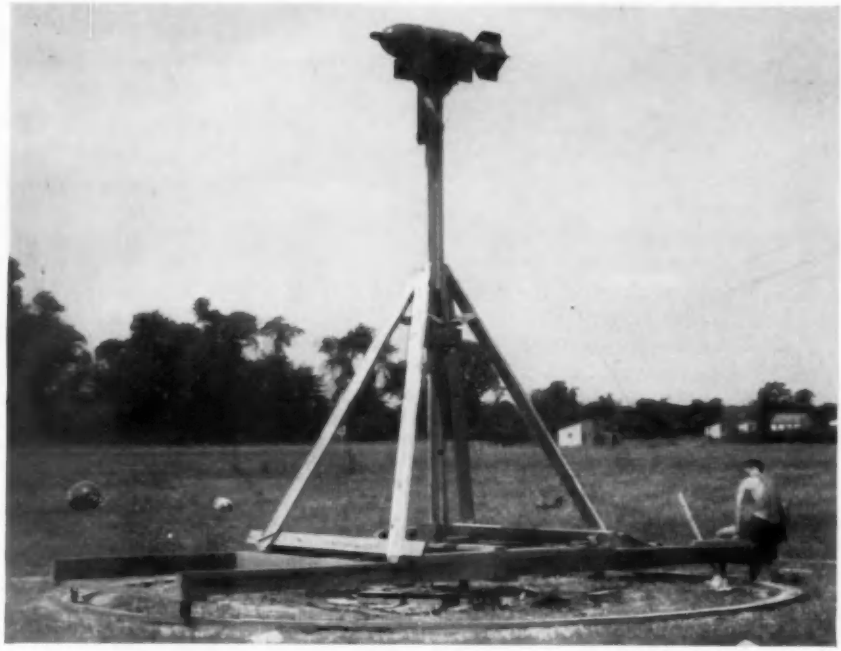

FIGURE 6.—*Test structure for obtaining fuze directivity envelope.*

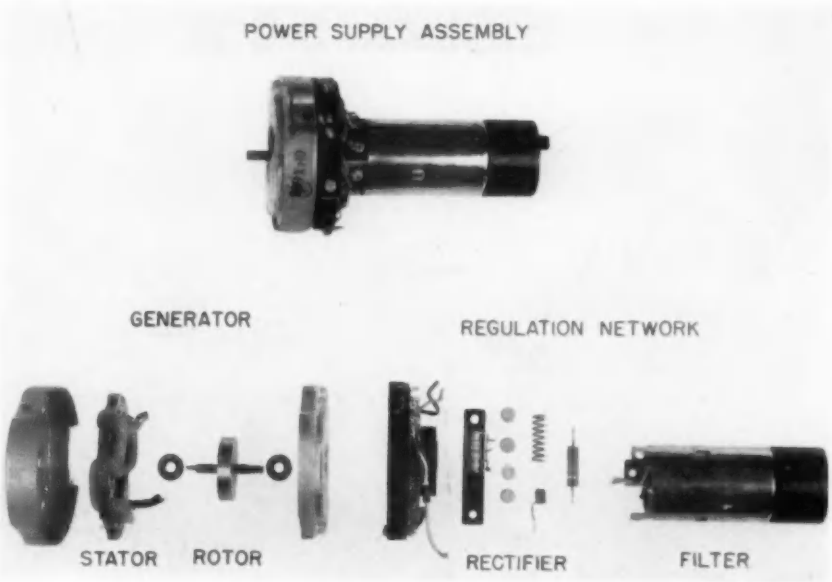

FIGURE 7.—*Power supply for bomb fuze.*

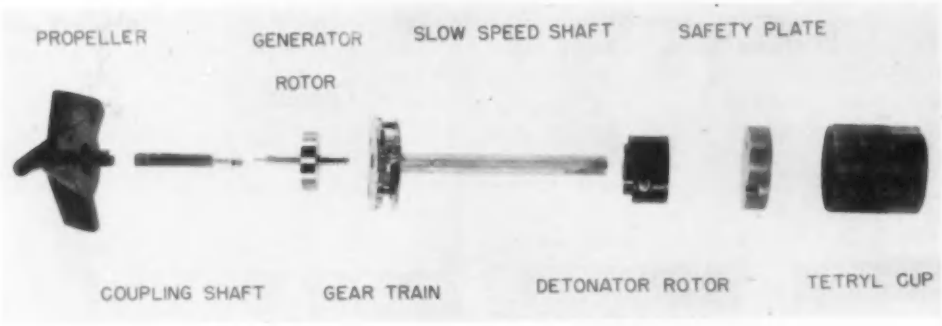

FIGURE 9.—*Mechanical drive and arming system.*

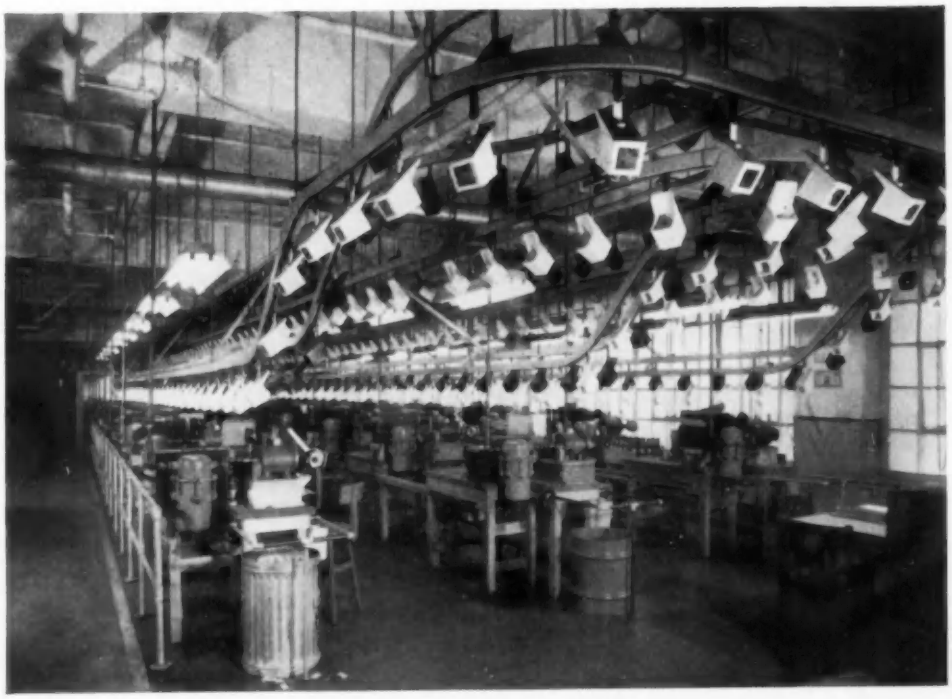

FIGURE 10.—*Fuze production line.*

V. Radiation, Reflection and Operating Range

The distance at which a reflected signal is large enough to operate the radio fuze and explode the projectile is dependent on several factors, both internal and external to the fuze. The internal factors that control the height of function are r-f sensitivity, over-all amplification, shaping of the amplifier, thyratron characteristics, and the time delays in all the electrical and explosive paths in the device. External to the fuze, controlling factors include the radiation pattern of the projectile acting as an antenna, external geometry of the fuze-projectile combination, radio frequency, reflection coefficient of the target, geometry of the target, angle of approach, and the relative velocity of projectile and target.

Although the above factors present a most unwieldy number of variables, it has been possible by a combination of theory with laboratory and field experiments to arrive at formulas for computing burst distances with considerable accuracy. The general method of solution is the same for any type of target provided some knowledge of the reflecting properties of the target is at hand. For an aerial target, the reflection coefficient, both in magnitude and phase, as a function of aspect angle, may be determined experimentally. Actually, however, the reflection coefficient of such targets varies so much with angle of approach and type of construction, i. e., metal, plastic, etc., that average figures are assumed for various targets and used for all computations regarding this target. Thus, for example, a certain type of airplane might be equivalent in reflecting properties to five half-wave electric dipoles (i. e., the reflection was five times that of a tuned half-wave doublet oriented for maximum reflection).

In the case of a bomb approaching level ground at an angle, the first step in the calculaion of height of function is to assume the earth to be an infinitely conducting plane. The signal reflected back to the bomb (which we shall call the driving antenna) is the same as that radiated by a mirror image of the bomb (or antenna) located as far below the conducting plane as the real bomb is above it. Thus, the field produced at the driving antenna by the image antenna is calculated in terms of current in the driving antenna, frequency, and geometry. To simplify the remainder of the derivation, the image antenna is now assumed to be a half-wave dipole and the voltage, e, induced in it by a given current in the driving antenna is calculated. Applying the reciprocity theorem, the same current at the center of the dipole gives the same induced voltage, e, at the feed-point of the driving antenna. Thus, the voltage induced in the driving antenna by the image dipole is found. If this voltage is multiplied by the ratio of the fields produced at the driving antenna by the image antenna and the image dipole, it will yield the true reflected voltage.

The field surrounding the antenna contains three components—the radiation field, the induction field, and the quasi-static field. For many practical purposes, only the radiation field need be considered. This simplifies the calculations and provides an easy working formula for determining operating heights. For the case of a bomb approaching ground at height, h, over terrain having a reflection coefficient, n, the Doeppler voltage detected by the fuze will be

$$V_R = \frac{knS}{h\beta_2}\phi(\theta) \text{ volts (rms)}, \qquad (1)$$

where

S = the r-f sensitivity of the fuze,

k = a constant that is principally a function of the wavelength

$$\beta_2 = \int_0^{\pi} \phi(\theta) \sin\theta d\theta$$ (this expression may be readily computed by numerical integration)

θ = the angle of the major axis of the bomb with respect to the vertical.

$\phi(\theta)$ = the directivity envelope (See fig. 3.)

Assume the input to the amplifier required to fire the thyratron is V_T volts (r. m. s.), measured at the Doeppler frequency corresponding to the altitude at which the bomb is dropped.[2] Inserting this value in place of V_R in equation (1) yields the height of function.

$$h = \frac{knS}{V_T\beta_2}\phi(\theta) \text{ feet.}$$

All the time delays in the fuze system total less than 5 milliseconds, so that at normal operating

[2] Frequency $= \frac{2V\lambda \cos\alpha}{V = \sqrt{2g \text{ (altitude)}}}$.

ranges and speeds, they can be neglected without appreciable error.

A structure for obtaining a directivity envelope for a fuze mounted on a 500-pound bomb is shown in figure 6. Provision was made for continuous rotation of the structure. In the figure, the operator is reading the angular position on the ground protractor. The signal radiated by the fuze-bomb combination is picked up by a receiver located approximately 100 feet away. The intensity of the signal is measured for each angular position of the bomb.

VI. Power Supply

In addition to the requirements of small size and reliable operation at substratosphere temperatures (−40° C.) and tropical conditions (+60° C., high humidity), the principal requirements that had to be met in the design of a universal type of power supply for the rocket, bomb, and mortar applications were that it must have a long shelf life, and be a permanent part of the fuze; i. e., should not have to be assembled to the fuze in the field.

A careful study of all methods of power supply led to the selection of a wind-driven a-c generator with a suitable rectifier-filter system as the most practicable solution to the problem. Considerably more than the necessary power to operate such a device was available in the wind stream, and with proper mechanical design, it could be harnessed without appreciably affecting the ballistics of the projectile. In fact, only a tiny fraction of the power available in the air stream was needed to supply the electrical energy for the fuze. The generator power supply not only met the requirements outlined above, but provided the additional feature of an exceptionally safe method of arming the fuze, to be described later. One of the power supplies used in the bomb and rocket fuzes is shown both in assembled and exploded views in figure 7.

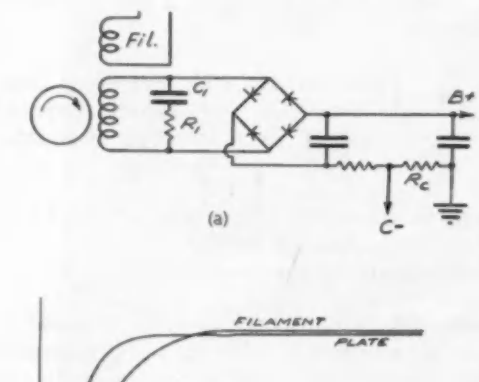

FIGURE 8.—*Generator circuit and characteristic.*
(a) Circuit arrangement, (b) voltage-speed characteristic.

The a-c generator consisted of a six-pole magnet rotating within a stator carrying the coils in which the voltage is generated. The rotor of this alternator was a simple cylinder approximately 1 inch in diameter and one-fourth inch thick. Composed of Alnico, it was magnetized in production by simply inserting it in a six-pole magnetizing fixture and sending a brief pulse of unidirectional current through the six coils on the fixture. For the stator, either a standard six-coil six-pole arrangement or a single-coil six-pole winding, little used in modern practice but of a type described in literature dating back to 1896,[8] was employed. Separate windings were used for the *A* and *B* supply. *C* bias was obtained from the rectified *B* voltage.

By properly shaping the amplifier gain-frequency characteristic, it was possible to use alternating current directly on the filaments of all tubes. A bridge rectifier was used for the plate and bias supply and filtered by means of a simple R-C filter, as shown in figure 8, a. An extra resistor (R_c) inserted at the low-potential side of the *B* output provided the necessary *C* voltage. This allowed the *C* voltage to be a definite fraction of the *B* voltage and to vary in the same manner as the *B* voltage. Thus, some compensation was provided for variations in *B* voltage from generator to generator in production.

The large leakage reactance of the high-voltage

[8] Edwin J. Houston and A. E. Kennelly, Electrodynamic machinery for continuous currents. (The W. J. Johnston Co., 1896.)

winding was made use of in achieving excellent voltage regulation with speed. In the various projectiles employed, speeds ranged up to 125,000 rpm, the higher speeds occurring in the turbine models. With care in design, the top speeds could be reduced to less than 100,000 rpm, but the range was still large. The normal open-circuit voltage of this type of alternator increases almost linearly with speed. The obvious step in obtaining good regulation was to raise the voltage at low speeds by resonating the leakage inductance with an external condenser. This was the method adopted. Using the shunt regulation components R_1 and C_1, speed regulation characteristics similar to that of figure 8, b were obtained. The plateau is reached at a speed below that at which the fuze is armed; that is, at which the fuze is ready to function electrically. The purpose of resistor, R_1, was to broaden the resonance effect of C_1 and the generator leakage inductance and thus limit the voltage at resonance to give constant voltage at all speeds above resonance.

By virtue of the inductive coupling between the A and B windings, the impedance reflected into the A voltage circuit, with the B regulation components and proper B load in place, was such as to provide an A voltage speed-regulation curve similar to that of the B circuit.

Full-wave rectification was obtained by means of selenium rectifiers in the four arms of the bridge. In some applications, a voltage-doubler rectifier circuit was employed, allowing good performance with half the number of rectifier cells.

One of the important factors which helped to make possible the tiny generator-powered radio proximity fuze was the development of small selenium rectifiers. The rectifier itself, in 1 of the applications, was composed of 10 cells, each about one-fourth inch in diamater.

Choice of the selenium rectifier was based on numerous considerations, including both the economical and the physical. Vacuum tubes would have provided a suitable solution to the problem of rectification; however, their cost and difficulties of production, including time, tools, and strategic materials needed, made it imperative that an inexpensive and easily produced substitute be found. Then, too, vacuum tubes draw filament power and in addition had to be made rugged. For example, in the trench mortar application, the fuze is designed to withstand a set-back force of 10,000 times that of gravity. This set-back occurs as the shell is fired. Although the ruggedness necessary was accomplished in the design of the tubes, in order to obtain it, special features of construction were necessary, with the attendant increase in cost and difficulty of production. It was felt that wherever possible, substitutes for vacuum tubes would be desirable in a device of this type.

Both selenium and copper oxide rectifiers were tested. The latter have especially desirable features and in the early stages of development appeared to be favorably adapted to the problem. In particular, they show a low reverse dynamic characteristic—that is, low conduction of current in the reverse direction. However, concentrated development on the selenium disk soon resulted in the obtaining of reverse characteristics which exceeded those of the copper-oxide rectifier. Also, the copper-oxide rectifier did not perform as well under the extreme ranges of temperature met in practice, especially at low temperatures, and full attention was soon focused on the selenium rectifier.

The exact method of manufacture of selenium cells is regarded as a trade secret. However, a general idea of the method may be told.

The cells are made on a base metal, such as steel, aluminum, etc. A large strip of metal is used and the individual cells are partially punched out, being held to the strip by 0.005 inch of metal, which keeps the cells on that particular strip together throughout all the subsequent manufacturing procedure.

Selenium powder is applied to the strips, which are then baked under pressure at approximately 115° C. The strips are again put into an oven, this time without pressure, and held at a temperature of slightly over 200° C. Care is exercised as this is very near the melting point of selenium. A shiny black appearance resulting from the first baking now changes to a crystalline grey. This practice is called annealing.

Following this, the cells are placed over a vapor of selenium dioxide. The material adhering to the selenium forms a thin layer and acts as a catalyst in the formation of the barrier layer. Finally, the counter-electrode is sprayed on, a mask being used to prevent a short circuit at the cell edges. The cells are now electroformed by connecting them to a source of d-c voltage.

The assembly of rectifier cells in their containers, shown in figure 7, met rigid microphonics tests.

Impellers of both propeller and turbine type were employed, the former on rocket and bomb fuzes and the latter on the mortar and also on one of the rocket fuzes. The propeller type was either molded of Bakelite or stamped out of steel. The turbine type was die cast. The pitch was selected at a value that gave the best compromise between fast starting and low top operating speeds.

The extremely high rotational speeds at which the generators were operated introduced severe mechanical problems. Even with the small degree of unbalance in early models, strong vibration resulted, and bearings were destroyed in a relatively short time. The introduction of commercial ball bearings in place of the sleeve bearings originally used gave a material improvement in performance.

The rotor, in addition to possessing excellent magnetic properties, required special metallurgical design to withstand the high speeds without tearing apart. Vanes were also balanced. End play in the rotating system was kept to minute figures hitherto thought impossible in small devices designed for very high production rates. For the higher generator speeds, more attention was given to balancing of the rotating system, and operation was so much improved that it was possible to return to the use of sleeve bearings.

VII. Safety and Arming

The radio proximity fuze, when armed, is sensitive to any sort of motion or action in its neighborhood that will change the amplitude of reflected waves (at a rate at which the amplifier is responsive). One may cause the fuze to operate by waving a Bakelite rod close to it, or by touching two wires together at a considerable distance from the fuze. Touching a metal pipe or any other ground or metal object may change the reflected signal enough to fire the fuze. For this reason, exceptional care must be taken to see that the fuze circuits are not completed until the fuze is well away from the firing or release point. A fuzed bomb or rocket must be many hundreds of feet away from the plane or the ground firing point before there is any possibility of the fuze functioning. Several safety means are employed. (1) A thick metal plate, usually called an interrupter plate, is interposed between elements of the explosive train so that if the electric detonator is discharged prematurely, the main explosive charge cannot be set off. (2) The electric detonator is disconnected from the power circuit. (3) With generator-powered fuzes, there is no power available to set off the detonator until the projectile is moving through the air at a high rate of speed.

Arming the fuze is accomplished through a gear train, driven by the same vane that drives the generator. Rotating the gear train removes the interrupter plate and connects the electric detonator. This occurs after the vane has made a preset number of revolutions corresponding to a fixed distance of air travel. The usual arming distance varies with type of projectile employed and may be as much as three or four thousand feet. Figure 9 includes a break-down of safety devices which, in the unit shown, are built into the power-supply assembly.

The detonator is set off-center in the detonator rotor, and its terminals are connected to contacts on the face of the rotor. When the fuze is not armed, the detonator is misalined a number of degrees from a small hole in the interrupter plate. The hole is filled with tetryl, a material widely used in explosive train elements. The tetryl cup holds a larger charge of tetryl, which is used to detonate the main explosive charge of the projectile. As the vane turns, the reduction gear train slowly turns the rotor by means of a slow-speed shaft. When the detonator is directly above the tetryl-filled hole in the plate, contact with the detonator leads is made; the rotor is released from the slow-speed shaft and locked in place, completing the arming of the fuze.

In using the bomb fuzes, an arming wire attached to the airplane is threaded through a metal pin on the fuze, which is arranged to block the fuze vane from turning. As the bomb is released, the wire is withdrawn, the metal pin falls out, and the vane is free to turn and arm the fuze.

Rocket and mortar fuzes require other safety means. These fuzes have accelerating forces of from 10 to 10,000 times gravity at the moment of firing. Mechanical locks, which release the vane under the forces of acceleration, prevent arming of the fuze except when it is fired.

VIII. Tubes and Other Components

Much of the effort expended on radio fuzes was directed toward the development and procurement of small and rugged components. Chief among these were the tiny tubes, as no suitable tubes were available at the start of the war. Work was started with various tube manufacturers on improving the hearing-aid types of tubes, the initial steps being taken by the Navy shell fuze development group of the Johns Hopkins Applied Physics Laboratory. Tube work on the Army phase of the fuze program at the same companies was directed primarily toward developing tubes free from microphonics in the presence of severe vibration.

Many new testing methods and procedures had to be developed, along with rigid manufacturing controls. As a result of this work, a very strong and stable line of inch-long tubes about five-sixteenths inch in major diameter were developed and produced in sufficient quantity to meet the heavy production requirements of the proximity fuzes. None of the production programs were ever delayed by lack of tubes.

For most of the other components, such as condensers, resistors, and coils, there was a continuous effort to reduce size and improve performance at extremes of temperature and humidity. Too much credit cannot be given to manufacturers of these items for the manner in which they engineered and produced the large quantities required.

Another important phase of the project was the development of suitable plastic materials for the nonmetallic parts of the fuzes. These parts included the nose cap, oscillator blocks, coil forms, and numerous housings for other components. Rigid mechanical requirements were imposed on the plastics by virtue of the severe strains to which the fuzes were subjected. In addition, those parts located in the high-frequency circuits had to have especially good electrical properties. These problems were solved by the close cooperation of plastics manufacturers.

IX. Production and Laboratory Testing

Perfection is a prime requirement of ordnance items. A bombing mission may carry 1 or 2 dozen bombs in a round trip of as much as 2,000 miles. Into the venture goes a bomber costing hundreds of thousands of dollars and a crew too valuable to reckon in money. For each fuze that fails to function, one bomb is lost to the mission and the whole mission may be jeopardized.

In order to assure the best possible fuze operation, a rigid system of production and field testing was instituted before release of the fuzes to the war theaters. Each fuze had to pass a comprehensive final test, and each subassembly was carefully checked prior to final assembly. Proper inspection on the line was of paramount importance. Usual production practices for electronic equipment could not be followed, for a device constructed to ordinary camera model radio set specifications could hardly withstand firing in a rocket or mortar.

Special inspection agencies were set up by the Army Signal Corps or Army Ordnance Department in each area of production to further the rigid inspection system.

The assembly lines were either of the conveyor or the pass-along system. Every fifth or tenth operator was an inspector, and a defect in a subassembly could not go far without detection. After passing minute inspection, both mechanical and electrical, samples of units were selected from each lot produced and shipped to the National Bureau of Standards. There they were tested to exhaustion in the specially built Control Testing Laboratory. They were put through life tests, low- and high-temperature tests, temperature cycling from one extreme to another, humidity tests, salt-spray baths, and a very rude jolt test, after which they were required to perform properly. After the units were packed in special hermetically sealed cans for shipment overseas, they were subjected to a packaging test.[4] This was somewhat akin to being dropped off a truck and jostled around in every conceivable direction hundreds of times. Again the units were expected to perform properly after the test.

At the Control Testing Laboratory, the sample units were disassembled and each subassembly and the principal components subjected to detailed analysis to determine potential sources of failure. Out of these tests came recommendations for

[4] By experts at Picatinny Arsenal.

improvement in design. A special production engineering section was set up at the National Bureau of Standards to act as liaison between development groups, pilot production lines, control testing, and mass-production plants. Valuable trade secrets were exchanged freely between manufacturers in the common interest.

The production line of one of the modern fuze plants is shown in figure 10.[8] This plant utilized an overhead conveyor system for passing units from the final assembly line to final test, thence into the packing room. A closeup of the conveyor system and a final test chamber is shown in figure 11. A fuze is within the chamber; the end of its power-supply assembly is seen projecting from the chamber face. A jet of high-pressure air drives the vane.

Throughout production, testing of completed fuzes remained the most pressing single problem, principally because of the difficulty of accurately simulating in a test fixture the actual conditions of a projectile in flight.

The final test chamber had to present both an electrical and a mechanical load to the unit. A dummy antenna was used to simulate the radiating body of the projectile. Mechanically the fuze was screwed into a mount that simulated the mechanical condition when screwed into the nose of a bomb, rocket, or mortar. Thus mechanical resonances in the fuze were allowed to play their full part in generation of electrical noise. Not only was the electrical noise measured on final test, but other parameters of oscillator, amplifier, and power-supply performance were determined with close-go and no-go limits. In this manner, uniform operation in the field was assured.

Women operators were generally used to operate these stations. It is a distinct credit to them that they were by far the majority of the workers who built and tested these complex electromechanical devices.

A subassembly test station is shown in figure 12. This station was used to check the r-f and a-f performance of one type of bomb fuze. The fuze head is shown clamped in the reclining side of the cube-shaped metal box. With the side moved up in place so as to close the box, an r-f load of approximately infinite impedance is presented to the oscillator. Any desired load may then be added by connecting a suitable r-f resistor from the oscillator antenna lead to the side of the box.

X. Field Testing

Before any lot of fuzes could be accepted for shipment to the field of action, a sample had to pass an Ordnance proving-ground test. In the case of bomb fuzes, they were tested in bombs dropped over land and water. The height of function was measured and the lot accepted if the units operated within specified limits. The height test was not the only test. Numerous safety tests with and without high explosives were made to assure proper operation of the arming and safety devices.

Interesting proving-ground tests of a fuze for the Army 4½-inch rocket were carried out at the Div. 4 N. D. R. C. proving ground at Fort Fisher, N. C., near Cape Fear. In the first tests at that station, an attempt was made to use aerial targets held aloft by small barrage balloons. Testing difficulties were many, for a radio fuze is sensitive to its departure from ground as well as to its approach to ground. Furthermore, early rocket projectors and aiming mechanisms were crude and did not permit accurate sighting on a target swaying in a wind. It was then realized that if the projectile could be fired with its trajectory parallel to a plane surface, free space conditions would be simulated, and fixed range conditions could be established. Such an arrangement is shown in figure 13. The rocket-firing tower is shown at the left and a simulated bomber at the right. The latter was made of plain chicken wire supported on four telephone poles. As the rockets were fired approximately horizontally, variations in the terrain between tower and target would produce undesired voltage ripples in the output of the amplifier. To eliminate this imperfection, the ground below was leveled off with a bulldozer. In this manner the fuze, which is insensitive to reflections of constant phase, was unaware of the fact that it was not traveling in free space. In figure 13, a puff may be seen below the end of the left wing where a rocket with a radio proximity fuze fired on passing the target. Smoke puffs were used in place of high explosives

[8] Courtesy Emerson Radio and Phonograph Corporation.

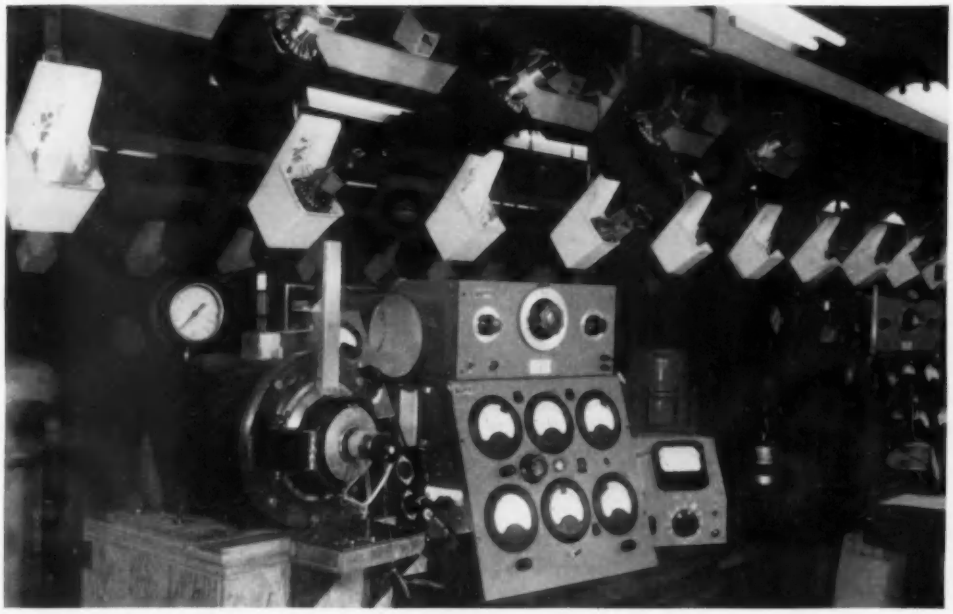

FIGURE 11.—*Final-test station.*

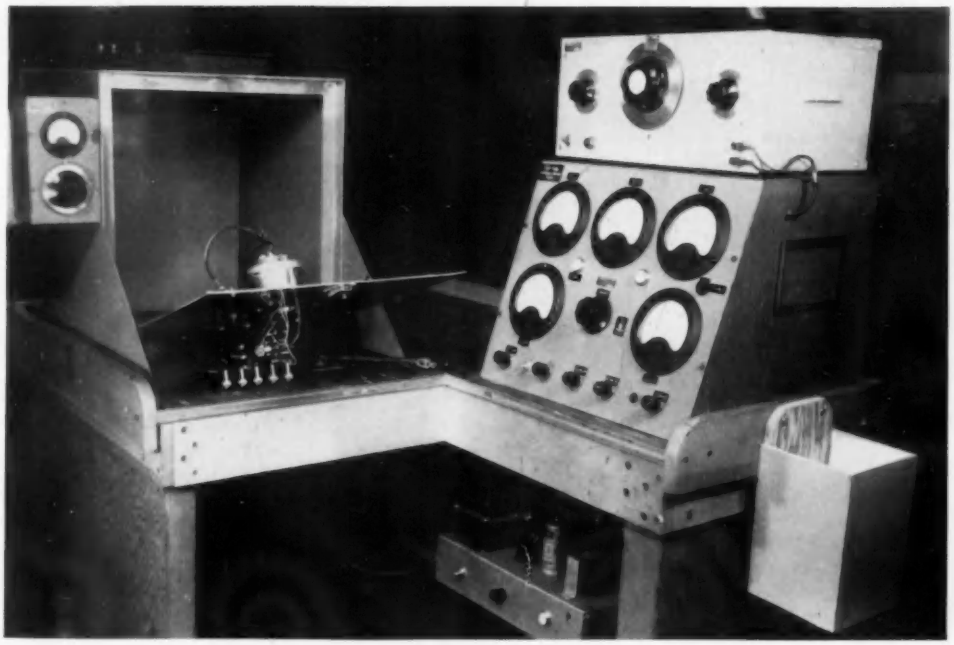

FIGURE 12.—*Subassembly test station.*

FIGURE 13.—*Target range at Fort Fisher, N. C.*

in the rocket to indicate the point of burst and avoid replacing the target after each shot. On passing the target, the rocket continued on into the waters of the Atlantic Ocean, which may be seen on the horizon.

In a treatment of this type, only a glimpse may be had of the large amount of testing that was carried out on the radio fuzes in proving in the design and quality of manufacture and determining the performance in the field. Thousands of acceptance tests were made at many proving grounds in this country, and innumerable operational tests were made here, in England, and on the continent. Added to this was the valuable information yielded by the enemy, who, so obligingly, supplied targets for numerous tests under actual battle conditions.

The program was conducted under the sponsorship of the Army Ordnance Department and the National Defense Research Council, and with the assistance of the Signal Corps.

The radio fuze development and production programs were successful because of the high order of cooperation between military and civilian Government agencies and the American manufacturers. The free exchange of information, even between normally competing manufacurers, contributed immeasurably to good fuze design and production. Principal manufacturers of bomb, rocket, and mortar fuzes were Emerson Radio & Phonograph Corporation, Friez Division of Bendix Corporation, General Electric Co., Globe-Union, Inc., Philco Corporation, Western Electric Co., Westinghouse Electric & Mfg. Co., The Rudolph Wurlitzer Co., and Zenith Radio Corporation. Principal tube manufacturers were General Electric Co., Raytheon Mfg. Co., and Sylvania Electric Products, Inc.

WASHINGTON, February 7, 1946

U. S. Department of Commerce
National Bureau of Standards

Research Paper **RP1724**
Volume 37, July 1946

Part of Journal of Research of the National Bureau of Standards

Assembly, Testing, and Operation of Laboratory Distilling Columns of High Efficiency[1]

By Charles B. Willingham and Frederick D. Rossini

A description is given of the assembly, testing, and operation of the laboratory distilling columns used at the National Bureau of Standards in the work of the American Petroleum Institute Research Project 6 on the analysis and purification of hydrocarbons and in the work on the preparation of NBS Standard Samples of hydrocarbons. The following topics are covered: Assembly of distilling columns, including pot, rectifying section, jacket, head, reflux regulator, receiving assembly, electrical heating system, thermometric systems, and controlled-pressure system; testing of distilling columns, including test mixtures and results; and operation of columns, for both regular and azeotropic distillations. Drawings of the equipment and apparatus are given, including the arrangement of the 15 distilling columns, measuring instruments, and auxiliary equipment in the distillation room. A view of the distillation room is given.

I. Introduction

This report describes the assembly, testing, and operation of the laboratory distilling columns used at the National Bureau of Standards in the work of the American Petroleum Institute Research Project 6 on the analysis and purification of hydrocarbons and in the work on the preparation of NBS Standard Samples of hydrocarbons.

These distilling columns have charging capacities ranging from ½ to 15 liters, with separating efficiencies in the range of 100 to 200 equivalent theoretical plates at total reflux. The distilling operations are performed continuously 24 hours a day, 7 days a week, with reflux ratios from 125/1 to 180/1 and rates of removal of product ranging from 2 to 12.5 ml of liquid an hour. The total time of distilling given charges ranges up to 1,800 hours.

Drawings of the equipment and apparatus are given, including the arrangement of the 15 distilling columns, measuring instruments, and auxiliary equipment in the distillation room.

[1] This investigation was performed at the National Bureau of Standards mainly as part of the work of the American Petroleum Institute Research Project 6 on the Analysis, Purification, and Properties of Hydrocarbons.

Contents

	Page
I. Introduction	15
II. Assembly of distilling columns	16
1. Complete assembly of individual column	16
2. Details of individual column	16
(a) Pot	16
(b) Rectifying section	17
(c) Jacket	18
(d) Head and reflux regulator	18
(e) Receiving assembly	18
(f) System for electrical heating	18
(g) Thermometric systems	19
(h) System for controlled pressures	21
3. Arrangement of columns and auxiliary equipment in the distillation room	21
III. Testing of distilling columns	21
1. Procedure	21
2. Test mixtures	21
3. Results	24
IV. Operation of distilling columns	26
1. Procedure for regular distillation	26
2. Procedure for azeotropic distillation	28
V. Conclusion	29
VI. References	29

693841—46——3

II. Assembly of Distilling Columns

1. Complete Assembly of Individual Column

Figure 1 shows a complete assembly of the main part of one of the distilling columns. All the glass parts of the column proper are sealed together, making one continuous closed system of glass from the pot to the receiver. Details of the assembly are given in the legend of figure 1 and in the following text.

Figure 2 gives the details of the mounting of the transite blocks (constituting the support for the glass pot) on the angle iron brackets (constituting the main support of the column). The position of the horizontal angle iron and supporting brackets on the wall of the room is shown.

2. Details of Individual Column

(a) Pot

Figure 3 gives the details of the 7-liter glass pot.

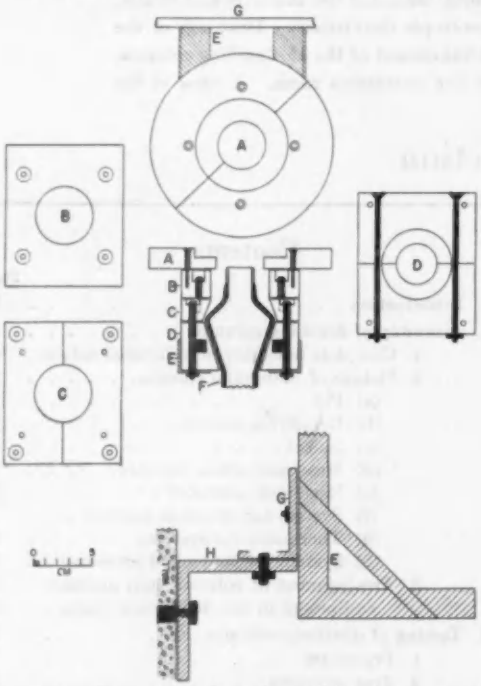

FIGURE 2.—*Transite blocks and metal bracket support for 7-liter still pot.*

A, *B*=transite blocks supporting jacket assembly.
C, *D*=transite blocks supporting glass still pot.
E=angle iron bracket supporting transite blocks.
F=neck of glass still pot.
G=angle iron running horizontally around room. (See fig. 12.)
H=brackets supporting angle iron *G*. (See fig. 12.)

The transite blocks for supporting this pot are shown in figure 2 and the details of the pot assembly are given in figure 1.

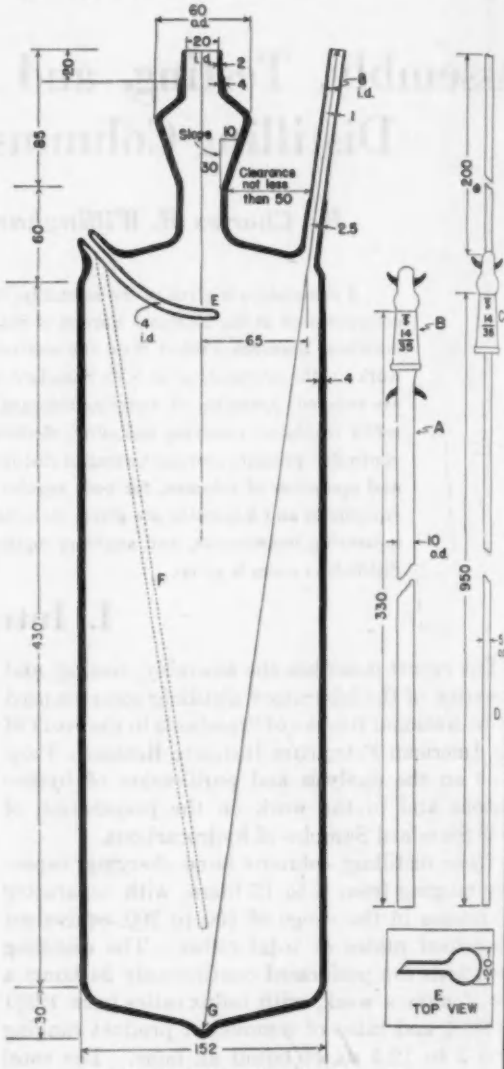

FIGURE 3

FIGURE 3.—*Details of the 7-liter glass still pot.*

The material is Pyrex laboratory glass.
A=filling tube, to be sealed to tube extending from pot.
B=cap of filling tube.
C=cap of withdrawal tube.
D=withdrawal tube.
E=tube for thermoelement.
F=position of tube for thermoelement, in earlier design.
G=recess in bottom of pot, to permit complete removal of undistilled material through the withdrawal tube.

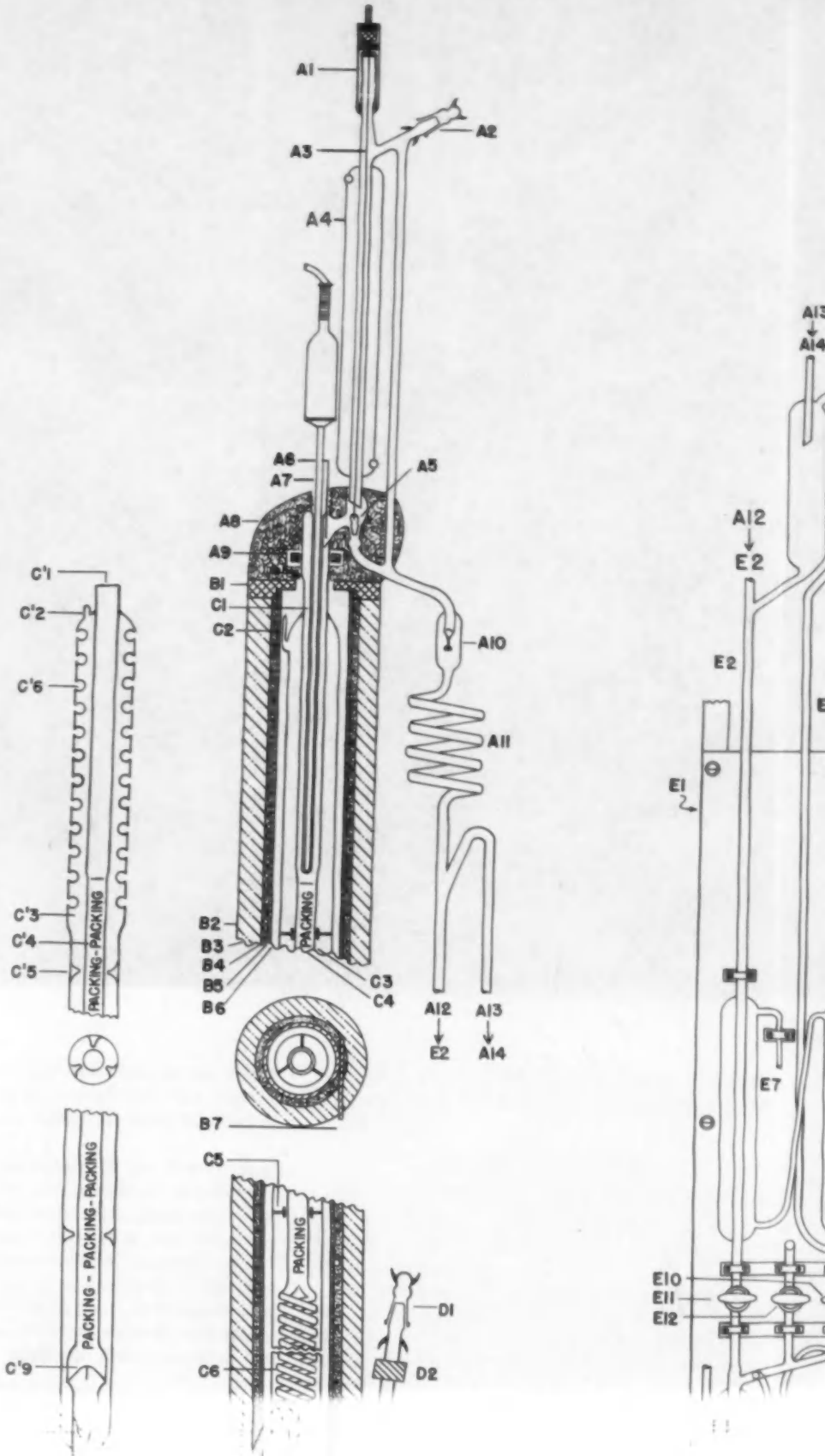
A1
A2
A3
A4
A5
A6
A7
A8
A9
B1
C1
C2
A10
A11
A12
E2
A13
A14
B2
B3
B4
B5
B6
B7
C3
C4
C5
C6
D1
D2
PACKING
C'1
C'2
C'6
C'3
C'4
C'5
C'9
PACKING - PACKING - PACKING
E1
E2
E7
E10
E11
E12

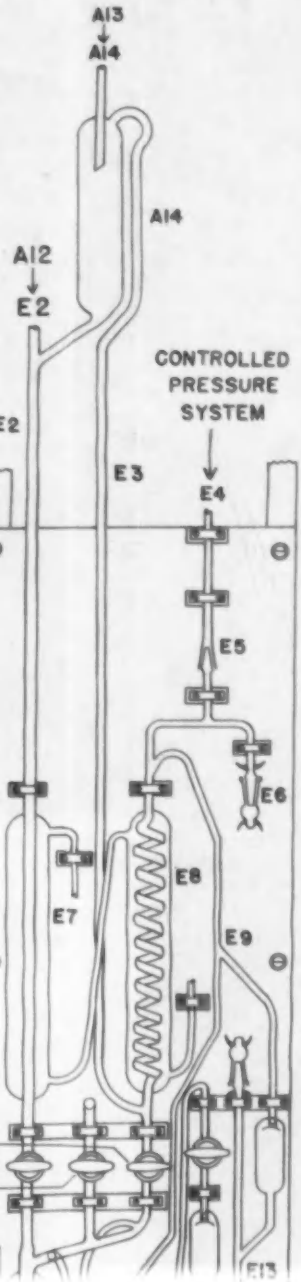

FIGURE 1.—*Assembly of distilling column.*

A = head and reflux regulator [*1*] (For details, see figs. 6 and 8).
A1 = metal regulator with metallic bellows [2].
A2 = capped opening, with standard ground joint 12/30.
A3 = tungsten rod, No. 12 AWG.
A4 = condenser.
A5 = ground-glass valve.
A6 = apron.
A7 = platinum resistance thermometer.
A8 = thermal insulation.
A9 = transite collar for lateral support.
A10 = drop counter.
A11 = expansion spiral.
A12 = product line to receiving assembly *E2*.
A13 = controlled pressure line.
A14 = trap to prevent liquid from entering controlled pressure line.
B = jacket assembly (see also fig. 7).
B1 = transite closure.
B2 = aluminum foil.
B3 = magnesia insulation.
B4 = electrical resistance heating wire, Nichrome, asbestos covered.
B5 = metal tube, steel or aluminum, split vertically, in two longitudinal sections, insulated with a silicone resin and asbestos paper.
B6 = air gap.
B7 = thermometer well, steel or aluminum, brazed to tube *B5*.
B8 = transite supports.
C = rectifying section for Heli-Grid packing.
C1 = open section for thermometer well.
C2 = seal-off tube for evacuated, silvered, jacket of rectifying tube.
C3 = wall of rectifying tube proper, showing depth of thermometer well and height of packing.
C4 = packing, Heligrid.
C5 = lateral support for rectifying tube proper (see also fig. 7).
C6 = double helix expansion section at bottom of rectifying tube proper.
C7 = throat to direct liquid to center.
C8 = drop counter.
C' = rectifying section for packing of helices.
C'1 = open section for thermometer well.
C'2 = seal-off tube for evacuated, silvered, jacket of rectifying tube.
C'3 = wall of rectifying tube proper, showing depth of thermometer well and height of packing.
C'4 = packing, stainless-steel helices $^{3}/_{32}$ inch in diameter of No. 30 AWG wire.
C'5 = indentations in jacket for centering rectifying tube.
C'6 = expansion bellows for jacket of rectifying tube.
C'7 = throat to direct liquid to center.
C'9 = support for packing, conical spider with four legs.
D = still pot assembly (see also figs. 3 and 4).
D1 = opening for introduction of charge, standard ground joint 14/35.
D2 = main support for charging tube.
D3 = tube connecting pot to manometer *E17*.
D4 = main support for glass still pot and rectifying tube (see also figs. 2 and 5).
D5 = electrical leads to heaters for still pot.
D6 = removable cover.
D7 = thermometer well
D8 = Pyrex-glass pot (4-mm wall).
D9 = special Glascol heater.
D10 = asbestos insulation.
D11 = aluminum foil.
D12 = air gap.
D13 = cylinder (Pyrex glass or sheet metal).
D14 = asbestos insulation.
D15 = aluminum foil.
D16 = well for removal of residue.
D17 = transite base.

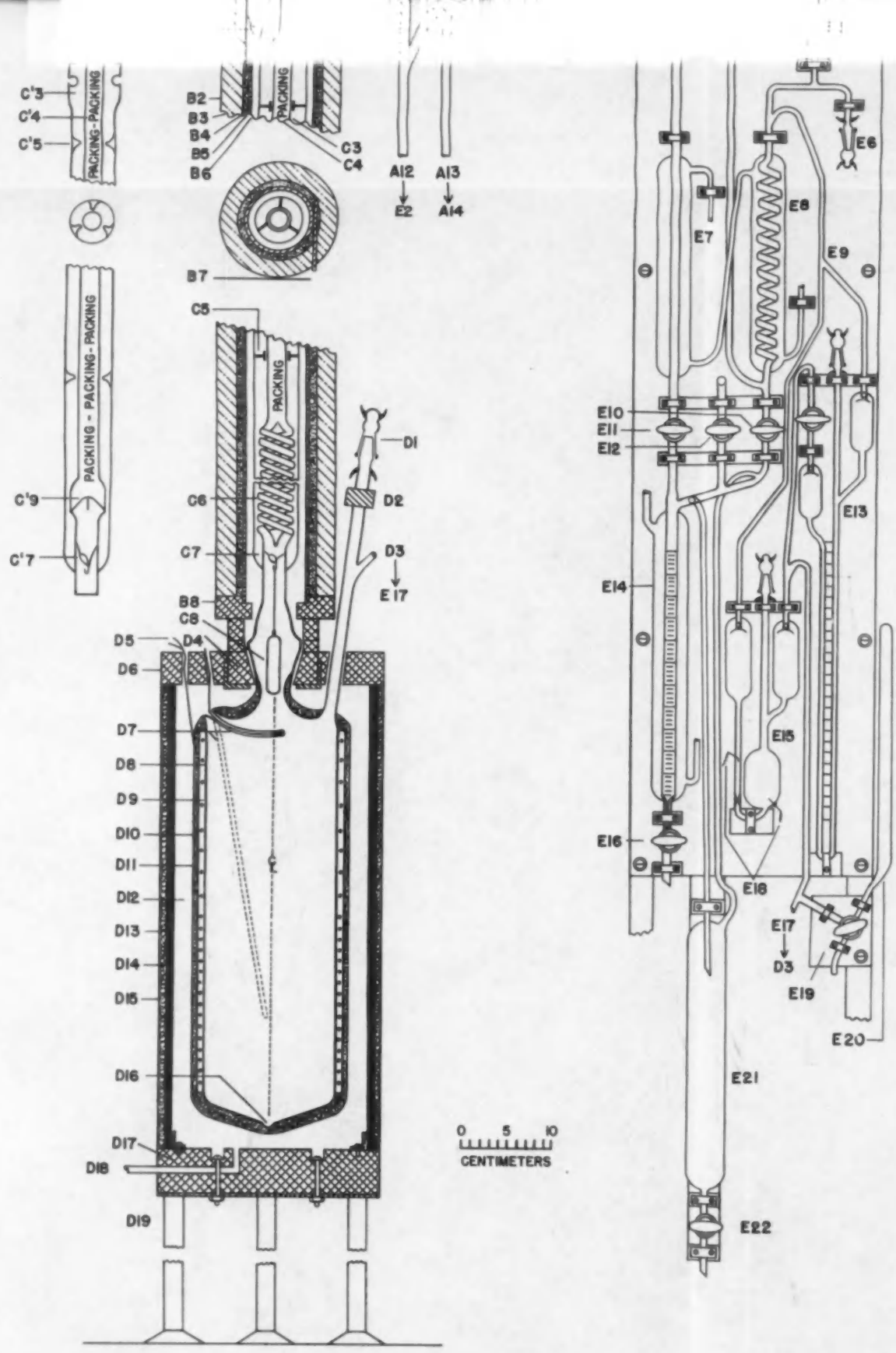
C'3
C'4
C'5
PACKING - PACKING
B2
B3
B4
B5
B6
PACKING
C3
C4
A12
A13
E2
A14
B7
C5
PACKING - PACKING - PACKING
PACKING
D1
C'9
C6
D2
C'7
C7
D3
E17
B8
C8
D5
D4
D6
D7
D8
D9
D10
D11
D12
D13
D14
D15
D16
D17
D18
D19
0 5 10
CENTIMETERS
E6
E7
E8
E9
E10
E11
E12
E13
E14
E15
E16
E18
E17
D3
E19
E20
E21
E22

=magnet.
B4=electrical resistance heating wire, Nichrome, asbestos covered.
B5=metal tube, steel or aluminum, split vertically, in two longitudinal sections, insulated with a silicone resin and asbestos paper.
B6=air gap.
B7=thermometer well, steel or aluminum, brazed to tube *B5*.
B8=transite supports.
C=rectifying section for Heli-Grid packing.
C1=open section for thermometer well.
C2=seal-off tube for evacuated, silvered, jacket of rectifying tube.
C3=wall of rectifying tube proper, showing depth of thermometer well and height of packing.
C4=packing, Heligrid.
C5=lateral support for rectifying tube proper (see also fig. 7).
C6=double helix expansion section at bottom of rectifying tube proper.
C7=throat to direct liquid to center.
C8=drop counter.
C'=rectifying section for packing of helices.
C'1=open section for thermometer well.
C'2=seal-off tube for evacuated, silvered, jacket of rectifying tube.
C'3=wall of rectifying tube proper, showing depth of thermometer well and height of packing.
C'4=packing, stainless-steel helices $\frac{3}{32}$ inch in diameter of No. 30 A WG wire.
C'5=indentations in jacket for centering rectifying tube.
C'6=expansion bellows for jacket of rectifying tube.
C'7=throat to direct liquid to center.
C'9=support for packing, conical spider with four legs.
D=still pot assembly (see also figs. 3 and 4).
D1=opening for introduction of charge, standard ground joint 14/35.
D2=main support for charging tube.
D3=tube connecting pot to manometer *E17*.
D4=main support for glass still pot and rectifying tube (see also figs. 2 and 5).
D6=electrical leads to heaters for still pot.
D6=removable cover.
D7=thermometer well
D8=Pyrex-glass pot (4-mm wall).
D9=special Glascol heater.
D10=asbestos insulation.
D11=aluminum foil.
D12=air gap.
D13=cylinder (Pyrex glass or sheet metal).
D14=asbestos insulation.
D15=aluminum foil.
D16=well for removal of residue.
D17=transite base.
D18=compressed-air line for cooling pot assembly.
D19=metal stand.
E=receiving assembly.
E1=transite board.
E2=product line from head *A12*.
E3=controlled-pressure line to head *A13*.
E4=copper line to controlled-pressure system.
E5=copper to glass standard taper joint.
E6=outlet to atmosphere, standard ground-glass joint 12/30.
E7=condenser for cooling product line, near 10° C.
E8=spiral condenser between receiver *E14* and controlled-pressure system. near 10° C.
E9=connection to manometers *E13* and *E15* from head *A* through spiral condenser *E8*.
E10=stopcock between receiver *E14* and controlled-pressure system.
E11=stopcock on product line.
E12=outlet from receiver *E14* to atmosphere.
E13=manometer (diethylene glycol monobutyl ether).
E14=receiver, graduated, water-jacketed.
E15=manometer (mercury, with tungsten contacts).
E16=stopcock at bottom of receiver *E14*.
E17=connection to manometers from pot *D*.
E18=tungsten contacts.
E19=stopcock for adding inert gas to manometer tube (*E17* to *D3*).
E20=overflow receiver.
E21=stopcock at bottom of overflow receiver.

UNIV.

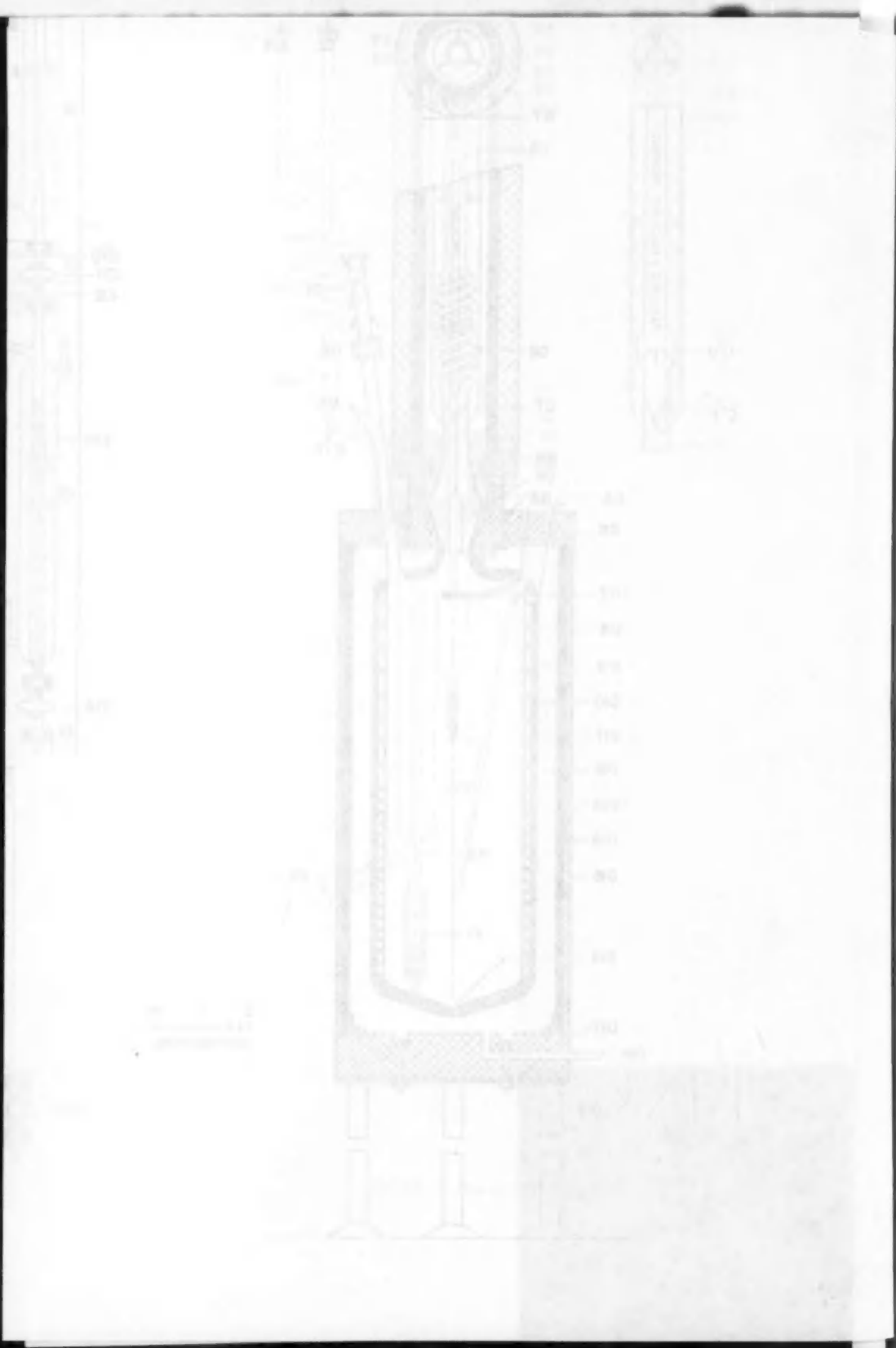

The 3-liter pot is made the same as the 7-liter pot shown in figure 3, except that the vertical dimension of 430 mm along the body is changed to 185 mm.

Figure 4 shows the details of the 18-liter glass pot. Figure 5 shows the details of the transite blocks for supporting the 18-liter glass pot. One of the important requirements in the manufacture [2] of these glass pots is that of thorough annealing. The transite blocks are made to fit the tapered neck of each individual pot. In the mounting of the pot in the transite block support, wet asbestos paper (1/64 inch thick) is placed around the tapered neck of the glass pot to insure a smooth fit against the corresponding tapered part of the transite block.

[2] Otto R. Greiner Co., Newark, N. J.

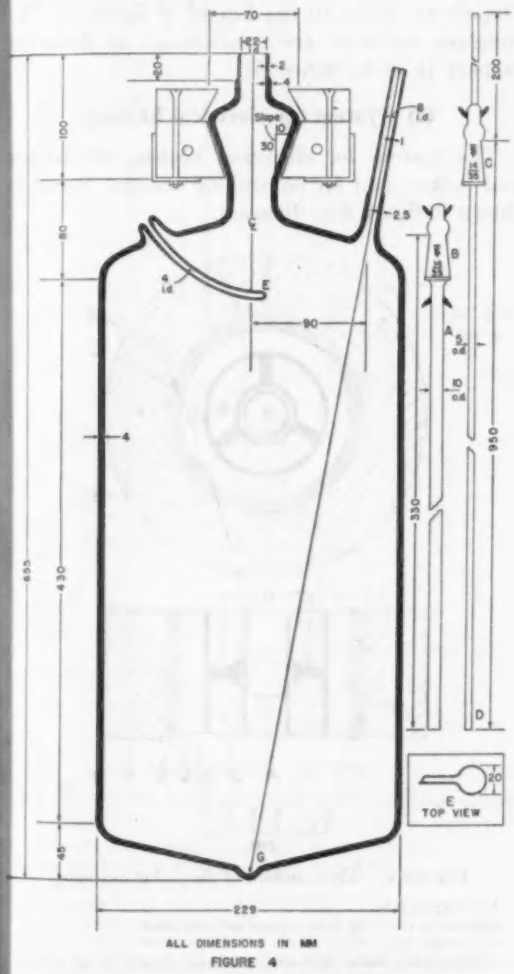

FIGURE 4

FIGURE 4.—*Details of the 18-liter glass still pot.*

The material is Pyrex laboratory glass. The letters have the same significance as the corresponding letters in figure 3.

(b) Rectifying section

The two different rectifying sections used are shown in figure 1. Both rectifying sections have directly sealed vacuum jackets, silvered and highly evacuated.

The rectifying section shown in figure 1 in position in the main assembly contains Heli-Grid packing [3] [3] and has an expansion element consisting of a double helical coil located at the lower end of the rectifying section inside the vacuum jacket [4].

The rectifying section shown in figure 1 at the side of the main assembly contains a packing of stainless steel helices (3/32 inch in diameter, made of No. 30 AWG wire) [5] and has an expansion element consisting of internal convolutions placed at the upper end of the jacket on the rectifying tube [6].

The upper end of each rectifying section is made to receive the thermometer well, which extends down inside the silvered vacuum jacket, as shown

[3] Figures in brackets indicate the literature references at the end of this paper.

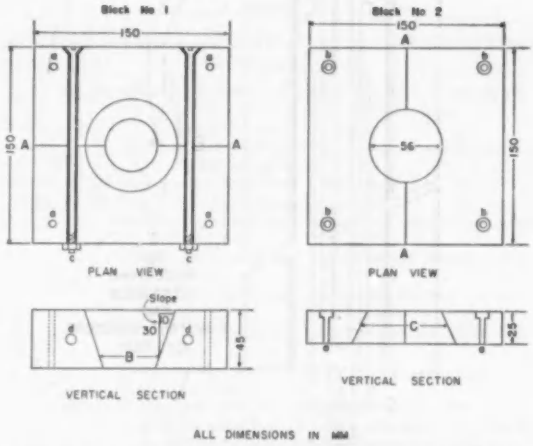

FIGURE 5.—*Details of the transite blocks for supporting the 18-liter glass still pot.*

Block No. 2 fits directly over block No. 1, with the cuts at right angle, as shown in figure 4.

AA=vertical cut through block.
B=taper, made to fit closely the taper on the neck of the corresponding still pot.
a=holes for 8-32 round-head machine screws.
b=countersink.
c=1/4-inch flat-head bolt.
d=holes for 1/4-inch bolt.

in figure 6. The place of sealing the head to the rectifying section is shown at *X* in figure 6.

(c) Jacket

The jacket surrounding the vacuum jacketed rectifying section over its entire length is shown in figures 1 and 6 and in cross section in figure 7. The metal tube, steel or aluminum, carries the insulated heating wire.

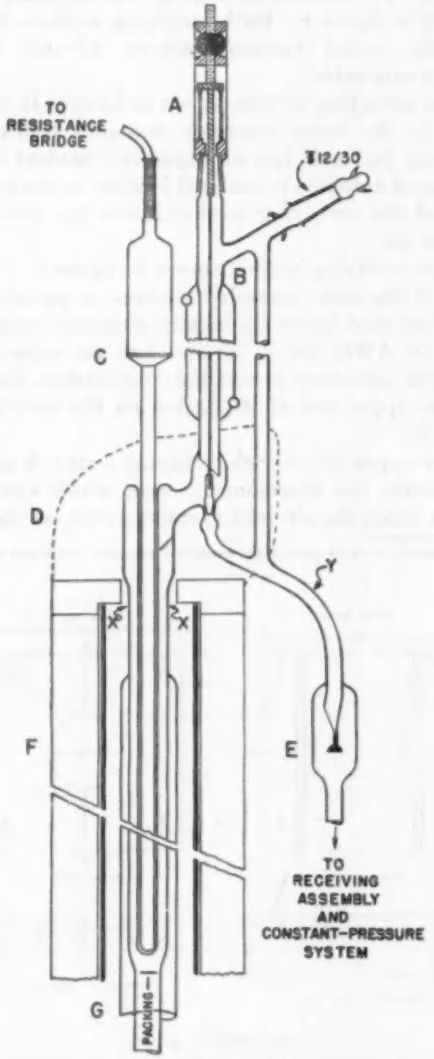

FIGURE 6.—*Assembly of head of distilling column.*

A=metal housing and control, with metallic bellows, as described in figure 3 of reference [2].
B=Pyrex-glass part of the apparatus.
C=platinum-resistance thermometer.
D=boundary of the thermal insulation on the finished head.
E=drop counter, with dimensions as shown in figure 2 of reference [2].
F=top of jacket assembly.
G=top of rectifying section, showing vacuum jacket.
X, *Y*=places where the glass head is sealed to the rectifying section and to the drop counter, respectively.

(d) Head and reflux regulator

The head and reflux regulator has been described previously [1], and is shown in assembly form in figures 1 and 6. Figure 8 shows the details of the glass part of the head and reflux regulator, with dimensions revised over those previously reported.

(e) Receiving assembly

The receiving assembly is shown in figure 1. Details are given in the legend of figure 1. The tungsten contacts are conditioned as described in part II of reference [7].

(f) System for electrical heating

The system for electrical heating of the pot and jacket, and for controlling the pot heater, is shown in figure 9 in diagram.

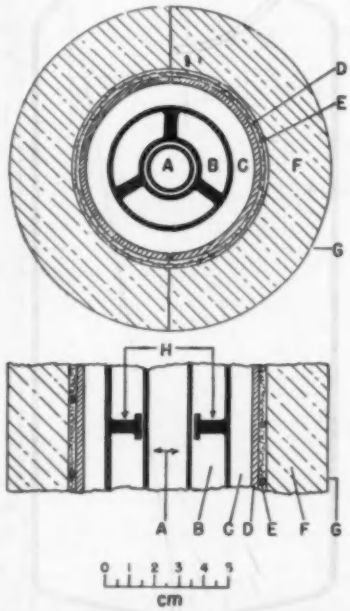

FIGURE 7.—*Cross section of the jacket assembly.*

A=rectifying tube.
B=jacket of rectifying tube, silvered and evacuated.
C=air gap.
D=metal tube, steel or aluminum, split longitudinally in two sections.
E=electrical resistance heating wire, Nichrome.
F=thermal insulation (85% magnesia).
G=aluminum-foil covering.
H=glass support for centering rectifying tube.

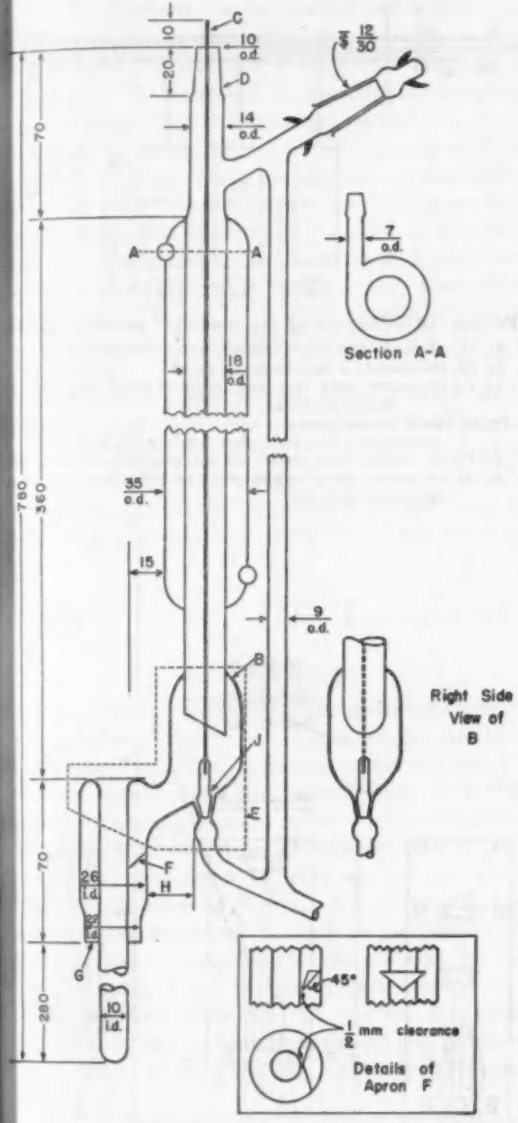

ALL DIMENSIONS IN MM

FIGURE 8.—*Details of the glass part of the distilling-column head.*

A=section showing opening in jacket of condenser.
B=portion connecting condenser with ground-glass valve.
C=tungsten rod, No. 12 AWG.
D=male ground joint, standard taper, 12/20.
E=portion having extra-heavy wall.
F=apron to direct liquid from the condenser to the thermometer well.
G=bottom edge for sealing to rectifying tube (should be smooth and have its plane perpendicular to the axis of the thermometer well).
H=clearance to be not less than 15 mm.
J=ground-glass valve, taper 1 in 5, small end 4 mm, large end 6 mm, length 10 mm, ground for high vacuum. Material is Pyrex laboratory glass.

(g) Thermometric systems

The thermometric systems are shown in diagram in figure 9.

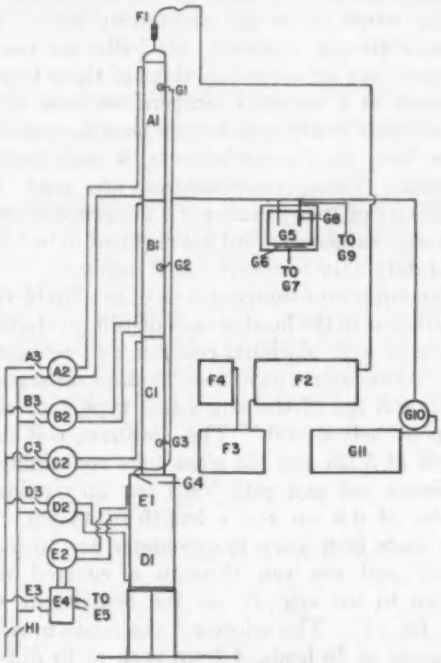

FIGURE 9.—*Diagram of the electrical heating and thermometric systems.*

A1, B1, C1=electrical heaters (300 watts, 110 volts a-c) for the top, middle, and bottom sections, respectively, of the jacket of the rectifying section.
D1, E1=lower and upper electrical heating units of sleeve-type Glascol heating mantle.
A2, B2, C2, D2, E2=variable transformers, 5 amperes, 110 volts, a-c.
A3, B3, C3, D3, E3=double-pole, single-throw switches.
E4=relay, enclosed mercury contacts with vacuum-tube circuit.
E5=mercury manometer with tungsten contact points (*E15*, fig. 1).
F1=platinum-resistance thermometer, 25 ohms, research grade.
F2=thermometer selector, for 19 thermometers with 4 leads each.
F3=resistance bridge, Mueller type.
F4=galvanometer.
G1, G2, G3=single-junction copper-constantan thermoelements for the top, middle, and bottom sections, respectively, of the metal tube surrounding the rectifying section.
G4=single-junction copper-constantan thermoelement for the still pot.
G5=reference junction for thermoelements, in constant-temperature air bath (40° C).
G6=space heater, 200 watts, 110 volts, a-c.
G7=variable transformer, 5 amperes, 110 volts, a-c.
G8=mercury-in-glass thermoregulator.
G9=relay, enclosed mercury contacts, with vacuum-tube circuit.
G10=selector switches.
G11=potentiometer.
H1=double-pole, single-throw switch on constant-voltage supply line.

The temperatures in the pot and at the top, middle, and bottom of the metal jacket tube are measured with single-junction copper-constantan thermoelements on a large portable-type potentiometer mounted on the instrument table. Two thermostatically controlled air baths are used to maintain the reference junctions of these thermoelements at a constant temperature near 40° C. Six 10-point rotary switches are used to receive the leads from 60 thermoelements, 4 each from 15 columns. These temperatures are read with sensitivity of about 1 mm per 0.4 degree centigrade on the galvanometer, but are required to be known accurately only to about 1 or 2 degrees.

The important temperatures of the liquid-vapor equilibrium in the head of each distilling column are measured with platinum resistance thermometers. The thermometers have near 25 ohms resistance at 0° C, and are of the strain-free type with single filament helical coil.[4] The platinum coil has a length of 5 cm and the glass tube containing the platinum coil and gold leads has an outside diameter of 0.9 cm and a length of 45 cm. The four leads from each thermometer are 50 feet in length and are run through a covered metal trough to the selector on the instrument table (see fig. 12). The selector [5] was made to receive as many as 76 leads, 4 from each of 19 different thermometers.[5] The resistance of the thermometer picked out with the selector is measured on a Mueller-type bridge,[6] of special design, with an internal commutator. On this bridge, the smallest units are 0.001 ohm, and the resistance of a given thermometer is measured to the nearest 0.001 ohm or 0.01 degree centigrade, with the sensitivity on the galvanometer scale being near 1 mm per 0.01 degree centigrade.

In normal operation, in analytical distillations of wide boiling (25° to 175° C) charges, it is found that the temperature of the liquid-vapor equilibrium in the head of the distillation column is "smooth" within ±0.01 degree centigrade. During distillations of highly purified hydrocarbons, it is usual for the temperature of the liquid vapor equilibrium in the head to be constant within ±0.01 degree centigrade for several hundred hours.

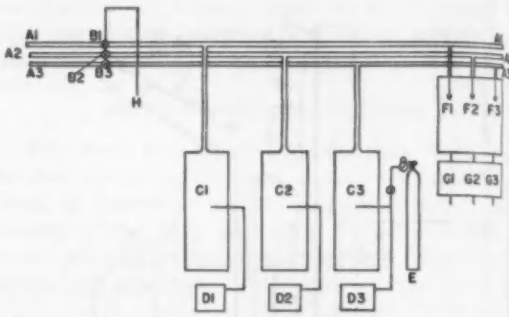

FIGURE 10.—*Diagram of the controlled pressure system.*

A1, A2, A3=copper pipe, 1-inch diameter, with soldered fittings.
B1, B2, B3=manifold of three-diaphragm valves.
C1, C2, C3=ballast tanks, cylindrical, 21 by 60 inches, with cover in thermal insulation.
D1, D2, D3=oil vacuum pumps.
E=cylinder of inert gas (carbon dioxide or nitrogen).
F1, F2, F3=mercury manometers in constant-temperature (35° C) air bath.
G1, G2, G3=relays and vacuum tube circuits for control of vacuum pumps.
H=connection to still.

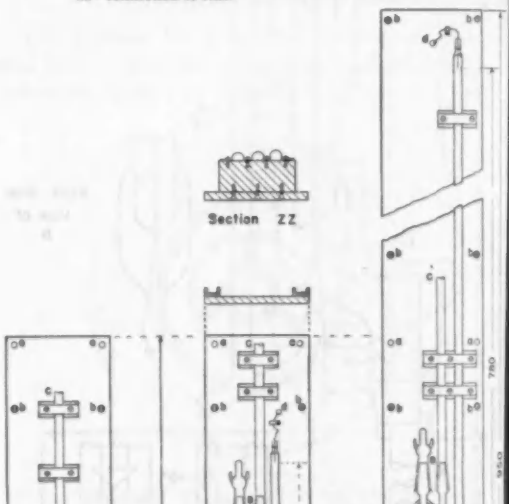

FIGURE 11.—*Details of the mercury manometer assembly for the controlled pressure systems.*

A=manometer proper, Pyrex glass.
B=standard taper (12/30) joint, copper female to glass male [8].
C=copper tube to controlled pressure system.
a=holes for mounting to main frame (not shown).
b=bolts holding transite to channel bars.
d=holes for leads to tungsten contacts.

[4] Twenty of these platinum resistance thermometers were made for this installation by C. H. Meyers.

[5] The selector and bridge were designed by E. F. Mueller and C. H. Meyers of this Bureau, and manufactured by the Rubicon Co., Philadelphia, Pa.

[6] See footnote 5.

(h) System for controlled pressures

The system for controlling the pressures during the distilling operations is shown in diagram in figure 10. The details of the mercury manometers used in controlling the pressures constant at given values are shown in figure 11. The operation of the system for controlling pressures is essentially identical with that previously described in another report from this laboratory [7]. All of the connections and joints in the system, including one metal to glass tapered joint [8] at each controlling manometer (*B*, fig. 11) and at the receiving assembly on each distilling column (*E*5, fig. 1), are soldered.

From hourly observations of temperature made over long periods of time during many distillations of highly purified hydrocarbons at a controlled pressure of 724.5 mm Hg, it is found that the immediate variations in pressure at the head of the column during the operation of the vacuum pump, as well as the long-time changes in the controlled pressure, normally do not exceed about ± 0.2 mm Hg.

The three controlled pressures normally maintained in the laboratory are 725, 217, and 57 mm Hg.

3. Arrangement of Columns and Auxiliary Equipment in the Distillation Room

Figure 12 gives a plan view of the first and second floor levels of the distillation room, together with a view of one wall, showing the location of the various services. The positions of the 15 distilling columns and of the auxiliary equipment are indicated. Figure 13 shows a view in the distillation room, including the instruments for the thermometric systems and the lower part of columns 5 to 10, inclusive.

III. Testing of Distilling Columns

1. Procedure

In this work, the testing of the distilling columns was performed under conditions similar to those encountered in actual operation. (See section IV.)

After equilibrium was established, with the column operating at total reflux, at the prevailing atmospheric pressure, small samples (about 2-ml in volume) were removed from the pot and head. The compositions of these samples were determined from measurements of refractive index. Twenty-four or more hours was allowed for the establishment of equilibrium in these tests.

The pressure drop through the column, from pot to head, was measured on the oil and mercury manometers in the receiving assembly (*E13* and *E15*, fig. 1).

The "through-put" was measured at the head of the column by collecting all the condensate formed in the condenser in a given time, usually 60 seconds or less. In these experiments, the head used was that described in reference [2].

2. Test Mixtures

For convenience in this and other investigations involving the use of mixtures of (a) *n*-heptane and methylcyclohexane and (b) 2,2,4-trimethylpentane and methylcyclohexane as test mixtures, values of refractive index as a function of composition were determined experimentally for these two mixtures. Known mixtures of the pure components were made up accurately by weight. The refractive index, n_D, at 25° C, of these known mixtures was measured, by reference to the refractive index of the pure components, to the nearest 0.0001 on an Abbe-type refractometer graduated directly to 0.0001. For the system *n*-heptane and methylcyclohexane, 26 mixtures were made up and measured. For the system 2,2,4-trimethylpentane and methylcyclohexane, 26 mixtures were also made up and measured. The results, expressed as the difference between the refractive index of the mixture and of *n*-heptane or of 2,2,4-trimethylpentane, are as follows:

For *n*-heptane and methylcyclohexane, at 25° C,

$$n_D(\text{mixture}) - n_D(n\text{-heptane}) = 0.0306N + 0.0048N^2, \quad (1)$$

where n_D is the refractive index and N is the mole fraction of methylcyclohexane in the mixture. (See reference [20].)

For 2,2,4-trimethylpentane and methylcyclohexane, at 25° C,

$$n_D(\text{mixture}) - n_D(2,2,4\text{-trimethylpentane}) = 0.0244N + 0.0072N^2, \quad (2)$$

where n_D is the refractive index and N is the mole fraction of methylcyclohexane in the mixture.

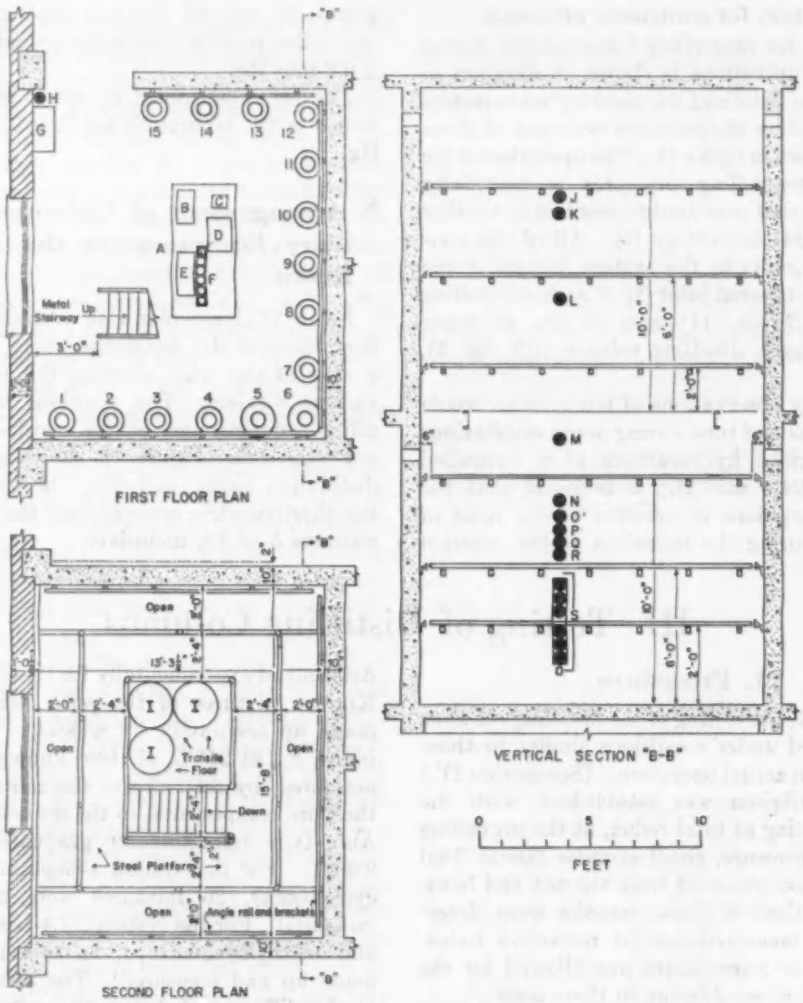

FIGURE 12.—*Arrangement of the distilling columns, auxiliary apparatus, and services in the distillation room.*

Plan views at the first- and second-floor levels, and a vertical view of one wall, are shown. The second-floor level has a 24-inch opening running around the four walls, a 28-inch metal walk with metal stairway to the first-floor level, and a center part covered with transite (on I-beams) for supporting the reservoir tanks of the controlled pressure systems.

The numbers adjoining the open double circle shown at three of the walls in the first-floor plan indicate the location of distilling columns 1 to 15. In each case, the larger circle shows the outside diameter of the pot assembly, and the inner circle shows the outside diameter of the jacket assembly. In the first-floor plan, the letters indicate the following:

A=table for mounting instruments.
B=resistance bridge.
C=galvanometer.
D=thermometer selector, for platinum-resistance thermometers.
E=potentiometer.
F=multiple switches for thermoelements.
G=pumps, manometers, relays, etc., for the controlled-pressure systems.
H=cylinder of carbon dioxide or nitrogen gas, for the controlled-pressure system.

In the second-floor plan, the letters *I* show the location of the three large reservoirs for the controlled-pressure system. The distilling columns have not been shown in the second-floor plan, for simplicity.

In the vertical section, "B–B", the solid circles show the location of the various services for one distilling column, as follows:

J=electric power outlet, 110 volts, a-c.
K, *M*=water outlet, house line.
L, *N*=drain, for discharged water.
O=connection to manifold of three valves, one to each controlled-pressure system.
P=refrigerated water, near 10°C.
Q=compressed air.
R=vacuum, house line.
S=battery of electric power outlets, 110 volts, a-c.

Each of the 15 distilling columns is provided with a similar set of services

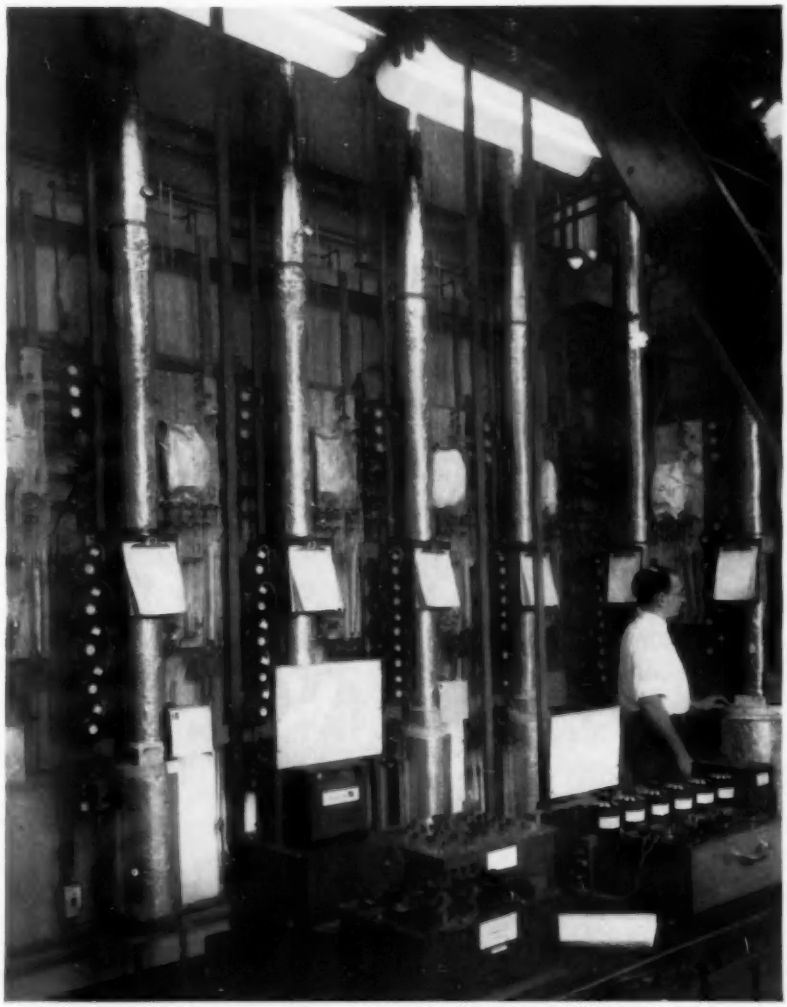

FIGURE 13.—*View in the distillation room, showing the instruments for the thermometric systems and the lower part of columns 5 to 10, inclusive.*

The foregoing equations reproduce each of the experimentally observed values of refractive index within ± 0.0001.

The purified hydrocarbons used in this work for making up the foregoing known mixtures for measurements of refractive index, and also for making up the mixtures for testing the distilling columns, were from lots of purified *n*-heptane, 2,2,4-trimethylpentane, and methylcyclohexane having a purity substantially identical with the same compounds described in another report from this laboratory [9], namely, *n*-heptane, 0.9993, 2,2,4-trimethylpentane, 0.9988, and methylcyclohexane, 0.9990 mole fraction.

The number of equivalent theoretical plates, n, in the actual rectifying section was calculated from the equation [10, 11]

$$n+1=[1/\log (P_A^\circ/P_B^\circ)] \log [(N_A/N_B)_{head}/(N_A/N_B)_{pot}], \quad (3)$$

where P° is the vapor pressure of the given component in the pure state at the mean temperature, N is the mole fraction of the given component in the liquid phase in the head or pot as indicated, A is the more volatile component, and B is the less volatile component.

Assuming that the two components in the binary mixtures are substantially ideal as regards the relation of vapor pressures to composition. (See references [18, 19]), the data on the vapor pressures of the pure components recently reported from this laboratory [7] were reduced to give values of P_A°/P_B° in the neighborhood of the normal boiling points of the components. From these data, P_A°/P_B° for *n*-heptane and methylcyclohexane has the values of 1.0738_0 at the normal boiling point of *n*-heptane (98.426° C) and 1.0758_4 at the normal boiling point of methylcyclohexane (100.934° C). For the 2,2,4-trimethylpentane and methylcyclohexane, these data yield values of P_A°/P_B° equal to 1.0492_2 at the normal boiling point of 2,2,4-trimethylpentane (99.238° C) and 1.0489_0 at the normal boiling point of methylcyclohexane (100.934° C).

With these values, and corresponding ones for neighboring temperatures, eq 3 giving the number of equivalent theoretical plates may be written as follows for the two mixtures:

For *n*-heptane and methylcyclohexane, in the range 96½° to 101½° C,

$$n+1=[32.15-0.34(t-99)] \log [(N_A/N_B)_{head}/(N_A/N_B)_{pot}]. \quad (4)$$

For 2,2,4-trimethylpentane and methylcyclohexane, in the range 97° to 101½° C,

$$n+1=[48.07+0.13(t-100)] \log [(N_A/N_B)_{head}/(N_A/N_B)_{pot}]. \quad (5)$$

In eq 4 and 5, t is the mean temperature in degrees centigrade. The numerical coefficients are estimated to have uncertainties not greater than about $\pm$½ percent for the ranges given.

In connection with the full-scale testing of columns having 200 or more theoretical plates, the authors consider the following binary mixtures as being suitable for trial:

(a) 2,3,4-Trimethylpentane and 2,3,3-trimethylpentane, with normal boiling points of 113.467° and 114.760° C, a difference of 1.293° C [7];

(b) 2,5-Dimethylhexane and 2,4-dimethylhexane, with normal boiling points of 109.103° and 109.429° C, a difference of 0.326° C [7]. From the data on vapor pressures recently reported on these compounds [7], and making the assumption of ideality as previously done above, the values of the constants of eq 3 applicable to these foregoing two test mixtures become as follows:

For 2,3,4-trimethylpentane and 2,3,3-trimethylpentane, over the range 111½° to 115° C,

$$n+1=[64.95-0.36(t-114)] \log [(N_A/N_B)_{head}/(N_A/N_B)_{pot}]. \quad (6)$$

For 2,5-dimethylhexane and 2,4-dimethylhexane, over the range 107° to 110° C,

$$n+1=[250.5-1.7(t-109)] \log [(N_A/N_B)_{head}/(N_A/N_B)_{pot}]. \quad (7)$$

As before, t is the mean temperature in degrees centigrade. The numerical constants have uncertainties estimated to be less than about $\pm$⅜ percent for the trimethylpentanes and about ± 3 percent for the dimethylhexanes.

Small samples (2 to 5 ml) of each of the foregoing binary mixtures may be readily analyzed with sufficient accuracy by means of infrared spectrometers. For the calibration of spectrometers for such analyses, small samples of these compounds of known high purity are available as NBS Standard Samples of hydrocarbons.[7]

Unfortunately, 2,5-dimethylhexane and 2,4-dimethylhexane are not at the present time available in sufficient quantity of adequate purity

[7] A complete list of the hydrocarbons available as NBS Standard Samples may be obtained by writing to the National Bureau of Standards, Washington 25, D. C.

for use in testing distilling columns, nor are pure mixtures of the two compounds available.

With regard to 2,3,4-trimethylpentane and 2,3,3-trimethylpentane, the situation is more favorable. Although neither compound is available separately in sufficient quantity of high purity, pure binary mixtures of the two compounds may be readily obtained by efficient distillation of a commercial mixture (alkylate) of branched-chain paraffins. (See figs. 17 and 18.) In such case (referring to figs. 17 and 18), the fractions to be used in making up the test mixtures would consist of the fractions of distillate containing about 85 percent 2,3,4-trimethylpentane and 15 percent 2,3,3-trimethylpentane and running through to those fractions of distillate containing about 10 percent 2,3,4-trimethylpentane and 90 percent 2,3,3-trimethylpentane. In the example just cited, about 700 ml of material free of components other than the two desired trimethylpentanes would have been obtained in a state suitable for blending for use as a test mixture.

3. Results

In figures 14, 15, and 16 are plotted the results of tests of rectifying sections 10, 15, and 25 mm in diameter and near 2.8 m in length, packed with stainless steel helices [5] ($\frac{3}{32}$ inch in diameter, made of No. 30 AWG wire). Results are given for the number of equivalent theoretical plates and the pressure drop per meter length of rectifying section, as a function of the through-put. The data are substantially in accord with observations on the same packing reported by Fenske and his collaborators [12, 13, 14].

Tests made on a rectifying section 13 mm in diameter and 1.83 m in length containing Heli-Grid packing [3] yielded the following results at atmospheric pressure: Number of equivalent theoretical plates at total reflux, 94, with a pres-

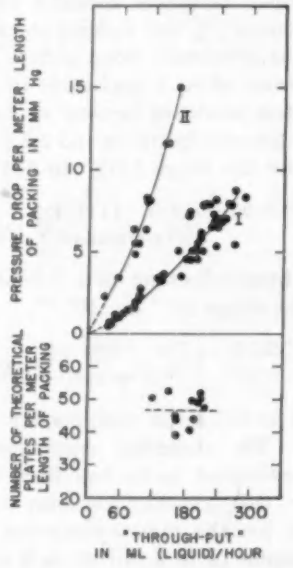

FIGURE 14.—*Results of performance tests on rectifying section of 10-mm diameter packed with stainless-steel helices.*

The upper scale of ordinates gives the pressure drop, in mm Hg, per meter length of packing; the lower scale of ordinates gives the number of equivalent theoretical plates per meter length of packing; and the scale of abscissas gives the "through-put" in milliliters (liquid) per hour. The rectifying section of the distilling column in which tests were made was 10 mm in inside diameter and 2.79 m in length, and was packed with stainless-steel helices, $\frac{3}{32}$ inch in diameter, of No. 30 AWG wire [5]. The test mixture was methylcyclohexane plus 2,2,4-trimethylpentane. For the pressure drop, curves I and II give results for controlled pressures of 770 mm and 217 mm Hg, respectively, at the head of the column. The mean value of the number of equivalent theoretical plates is 46.9, with an average deviation of ±3.7. Determination of the number of equivalent theoretical plates was made at the prevailing atmospheric pressure.

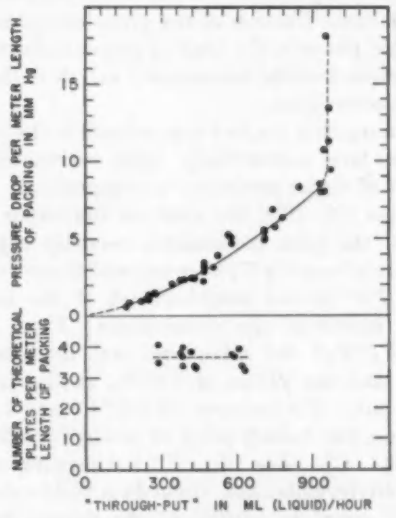

FIGURE 15.—*Results of performance tests on rectifying section of 15-mm diameter packed with stainless-steel helices.*

The upper scale of ordinates gives the pressure drop, in mm Hg, per meter length of packing; the lower scale of ordinates gives the number of equivalent theoretical plates per meter length of packing; and the scale of abscissas gives the "through-put" in milliliters (liquid) per hour. The rectifying section of the distilling column H in which these tests were made was 15 mm in inside diameter and 2.71 m in length, and was packed with stainless-steel helices, $\frac{3}{32}$ inch in diameter, No. 30 AWG wire [5]. The test mixture was methylcyclohexane plus 2,2,4-trimethylpentane. The measurements of pressure drop were performed at a controlled pressure of 770 mm at the head of the column. The mean value of the number of equivalent theoretical plates is 36.4, with an average deviation of ±2.1. Determination of the number of equivalent theoretical plates was made at the prevailing atmospheric pressure.

FIGURE 16.—*Results of performance tests on rectifying section of 25-mm diameter packed with stainless-steel helices.*

The upper scale of ordinates gives the pressure drop, in mm Hg, per meter length of packing; the lower scale of ordinates gives the number of equivalent theoretical plates per meter; and the scale of abscissas gives the "through-put" in milliliters (liquid) per hour. The rectifying sections of the five different distilling columns in which these tests were made were as follows: Column *E*, points marked ×; column *F*, points marked ■; and column *G*, points marked □, inside diameter of 25 mm and length of 2.75 m; column *M*, points marked ●; and column *N*, points marked △, inside diameter of 25 mm and length of 2.73 m. The test mixtures were methylcyclohexane plus 2,2,4-trimethylpentane for columns *E*, *F*, *M*, and *N*, and methylcyclohexane plus n-heptane for column *G*. For pressure drop, curves I, II, and III give results for controlled pressures of 770, 217, and 57 mm Hg, respectively, at the head of the column. The mean value of the number of equivalent theoretical plates is 33.2, with an average deviation of ±1.6. Determination of the number of equivalent theoretical plates was made at the prevailing atmospheric pressure.

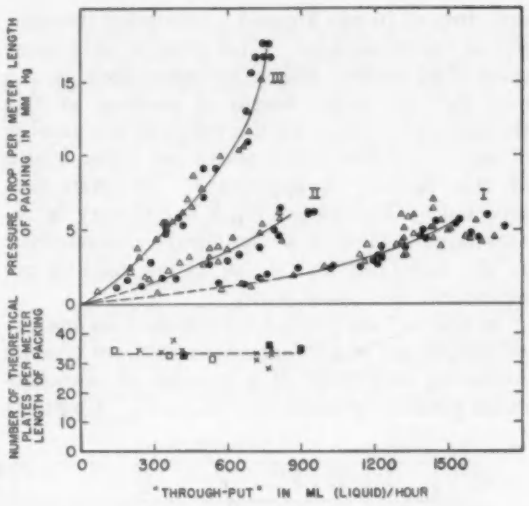
PRESSURE DROP PER METER LENGTH OF PACKING IN MM Hg
NUMBER OF THEORETICAL PLATES PER METER LENGTH OF PACKING
"THROUGH-PUT" IN ML (LIQUID)/HOUR
I
II
III

FIGURE 17. *Results of an analytical distillation of a commercial mixture of branched-chain paraffin hydrocarbons in a distilling column of 16-mm diameter, packed with Heli-Grid packing.*

One scale of ordinates gives, as indicated, the temperature of the liquid-vapor equilibrium at the head of the column under a controlled pressure of 25 mm Hg. The other scale of ordinates gives the refractive index, N_D, at 25° C, of the fractions (18 ml) of distillate collected. The scale of abscissas gives the volume of the distillate in milliliters. The data were analyzed [15] to give the components indicated in the upper part of the chart. This distillation was performed in column 4, which has a rectifying section 16 mm in diameter with 3.66 m of Heli-Grid packing [3], under the following conditions, with preflooding of the column at the start of the distillation: Time allowed for attainment of equilibrium at start, 24 hours; rate of removal of distillate, 4.5 ml/hour; pressure drop, 18.6 mm Hg; calculated reflux ratio 150/1; controlled pressure, 725 mm Hg; total elapsed time, 1,087 hours. The numbers in the lower part of the chart refer to lots in which the fractions of distillate were blended for spectrographic analysis. (See text and fig. 17.)

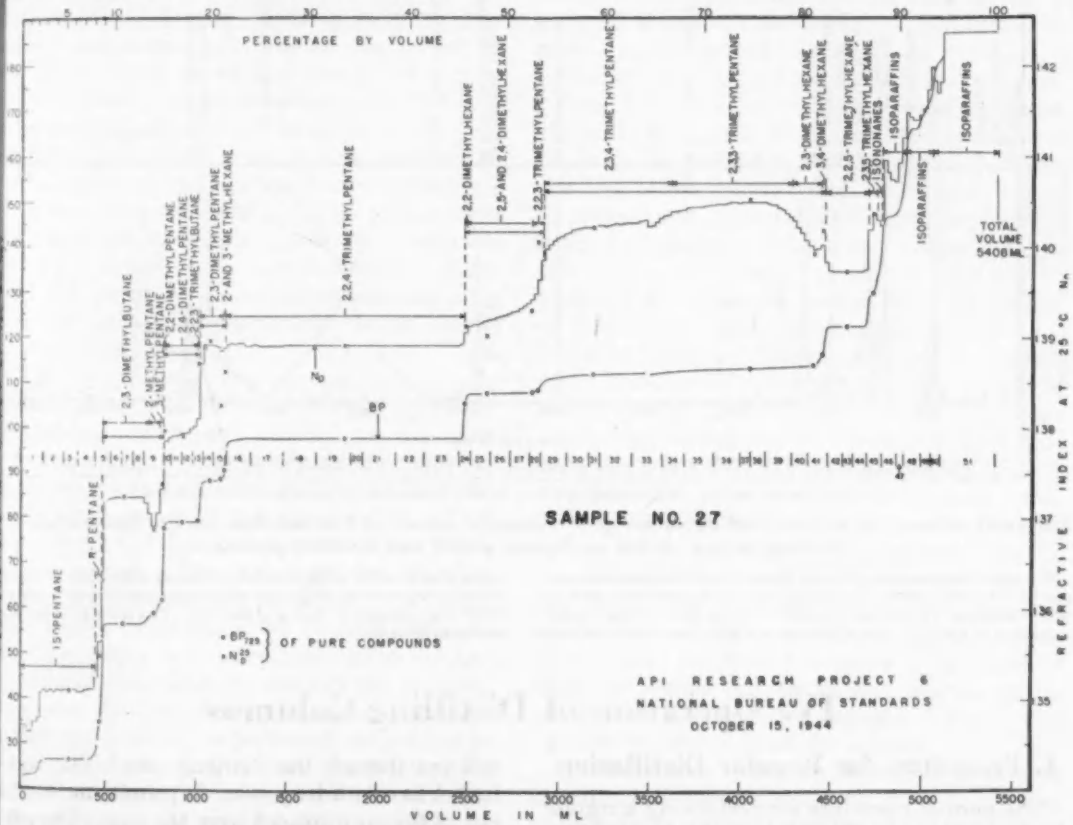

sure drop of 10 mm Hg and a calculated through-put of 340 ml an hour. This gives 51 equivalent theoretical plates, and a pressure drop of 5.5 mm Hg, per meter length of packing at this through-put. Although the values of the number of equivalent theoretical plates per meter length of this packing is appreciably less than that reported by Podbielniak [3], it is still very favorably large. Another advantageous characteristic of the Heli-Grid packing is its low hold-up per equivalent theoretical plate.

In figure 17 are plotted the results of an analytical distillation of a commercial petroleum product consisting essentially of a mixture of branched-chain paraffin hydrocarbons C_5 to C_9. Complete details of this test are given in the legend of figure 17.

The fractions of distillate from the above-mentioned distillation were subsequently blended into larger lots, as indicated by the horizontal row of numbers through the lower middle of figure 17. These lots of material were analyzed for the actual amounts of the individual components by means of infrared spectrographic analysis in the Research Laboratory of the Socony Vacuum Oil Co., Paulsboro, N. J. Figure 18 is a plot of the results giving the composition of the distillate in terms of individual components as interpreted from the infrared spectrographic analyses. Details are given in the legend of figure 18.

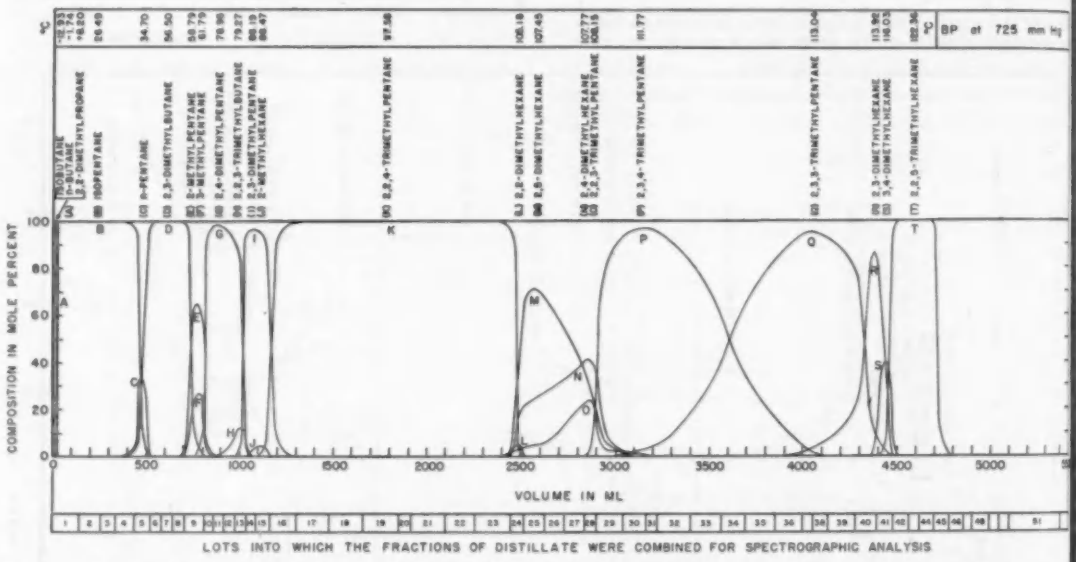
BP at 725 mm Hg
COMPOSITION IN MOLE PERCENT
VOLUME IN ML
LOTS INTO WHICH THE FRACTIONS OF DISTILLATE WERE COMBINED FOR SPECTROGRAPHIC ANALYSIS

FIGURE 18.—*Results of an analytical distillation of a commercial mixture of branched-chain paraffin hydrocarbons in distilling column 16 mm in diameter packed with Heli-Grid packing.*

The scale of ordinates gives, in terms of individual components, the composition of the distillate as a function of its volume, which is plotted along the scale of abscissas. The continuous smooth curve for the percentage of each component in the distillate as a function of volume was synthesized from actual analyses of the lots indicated at the bottom of the chart. The boiling points of the individual components at the controlled distillation pressure of 725 mm are indicated at the top of the chart. This is the same distillation plotted in figure 17.

IV. Operation of Distilling Columns

1. Procedure for Regular Distillation

The normal procedure for performing a regular distillation at one of the controlled pressures is as follows:

The material to be charged is appropriately cooled, if volatile, and then introduced into the still pot through the charging tube[6], *D1*, with a funnel having a long stem to permit undisturbed exit of the air displaced from the pot. The reflux regulator, *A1*, at the head of the column is closed

[6] The letters and numbers following in the text in this section refer to figure 1, unless otherwise stated.

the rates of flow of water through the condenser, *A4*, at the head and those at the receiving assembly, *E7* and *E8*, are adjusted; and the valve to the proper controlled pressure is opened.

The electric current is switched on to the pot heaters and, if necessary (see below), to the jacket of the column. For material boiling below about 50° C at the given pressure, no heating is applied to the jacket. For material boiling between 50° and about 150° C at the given pressure, the electric power is applied simultaneously to pot and jacket heaters. For material normally boiling above about 150° C, electric power is applied to the jacket heaters about 1 hour in advance of the pot heaters. This procedure reduces the difference in temperature between the inside and outside of the rectifying section at the time boiling starts and throws less strain on the expansion elements in the vacuum-jacketed rectifying section. The variable transformers controlling the power to each section of the jacket are initially set to produce a maximum temperature about 10° C below the initial boiling point of the material.

Following the usual practice with packings of the kind used in these columns, the rectifying section is flooded at the start [3, 11] by adding sufficient extra heat to the pot to force liquid into the head of the column. As soon as flooding occurs, the electric power to the pot is reduced and compressed air, *D18*, is introduced into the pot assembly to accelerate cooling.

When the pressure drop through the column decreases to a value below the normal operating pressure drop (previously selected on the basis of the desired through-put), the electric power to the pot heaters is adjusted to normal, and the electric relay control system is connected. This relay controls the upper or intermittent one of the two pot heaters. The lower pot heater is on continuously, but is set at a power input that is not quite enough to maintain the required through-put. The upper pot heater, controlled by the relay circuit, *E4*, figure 9, through the mercury manometer, *E15*, supplies power intermittently to maintain the pressure drop through the column at the constant preselected value. As the temperature of the material being distilled increases, additional power is required to be added to the lower pot heater which is on continuously.

The temperature of the metal tube, *B5*, in the jacket assembly is manually controlled by means of variable transformers, *A2*, *B2*, and *C2* in figure 9, so that the temperatures at the bottom, top, and middle thermometer wells, *B7*, are maintained as follows: The bottom, *G3* in figure 9, at the same temperature as the material in the pot (preferably the temperature of the liquid returning to the pot) *G4*, fig. 9,; the top, *G1*, in figure 9, at the same temperature as the liquid-vapor equilibrium in the head, *F1* in figure 9; and the middle, *G2* in figure 9, at the mean of the top and bottom temperatures. As the metal tube is separated from the material inside the rectifying section by an air gap, *C* in figure 7, and a silvered, evacuated, jacket, *B* in figure 7, its temperature need be controlled only within 1 or 2 degrees of the desired value.

After the through-put, as measured by the pressure drop, reaches its normal operating value, the column is operated at total reflux for a period of from 24 to 36 hours to permit attainment of equilibrium in the rectifying section.

Following the period of establishment of equilibrium, an initial setting of the metal regulator, *A1*, and glass valve, *A5*, at the reflux regulator is made on the basis of the time of fall of 1 drop at the drop counter, *A10*. (For this purpose, 1 drop of hydrocarbon material of the gasoline range is assumed to be equal to 0.04 ml). Adjustment of this rate to the prescribed value is subsequently made on the basis of the actual hourly increment of volume of liquid in the receiver, *E14*.

At the prescribed intervals of time, the product in the receiver is removed as a "fraction." In this operation, the receiver is isolated from the column by closing the stopcocks *E10* and *E11*, and then opened to the atmosphere by opening stopcock *E12*. The material is carefully withdrawn from the bottom of the receiver through stopcock *E16*, with appropriate drainage from the tip of the receiver into the receiving bottle. After the material has been carefully capped, the stopcocks *E16* and *E12* are closed, and stopcocks *E10* and *E11* are opened to the column, slowly in order to permit the air in the receiver to be reduced to the operating pressure without disturbing the operation of the column.[9]

Up to the time that the still reaches its normal operating through-put after flooding, the operations have been conducted by the supervisor or assistant supervisor of the distillation laboratory.

[9] For very low pressures, a separate evacuating system may be used to bring the receiver to the operating pressure before it is reopened to the column.

From this point on, the operation of the distilling column is turned over to the distillation operator, who may have as many as 15 of the distilling columns to care for. The laboratory has one distillation operator on duty each shift of 8 hours, with the distilling columns being operated 24 hours a day, 7 days a week.

The assignment sheets for each new distillation prescribe the pressure at which the distillation is to be performed, the normal operating pressure drop, the rate of collection of product, the size of the "fractions" to be collected, and the time interval between collection of fractions.

The distillation operator checks each of the distilling columns once every hour, making the following observations and entering them on printed record sheets:

(a) The resistance of the platinum thermometer giving the temperature of the liquid-vapor equilibrium in the head is measured. This resistance is recorded accurately to the nearest 0.001 ohm (equivalent to 0.01 degree centigrade).

(b) The foregoing resistance is converted roughly to degrees centigrade from a table giving average values of resistance with respect to temperature for the 15 platinum thermometers in the system. This conversion [10] is made roughly, for purposes of operation, with a precision of 0.1 degree centigrade and an accuracy of about one-half degree.

(c) The volume of the liquid in the receiver is recorded, to 0.1 ml or 0.01 ml, depending upon the size of the receiver.

(d) The hourly increment of volume in the receiver, obtained by subtraction of the preceding volume in the receiver, is recorded, for the purpose of checking adherence to the prescribed rate of collection of product.

(e) The pressure drop through the column, as measured on the oil manometer, *E13*, is recorded to 0.1 cm.

(f) The emf of the three thermoelements giving the temperatures of the top, middle, and bottom of the metal tube in the jacket assembly, and of the one thermoelement giving the temperature of the pot, are measured.

(g) These emf are converted to temperature in degrees centigrade, recording to the nearest 1.0 degree.

(h) Appropriate adjustments to the settings of the variable transformers controlling the power to the lower pot heater and to the three sections of the jacket are made.

(i) The scale readings (voltage) on the five variable transformers controlling the two pot heaters and the three jacket heaters are recorded.

As the end of the distillation approaches, an accurate comparison is made of the volume of material collected and the volume charged, to permit a reliable estimate of the day on which the distilling column will be shut down. Normally the distillation is halted when the rapid fall of the pressure drop from its normal operating value indicates depletion of the liquid in the pot. At this point, the valve to the controlled pressure system is closed, all electric power is cut off, and the pot and jacket are allowed to cool to room temperature. The cooling of the pot is accelerated by a flow of air into the pot assembly, *D1*. After the pot has cooled, the residue is withdrawn from the pot through the withdrawal tube (see *D*, fig. 3) inserted down through the charging tube, *D1*, in close proximity to the recess in the bottom of the pot. (See *G*, fig. 3.)

After the residue has been removed, acetone is charged to the pot and distilled at total reflux to clean out the column. After the acetone is removed, air is drawn through the pot and rectifying section to "dry out" the column. Before the next distillation the stopcocks on the receiver assembly are cleaned and relubricated, normally with tetraethylene glycol citrate [16].

2. Procedure for Azeotropic Distillation

The procedure followed in the operation of the distilling columns for azeotropic distillation is the same as for the regular distillation described in the preceding section except that, normally, an excess of the added azeotrope-forming substance is added to the hydrocarbon charge in the pot and the distillation is carried through to the point where no hydrocarbon remains in the columns, as evidenced by the rise of the temperature of the liquid-vapor equilibrium in the head to that corresponding to the pure azeotrope-forming substance. The operator is normally instructed to halt the distillation when there have been collected two fractions with boiling points equal to that of the azeotrope-forming substance at the given pressure.

[10] After the distillation is completed, the record of the temperature of the liquid-vapor equilibrium is given to the appropriate research investigator, who makes the conversion of the temperature of the liquid-vapor equilibrium accurately to 0.01 degree from the individual table for the given platinum thermometer used.

V. Conclusion

As of December 31, 1945, the 15 distilling columns assembled in the distillation room described in section II–3 and figures 12 and 13 of this report had the characteristics shown in table 1. It is planned to make improvements in the apparatus and equipment as new information from this and other laboratories becomes available. The earlier distilling apparatus in this laboratory is described in reference [17].

TABLE 1.—*Characteristics of the 15 distilling columns installed as of December 31, 1945*

Number of distilling column [a]	Rectifying section			Pot		Minimum operating residue (approximate)	Operating pressure drop	Operating throughput	Rate of collection of product	Operating reflux ratio (approximate)	Estimated number of theoretical plates (at total reflux)
	Diameter	Length	Packing [b]	Actual volume	Maximum charging capacity						
	mm	*m*		*Liters*	*Liters*	*ml*	*mm Hg*	*ml/hour*	*ml/hour*		
1	11	2.74	HG	3.2	2.7	40	12.1	300	2.0	150/1	150
2	13	1.83	HG	7.2	6.0	50	8.5	300	2.2	135/1	100
3[c]	13	1.83	HG	7.2	6.0	50	8.5	300	2.2	135/1	100
4	18	3.66	HG	7.2	6.0	100	19.2	720	4.0	180/1	200
5	25	3.66	SSH	18.0	15.0	300	21.3	1,560	12.5	125/1	125
6	25	3.66	SSH	18.0	15.0	300	21.3	1,560	12.5	125/1	125
7	20	3.66	SSH	7.2	6.0	135	21.3	1,240	8.5	145/1	130
8	20	3.66	SSH	7.2	6.0	135	21.3	1,240	8.5	145/1	130
9	15	3.66	SSH	7.2	6.0	100	21.3	740	4.5	165/1	135
10	15	3.66	SSH	7.2	6.0	100	21.3	740	4.5	165/1	135
11A	18	3.66	HG	7.2	6.0	100	19.2	720	4.0	180/1	200
12	15	3.66	SSH	3.2	2.7	80	21.3	740	4.5	165/1	135
13	20	3.66	SSH	7.2	6.0	135	21.3	1,240	8.5	145/1	130
14	25	3.66	SSH	7.2	6.0	175	21.3	1,560	12.5	125/1	125
15[c]	25	3.66	SSH	7.2	6.0	175	21.3	1,560	12.5	125/1	125

[a] "A" attached to the number of the distilling column indicates that the original rectifying section was changed. The rectifying section in the original column 11 was one of the same length 10 mm in diameter packed with the stainless steel helices described in footnote "b".

[b] SSH represents stainless-steel helices, 3/32 inch in diameter, made of No. 30 AWG wire [5]; HG represents Heli-Grid packing [3].

[c] Columns 3 and 15 are planned to be changed so that their rectifying sections will be similar to that of column 4.

Acknowledgment is made to P. V. Keyser, Jr., C. H. Schlesman, and F. P. Hochgesang, of the Research Laboratories of the Socony-Vacuum Oil Co., Paulsboro, N. J., for permission to use the results of their infrared spectrographic analysis of the fractions of the distillate shown in figures 17 and 18.

VI. References

[1] C. B. Willingham and F. D. Rossini, J. Research NBS **33,** 383 (1944) RP1615.

[2] F. D. Rossini and A. R. Glasgow, Jr., J. Research NBS **23,** 509 (1939) RP1249.

[3] W. J. Podbielniak, Ind. Eng. Chem., Anal. Ed. **13,** 639 (1941).

[4] Podbielniak, Inc., Chicago, Ill.

[5] M. R. Fenske, C. O. Tongberg, and D. Quiggle, Ind. Eng. Chem. **26,** 1169 (1934).

[6] D. J. Pompeo and E. Meyer, Rev. Sci. Instr. **12,** 368 (1941).

[7] C. B. Willingham, W. J. Taylor, J. M. Pignocco, and F. D. Rossini, J. Research NBS **35,** 219 (1945) RP1670.

[8] C. H. Meyers, J. Am. Chem. Soc. **45,** 2135 (1923).

[9] A. F. Forziati, A. R. Glasgow, Jr., C. B. Willingham, and F. D. Rossini, J. Research NBS **36,** (1946) RP1695.

[10] M. R. Fenske, Ind. Eng. Chem. **24,** 482 (1932).

[11] M. R. Fenske, Science of petroleum, **II,** 1629–1661. (Oxford University Press, London, 1938).

[12] C. O. Tongberg, D. Quiggle, and M. R. Fenske, Ind. Eng. Chem. **26,** 1213 (1934).

[13] C. O. Tongberg, S. Lawroski, and M. R. Fenske, Ind. Eng. Chem. **29,** 957 (1937).

[14] F. C. Whitmore, M. R. Fenske, D. Quiggle, H. Bernstein, T. P. Carney, S. Lawroski, A. H. Popkin, R. B. Wagner, W. R. Wheeler, and J. S. Whitaker, J. Am. Chem. Soc. **62,** 795 (1940).

[15] A. R. Glasgow, Jr., and F. D. Rossini. American Petroleum Institute Research Project 6. National Bureau of Standards. (Unpublished.)

[16] T. P. Sager. Ind. Eng. Chem. **4,** 388 (1936).

[17] J. H. Bruun and S. T. Schicktanz, J. Research NBS **7,** 851 (1931) RP379.

[18] G. Calingaert and H. A. Beatty, Ind. Eng. Chem. **26,** 504 (1934).

[19] J. M. Harrison and L. Berg, Ind. Eng. Chem. **38,** 117 (1946).

[20] E. C. Bromiley and D. Quiggle, Ind. Eng. Chem. **25,** 1136 (1933).

WASHINGTON, January 28, 1946.

U. S. Department of Commerce
National Bureau of Standards

Research Paper RP1725
Volume 37, July 1946

Part of Journal of Research of the National Bureau of Standards

Nickel Plating on Steel by Chemical Reduction

By Abner Brenner and Grace E. Riddell

A process has been developed for the production of adherent nickel deposits of good quality on steel without the use of an electric current. The deposition of nickel is brought about by chemical reduction of a nickel salt with hypophosphites in a hot ammoniacal solution. The reaction is catalytic and, under the prescribed conditions of concentration and pH, no reduction occurs in the solution unless certain metals, such as steel or nickel, are introduced into the bath. The reduction then occurs only at the surface of the immersed metal with the production of a coating of nickel of 96 to 97 percent purity.

I. Introduction

In the course of an investigation on a nickel plating bath an unusual chemical reaction was accidentally encountered, by means of which nickel deposits of good quality can be produced on a steel or nickel surface without the use of an electric current. The reaction involves reduction by hypophosphites in a heated nickel solution. In the nickel bath being investigated, trouble was had with the oxidation of some constituents of the bath at an insoluble anode, and to obviate this difficulty typical reducing agents were added. In one of the experiments the surprising result of an apparent cathode current efficiency of 130 percent was obtained, although during the plating there was considerable gassing at the cathode, which usually indicates a low current efficiency. Furthermore, the object being plated, which was a tube with an inside anode, was found to have been completely plated on the outside, although no external anodes had been used. Although this process will not replace electrodeposition of nickel, it may prove useful for special applications.

Contents

	Page
I. Introduction	31
II. Literature	32
III. General principles	32
IV. Bath composition and operating condition	33
V. Other methods of chemical reduction	34

693841—46—5

II. Literature

The foregoing experience with the hypophosphite reduction occurred before it was noted that this reaction had been previously reported. An investigation of the literature disclosed that the reduction of nickel solutions with hypophosphite to produce metallic nickel had been observed by Wurtz.[1] The reaction was studied in detail by Bretau,[2] Paal and Friederici,[3] Scholder and Heckel,[4] and Scholder and Haken.[5] These workers used high concentrations of hypophosphite, usually several hundred grams per liter, to effect the reduction. The solution containing the nickel salt was heated on a steam bath for several hours, if necessary, until the reaction began. The reaction was usually quite vigorous, much hydrogen was evolved, and the mass bubbled up to 10 or 20 times its original volume. The nickel was obtained mainly as a dark powder, but occasionally it deposited on the walls of the flask as a mirror, which gradually became detached and broke up into thin flakes.

The reaction by which nickel is produced is

$$NiCl_2+NaH_2PO_2+H_2O\rightarrow Ni+2HCl+NaH_2PO_3 \quad (1)$$

or

$$Ni^{++}+H_2PO_2^-+H_2O\rightarrow Ni^{\circ}+2H^+H_2PO_3^-.$$

Concurrently, some of the hypophosphite is oxidized by the water, particularly in the presence of certain metals, to phosphite, and hydrogen is liberated:

$$NaH_2PO_2+H_2O\rightarrow NaH_2PO_3+H_2. \quad (2)$$

These equations show that the reaction mixture becomes more acid, as either an acid salt or free acid is produced. The reduction of nickel ion (eq. 1) is catalyzed by certain metals, including nickel, and as nickel is produced by the reaction, it is therefore autocatalytic. This explains why the reaction, which is rather slow in starting, proceeds with so much vigor after it once begins.

Some of the above investigators obtained cobalt by a hypophosphite reduction similar to that used for nickel. Only alkaline solutions could be used, and the reduction was slower than that of nickel.

The product which these workers (see footnotes 3 and 4) obtained from an initially neutral nickel solution was not pure nickel but a mixture of phosphides, probably as Ni_2P and Ni_5P_2 (see footnote 3), with perhaps some uncombined nickel. The precipitate usually contained 85 percent of nickel and about 12 percent of phosphorus, with small amounts of moisture and oxygen. The product obtained from an alkaline solution was much purer. It contained about 97 percent of nickel and 3 percent of phosphorus, and hence consisted largely of uncombined nickel. The nickel phosphides obtained by the hypophosphite reduction are more similar to an intermetallic compound, in which the phosphorus behaves as a metal, than to a phosphine derivative. They are soluble in acids only with difficulty and do not give off phosphine when so treated.

III. General Principles

In an extension of the work of the previous investigators, it was found that the reduction of nickel compounds to nickel could be so controlled as to cause the catalytic reduction to occur, with the virtual exclusion of the purely chemical reduction. Thus an adherent compact nickel coating could be deposited on certain metal surfaces immersed in the bath without any appreciable precipitation of nickel occurring throughout the bulk of the solution or on the walls of the glass vessel. This preferential deposition was made possible by employing dilute solutions of hypophosphite, about 10 grams per liter instead of several hundred grams per liter. Under these conditions, the deposition of nickel occurs on the surface of iron, nickel, gold, cobalt, palladium, and aluminum, but not on platinum, copper, zinc, or lead.

The method differs from the common methods of chemically depositing metallic coatings from aqueous solutions. The formation of coatings by chemical replacement, such as the formation of a copper film on steel dipped in copper sulfate, involves solution of the base metal. The formation of metallic films, such as silver, copper, or gold by reduction, does not necessarily involve any catalytic action, as the metal precipitates indiscriminately over all articles immersed in it, as well as on the walls of the vessel.

[1] Compt. rend. **21**, 169 (1845).
[2] Bul. soc. chim. [4] **9**, 518 (1911).
[3] Ber. deut. chem. Geo. **64**, 1766 (1931).
[4] Z. anorg. allgem. Chem. **198**, 329 (1931).
[5] Ber. deut. chem. Ges. **64**, 2870 (1931).

IV. Bath Composition and Operating Conditions

The composition of the baths may vary within wide limits. Some typical formulas are shown in table 1. The baths are operated at or above 90° C (194° F). As already noted, they produce a deposit only on certain metals. In the absence of metals that catalyze nickel deposition, the baths are fairly stable. A bath containing hypophosphite has been kept at 90° C for 5 hours without deteriorating very much. At room temperature, a bath is stable for several days.

The nickel deposits contained about 97 percent of nickel, and therefore are similar to those that Paal and Friederici obtained from an alkaline solution.

TABLE 1.—*Bath compositions*

	Bath		
	1	2	3
Nickel chloride, $NiCl_2.6H_2O$	30 g/liter	30 g/liter	30 g/liter.
Sodium hypophosphite, NaH_2PO_2	10 g/liter	10 g/liter	10 g/liter.
Ammonium chloride, NH_4Cl	50 g/liter	100 g/liter	
Sodium citrate, $Na_3C_6H_5O_7$. $5½H_2O$	100 g/liter		100 g/liter.
Rate of deposition { mm/hr	0.006	0.012	0.005.
Rate of deposition { in./hr	0.00025	0.0005	0.0002.
Appearance of deposit	Semibright	Dull	Bright.
Alkali for neutralizing bath	NH_4OH	NH_4OH	NaOH.
pH	8 to 9	8 to 9	8 to 9.

Steel objects to be plated are cleaned by any of the accepted procedures and are given an acid dip before being placed in the bath. The parts to be plated are suspended in the bath, for example, by a string. Small objects may be held on cloth stretched over a frame and should be agitated occasionally, although there is no need of constant motion, as in barrel plating, because current distribution is not involved. During the deposition a considerable amount of hydrogen is evolved from the surface of the metal. Under the conditions of operation outlined, nickel deposits only on the steel. However, after a bath has operated in a glass vessel for about 5 hours, a small amount of a precipitate containing nickel may deposit on the bottom of the vessel where the source of heat has been applied. If this precipitate is not removed, it may cause decomposition of some of the hypophosphite, just as another metal surface does.

The thickness of nickel deposited in a given time depends in part on the relation of the steel surface to the volume of the bath. The values in the above table were obtained with an area of 1 square decimeter (16 square inches) in 1 liter (1.1 quart) of solution. The rate of plating is less than that usually employed in nickel electroplating in a tank, but is about the same as in barrel plating. Because of the gradual exhaustion of the hypophosphite, less nickel will deposit during each succeeding interval of time. Most of the nickel is deposited during the first hour, and the reaction is virtually complete in 2 hours, unless more hypophosphite is added.

As the hypophosphite is gradually exhausted, more must be added if thick deposits are required, especially if the area to be plated is relatively large compared to the volume of solution. Additions of 5 grams of hypophosphite per liter may be made at half-hour or 1-hour intervals. Thereby, deposits 0.002 inch (0.05 mm) thick have been obtained in about 6 hours. As pointed out in equations 1 and 2, the hypophosphite becomes converted into phosphite, which, however, does not interfere with the operation of the bath. When the bath becomes too concentrated with this compound, it would be more economical to discard the bath than to try to remove the phosphite.

When the bath becomes depleted in nickel, additional nickel must be added in the form of soluble nickel salts. The function of the ammonium salts or the citrates is to keep nickel in solution at a pH of 8 to 9. Ammonia has the disadvantage of being volatile at the temperature at which the bath is operated, but it is more satisfactory than organic amines, which were tried as substitutes. The citrate can be replaced by other hydroxy-organic acids, such as tartaric, without affecting the operation of the bath. Bath 1 (see table 1) is the preferred composition. Bath 2, which does not contain any citrate, plates more rapidly than bath 1, but the deposits are dull and more likely to be rough, and the bath does not remain as clear during operation. Bath 3, with no ammonium salts, gave the brightest deposits, but had the disadvantage that after the deposits had reached a thickness of about 0.0002 inch, they ceased to become thicker even after several hours.

The reason for using a low concentration of hypophosphite, as already pointed out, is to obtain a deposition on the articles without producing

"nickel black" throughout the bath. A similar consideration governs the chosen concentration of ammonium salts, too high a concentration of which will cause the chemical reduction to take place with liberation of nickel on the walls of the vessel. A higher nickel concentration tends to produce rough deposits.

The temperature of operation of the bath is important. At temperatures below 90° C. the rate of deposition of nickel is slower, and the deposit is more likely to contain impurities. For example, at 60° C. the rate of deposition is about half that at 90° C. Nickel may be slowly deposited on steel at room temperature from a bath that has a high concentration of hypophosphite.

The pH of the bath should be kept between 8 and 9 to obtain the best deposits. On operation of the bath the pH drops because of the formation of hydrogen ions, as shown in equations 1 and 2. Also, the volatilization of the ammonia causes a drop in the pH. The pH is readily kept at the required value by adding ammonia water occasionally, so as to keep the bath perceptibly ammoniacal in odor.

The efficiency of the reduction of nickel salts to nickel is not very high because, as pointed out in connection with reaction 2, some of the hypophosphite is catalytically oxidized by water with the liberation of hydrogen. The best yield of nickel that has been obtained was about 37 percent, based on the conversion of the hypophosphite to phosphite. This yield, obtained with a large area of metal in the bath, amounts to a reduction of about 2 grams of nickel by 10 grams of hypophosphite. With a small area of metal in the bath the efficiency of deposition is likely to be about 20 percent.

The adhesion of the nickel deposit to mild steel is such that it cannot be flaked off by bending. However, the adhesion is less satisfactory on high-carbon steel.

Salt-spray tests were made on steel coated with 0.0002, 0.0005, and 0.001 inch of this reduced nickel, in comparison with similar panels coated with electrodeposited nickel. The protective value of the two types of nickel was virtually the same.

The chemical method of plating nickel is not economical to operate because the hypophosphite is expensive (about 70 cents a pound) and its utilization is inefficient. On the other hand, no special equipment is required, such as generators, rheostats, and racks. The utility of the method will lie in special applications, for example, plating small lots of small steel parts, which cannot be plated economically in a barrel. Another advantage of the method is that it can be employed to plate the inside of an article that cannot be plated with an inside anode. For example, by this method a nickel deposit was applied to the inside of a bent steel tube one-fourth inch in diameter.

V. Other Methods of Chemical Reduction

The reduction of nickel and cobalt salts to the metal is a rather rare chemical phenomenon, of which we have found no recorded examples other than the method employing hypophosphites. In the course of some other work another system was encountered in which nickel and cobalt salts can be reduced to metal, but the reduction is not as simple or practicable as the hypophosphite method. This reaction involves the reduction of nickel or cobalt in an alkaline solution with lower valent molybdenum compounds. The molybdenum, in the form of molybdate in a strongly acid solution, is electrolytically reduced in a porous cell, preferably with a lead cathode, to the reddish-brown solution of the lower valent salt. When this solution is added to an alkaline metal solution containing hydroxyacetates (to keep molybdenum and cobalt compounds from precipitating), a thin mirror of nickel or cobalt will form on the walls of the test tube and some gas will be liberated.

Cobalt deposits have been obtained by another reaction, which was not conducted in aqueous solution. A cobalt salt was dissolved in molten potassium formate or hydroxyacetate or a mixture of the two, which melts at about 150° C. When a rod of copper or gold was left in the melt for some hours, a thin, bright coating of cobalt was obtained as a result of chemical reduction.

WASHINGTON, April 11, 1946.

U. S. Department of Commerce
National Bureau of Standards

Research Paper RP1726
Volume 37, July 1946

Part of Journal of Research of the National Bureau of Standards

Temperature Coefficients for Proving Rings

By Bruce L. Wilson, Douglas R. Tate, and George Borkowski

Proving rings for calibrating testing machines are not compensated for change in elastic properties and dimensions with temperature. For this reason, temperature-correction factors must be used in computing ring loads from deflections obtained at temperatures that differ from the temperature of calibration. Temperature coefficients for 14 representative rings were computed from calibration results obtained at temperatures of 70° and 100° F. The temperature coefficient of one ring for the range +70° to −93° F was determined from measurements of the natural frequencies at these temperatures. The temperature coefficient of a proving ring is shown to be equal to the temperature coefficient of Young's modulus of elasticity plus twice the coefficient of thermal expansion of the material of the ring.

I. Introduction

The proving ring is the most widely used elastic calibration device [1][1] for calibrating testing machines that apply forces to engineering materials and structures. About four-fifths of such devices submitted to the National Bureau of Standards for calibration during the past year were proving rings. The rings are not compensated for the change in elastic properties and dimensions with temperature, therefore, a knowledge of the temperature coefficient is required for use in computing ring loads from deflections obtained at temperatures that differ from the temperature during the calibration of the ring.

The tests described were undertaken (a) to determine experimentally the temperature coefficients of a number of representative proving rings for the usual range of room temperatures, (b) to determine the coefficient of a representative

[1] Figures in brackets indicate the literature references given at the end of this paper.

Contents

	Page
I. Introduction	35
II. Description of proving ring	36
III. Theory of thermal effects	36
1. Relationship between temperature coefficient and deflection for proving rings	36
2. Relationship between temperature coefficient of proving ring and temperature coefficient of Young's modulus of elasticity and coefficient of thermal expansion	36
3. Relationship between temperature coefficient and spring constant for proving rings	37
IV. Experimental procedure	38
1. Temperature range 70° to 100° F	38
2. Temperature range +70° to −93° F	38
V. Results	39
1. Temperature range 70° to 100° F	39
2. Temperature range +70° to −93° F	40
VI. Conclusions	40
VII. References	41

ring at a temperature near −100° F, and (c) to determine whether the temperature coefficient may be calculated with sufficient accuracy from measured values of the temperature coefficient of Young's modulus of elasticity and the coefficient of thermal expansion for the material of a ring.

II. Description of Proving Ring

The proving ring has been described in a previous paper [2]. Briefly, it is an elastic ring in which the deflection of the ring, when loaded along a diameter, is measured by means of a micrometer screw and a vibrating reed mounted diametrically in the ring. One of the rings used in the tests reported is shown in figure 1. This ring, which was used for the tests at −93° F, was made of steel having the following chemical composition: C, 0.50 percent; Cr, 1.00 percent; and Ni, 1.75 percent. It was heat treated to show a Vickers number of about 475 (diamond indenter, load=120 kg). It is believed that each of the proving rings tested had a total alloying content not exceeding 5 percent.

Proving rings are usually calibrated in dead-weight machines [3], in which their deflections are determined for 10 uniformly spaced loads. The calibration factor, the ratio of the load to the deflection of the ring, is calculated, and the results are shown graphically as in figure 2. When a ring is used to measure loads, the observed deflection is multiplied by the product of the calibration factor read from the calibration graph and a temperature correction factor.

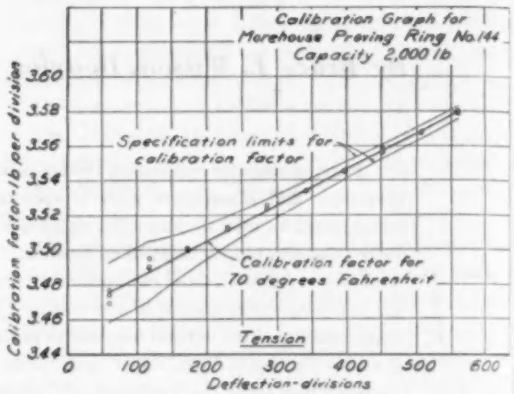

FIGURE 2.—*Calibration graph for Morehouse proving ring No. 144.*

III. Theory of Thermal Effects

1. Relationship Between Temperature Coefficient and Deflection for Proving Rings

The temperature coefficient, k, of a proving ring is defined by the equation

$$k=(1/F_c)(dF/dt), \tag{1}$$

in which F_c is the calibration factor for the ring at the standard temperature of calibration.

The calibration factor F_t for any temperature, t, becomes

$$F_t=F_c[1+k(t-t_c)], \tag{2}$$

where

F_t=calibration factor for a temperature of t degrees

t_c=standard temperature of calibration.

Equation 2 may be written in terms of deflections measured in dial divisions as

$$d_c=d_t[1+k(t-t_c)], \tag{3}$$

in which

d_c=deflection of the ring at a temperature of t_c degrees

d_t=deflection of the ring at a temperature of t degrees.

Solving equation 3 for the temperature coefficient

$$k=\frac{d_c-d_t}{d_t(t-t_c)}. \tag{4}$$

By means of equation 4 the temperature coefficient for a ring may be computed from deflections for the same load obtained at different temperatures.

2. Relationship Between Temperature Coefficient of Proving Ring and Temperature Coefficient of Young's Modulus of Elasticity and Coefficient of Thermal Expansion

The deflection in the direction of the load of a closed circular ring of rectangular cross section

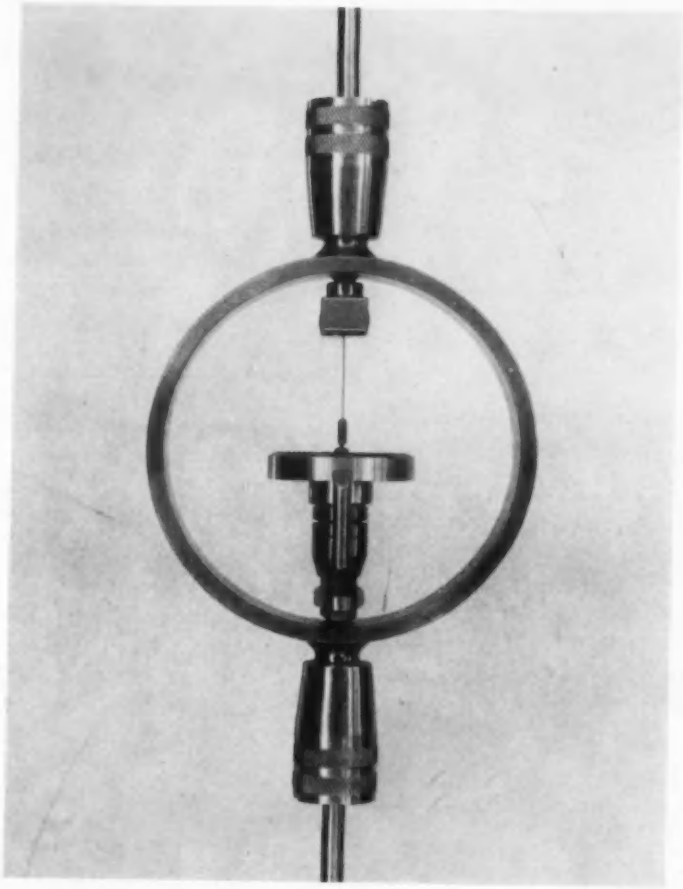

FIGURE 1.—*Morehouse proving ring No. 144, capacity 2,000 lb, with tension fittings attached to external bosses.*

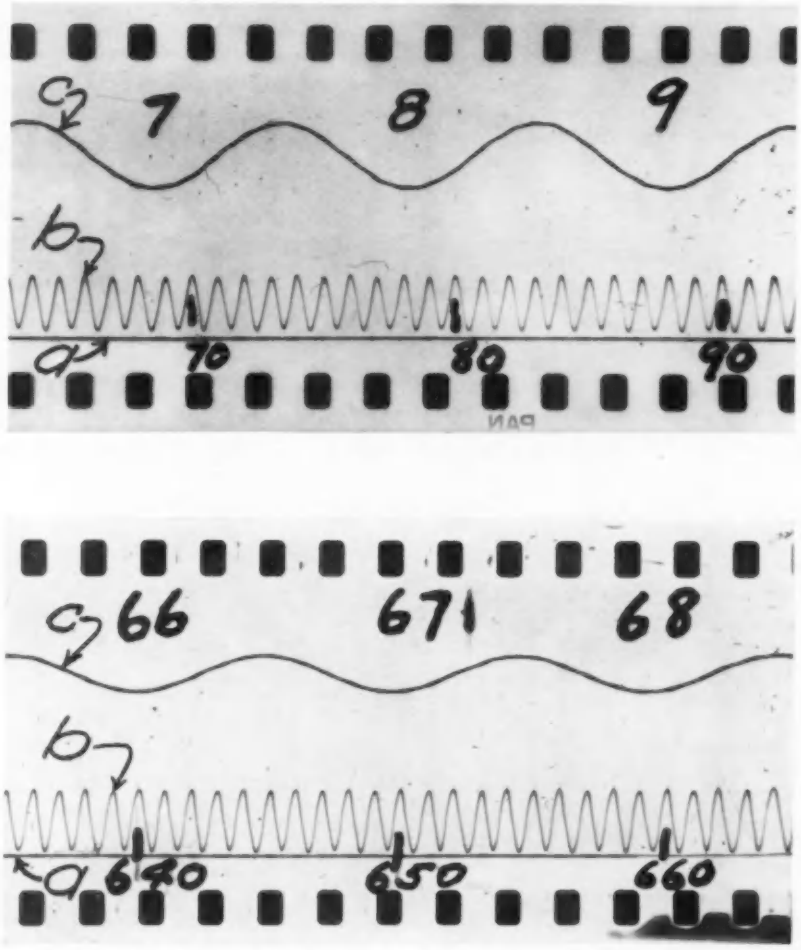

FIGURE 4.—*Reproductions from film exposed in the autographic autocollimator; (a) reference line, (b) time scale, (c) ru vibration as indicated by Tuckerman strain gage.*

loaded at opposite ends of a diameter is given approximately by the expression eq 4 where

$$d=APr^2/Elh^3, \tag{5}$$

d=deflection of the ring in the direction of the forces
A=a numerical constant
P=load on the ring
r=initial radius of curvature of the neutral surface
E=Youth's modulus of elasticity of the material of the ring
l=width of the cross section of the ring
h=thickness of the cross section of the ring.

The deflection of a proving ring is not exactly proportional to the load as indicated in equation 5. The calibration factor increases slightly with increasing tensile load as shown in figure 2. Usually the calibration factor for 10-percent capacity load differs from the calibration factor for capacity load by less than 3 percent.

As the calibration factor of a proving ring is, by definition, the ratio of the load to the deflection of the ring measured in dial divisions, the effect of changing temperature on the micrometer screw should be included in the expression for the calibration factor. Usually the micrometer screw is made of steel and has about the same coefficient of thermal expansion as the ring. If the axial travel of the micrometer screw per unit dial division is denoted by N, the calibration factor F may be written as

$$F=(PN/d). \tag{6}$$

After combining equations 5 and 6 the result may be expressed as

$$F=BEL^2, \tag{7}$$

in which

B=a numerical quantity, constant for a given ring
E=Young's modulus of elasticity, lb/in.^{2}
L=a quantity having the dimensions of length, in.

Differentiating equation 7 with respect to temperature and then dividing by equation 7,

$$\frac{1}{F}\frac{dF}{dt}=\frac{1}{E}\frac{dE}{dt}+\frac{2}{L}\frac{dL}{dt}. \tag{8}$$

Since the value of F changes by less than 1 percent over the temperature range in which proving rings are ordinarily used, it is permissible to write

$$\frac{1}{F}\frac{dF}{dt}=\frac{1}{F_c}\frac{dF}{dt}=k,$$

the temperature coefficient of the ring.
Since

$$\frac{1}{E}\frac{dE}{dt}=e,$$

the temperature coefficient of Young's modulus of elasticity

$$\frac{1}{L}\frac{dL}{dt}=\alpha,$$

the coefficient of linear thermal expansion.
Equation 8 may be written

$$k=e+2\alpha. \tag{9}$$

By means of equation 9 the temperature coefficient of a proving ring may be calculated from the temperature coefficient of Young's modulus of elasticity and the coefficient of thermal expansion.

3. Relationship Between Temperature Coefficient and Spring Constant for Proving Rings

The temperature coefficient of a proving ring may be computed from measurements at two temperatures of the natural frequency of the elastic system consisting of the ring and its load of dead

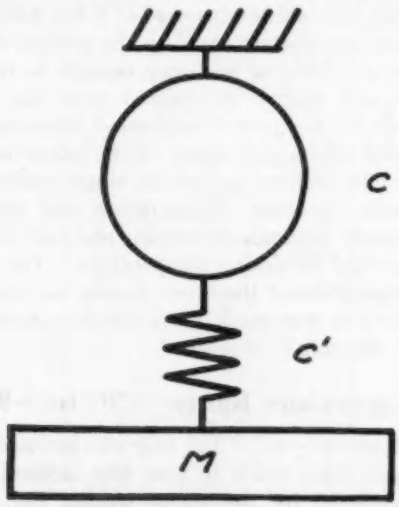

FIGURE 3.—*Elastic system used in the vibration tests.*

The load applied to the ring is represented by M, the spring constant of the ring by c, and the spring constant of the loading fixtures by c'.

weights shown in figure 3. The natural frequency of the system may be written [5]

$$f=\frac{1}{2\pi}\sqrt{\frac{cc'}{(c+c')m}}, \tag{10}$$

in which

f=natural frequency of the system
c=spring constant, load per unit deflection, for the proving ring
c'=spring constant for the loading fixtures
m=mass suspended from the ring.

From equation 10 the spring constant for the ring at any temperature, t, is

$$c_t=\frac{mc'(2\pi f)^2}{c'-m(2\pi f)^2}. \tag{11}$$

An expression for the temperature coefficient in terms of the spring constants of the ring may be derived from equation 4, which gives the relationship between the temperature coefficient and the deflections of the ring. It may be shown that

$$k=\frac{c_t-c_c}{c_c(t-t_c)}+\alpha, \tag{12}$$

in which

c_t=the spring constant of the ring for the temperature t degrees
c_c=the spring constant of the ring for the temperature t_c degrees
α=the coefficient of linear thermal expansion.

The last term in equation 12 is due to the change in pitch of the micrometer screw with temperature. By means of equation 12 the temperature coefficient of a proving ring may be calculated from the spring constants of the ring for two different temperatures and the thermal coefficient of linear expansion of the material of the ring.

IV. Experimental Procedure

1. Temperature Range 70° to 100° F

The tests were made in dead-weight testing machines [3], the loading frames of which are inclosed in a temperature controlled room. The air temperature of the room could be maintained near 70° or 100° F and held constant to within one-half degree Fahrenheit.

During the calibrations a steel block having a section approximately equal to the section of the ring being calibrated and long enough to reduce thermal end effects was placed near the ring. The bulb of a sensitive calibrated thermometer was sealed into a hole bored to the center of the block. The calibrations of the rings were made with both the block temperature and the air temperature maintained within one-half degree Fahrenheit of the desired temperature. The average temperature of the block during the interval of calibration was taken as the average temperature of the ring.

2. Temperature Range +70° to −93° F

For tests at −93° F the ring was inclosed in a wire-mesh cage, which in turn was inclosed in a box supported by the upper pulling rod. For the low-temperature tests the space between the wire-mesh cage and the box was packed with solid carbon dioxide. The box and cage were so designed that, although the ring was almost completely surrounded by solid carbon dioxide, sufficient clearance was provided for the ring to vibrate without damping effects produced by friction with the cage or the walls of the box. Vibration tests at 70° were made with the box in place.

The temperature of the ring was measured by means of five calibrated chromel P-alumel thermocouples in contact with the surface of the ring. It is believed that the errors of the temperature measurements did not exceed 1 degree Fahrenheit. During the low-temperature tests, the temperature of the ring differed from point to point due to conduction of heat along the pulling rods, but in no case did the temperature measured at any point differ from the average temperature by more than 5 percent of the total temperature range.

Vibration of the ring was produced by a single impact of a small hammer swung from a constant height about a fixed axis. The hammer swung freely, struck a rubber pad, and was caught on the first rebound. Therefore, the initial amplitude of the ring vibration was very nearly constant.

The natural frequency of the vibration of the 2,000-lb-capacity ring loaded to about 60-percent-capacity load was measured by means of a Tucker-

man strain gage attached to projections on the pulling rods of the ring. The images from the gage, a reference mirror, and a vibrating mirror controlled by the standard 60-cycle-frequency signal from the Bureau's Radio Section were photographed in an autographic autocollimator. The film was moved continuously by a synchronous motor at a speed of approximately 10 inches per second. The length of film exposed during each run was sufficient to photograph at least 60 complete wavelengths of the ring vibration. Typical records are shown in figure 4.

The frequency was determined from measurements of the number of time waves corresponding to a fixed number of wavelengths of the ring vibration. By projection, the number of time wavelengths was determined to within 0.1 time wavelength. In no case, it is believed, did the error in the measurement of the frequency exceed 0.02 percent.

The effect of damping on the frequency was calculated from measurements of the amplitudes on each film. In no case was the calculated error due to damping greater than 0.001 percent.

Under ordinary conditions of use sufficient time elapses after the application or removal of load to a proving ring to permit almost complete temperature equalization before readings are observed, and the action may, therefore, be considered isothermal [6]. During the vibration tests the frequency was about 12 cycles per second, and the action was nearly adiabatic. As the difference between temperature coefficients for steel rings determined under isothermal and adiabatic conditions can be shown to be less than 1 percent [7], no correction was considered necessary.

The spring constant of the loading fixtures (c', equation 10) was nearly independent of the temperature of the ring as the temperature of the air surrounding the rods and frame of the deadweight machine was constant. The constant c' was evaluated by substituting in equation 11 a value of c_t derived from the calibration graph of the ring for 70° F and the measured natural frequency of the system for a ring temperature of 70° F.

V. Results

1. Temperature Range 70° to 100°F

The temperature coefficients were determined for 14 proving rings for the range of temperatures from 70° to 100° F. In preliminary tests it was observed that the result obtained by computing the coefficient for the three highest of the 10, uniformly spaced test loads applied to the ring, e. g., 80, 90, and 100 percent of capacity, did not differ significantly from the result computed for 10 uniformly spaced test loads. Therefore, the temperature coefficients were determined for the three highest test loads. The temperature coefficient, k (equation 4) was computed for each ring by the method of least squares.

Typical average deflections for a 100,000-lb-capacity compression proving ring are as follows:

	Applied load—		
	80,000 lb	90,000 lb	100,000 lb
Deflection, for 101.6° F, divisions	484.21	545.33	606.67
Deflection, for 70.2° F, divisions	482.07	542.82	603.82
Difference, divisions	2.14	2.51	2.85

TABLE 1.—*Temperature coefficients for proving rings for the temperature range 70° to 100° F*

Capacity	Temperature coefficient, k	
	Compression per ° F	Tension per ° F
MOREHOUSE MACHINE CO. PROVING RINGS		
Pounds		
2,000	−0.000144	−0.000134
10,000	−.000148	.....
10,000	−.000143	.....
10,000	−.000152	.....
10,000	−.000146	.....
20,000	−.000155	−.000147
50,000	−.000155	.....
100,000	−.000160	−.000149
100,000	−.000146	.....
100,000	−.000150	.....
100,000	−.000158	.....
TINIUS OLSEN TESTING MACHINE CO. PROVING RINGS		
2,000	−0.000123	.....
20,000	−.000155	.....
100,000	−.000151	.....

Average value of the temperature coefficient for proving rings, $k = -0.000148$/° F

The temperature coefficient calculated from these data by the method of least squares is

$$k = -0.000146 \text{ per degree Fahrenheit}$$

Temperature coefficients for the 14 proving rings are given in table 1.

The temperature coefficients for proving rings varied from −0.000123 to −0.000160, the mean value being −0.000148 per degree Fahrenheit. This value corresponds to the value −0.000149 per degree Fahrenheit calculated by means of equation 9 from values for the coefficients of Young's modulus of elasticity and thermal expansion reported by Dadourian [8]. Keulegan and Houseman [9] reported results from which computed values were obtained ranging from −0.000132 to −0.000146 per degree Fahrenheit for steels of less than 5 percent total alloying content.

The temperature coefficient of one of the rings differed from the average value for all of the rings by 0.000025 per degree Fahrenheit. For this ring, correction by means of the average value for a temperature difference of 30° F, a considerably greater temperature difference than is ordinarily encountered, would result in an error of 0.075 percent. This is less than the tolerance (0.1 percent) for proving rings [2].

2. Temperature Range +70° to −93° F

Low-temperature measurements were made on the proving ring shown in figure 1. The calibration graph for this ring for a temperature of 70° F is shown in figure 2.

The temperature-correction coefficient was calculated from measurements of the natural frequency of vibration recorded on six films. The following results were obtained.

Temperature	Frequency	Spring constant of ring	Temperature coefficient per °F
°F	c/s	lb/in.	
69.4	12.391	23,050	−0.00023
−93.2	12.585	23,940	.....

The value −0.00023 obtained for the temperature range +70° to −93° F differs considerably from the average value of −0.00015 obtained for the temperature range 70° to 100° F. Benton [10] also reported a considerable increase in the temperature coefficient of Young's modulus at low temperatures. The greatest source of error in the low-temperature tests was the nonuniformity of the temperatures of different portions of the ring. Nevertheless, it is believed that the value reported is not in error by more than 1 part in 23.

As a check on the method used in the low-temperature tests, the temperature coefficient of a ring was measured by the same method over a temperature range of 70° to 178° F by means of heaters mounted in the box used for the low-temperature tests. A value $k = -0.000153$ per degree Fahrenheit was obtained, which agrees with values obtained in the dead-weight machines.

VI. Conclusions

The temperature coefficients of a group of 14 proving rings were measured for the temperature range 70° to 100° F and found to average −0.00015 per degree Fahrenheit. This value is in agreement with values calculated from the results of other observers for this temperature range.

The work of Keulegan and Houseman [9] has indicated that the temperature coefficient of Young's modulus changes very slowly in the range of temperatures ordinarily encountered in the operation of testing machines. It is believed, therefore, that for rings made of steel having a total alloying content not exceeding 5 percent, the temperature coefficient will not vary more than 10 percent from 30° to 120° F. An error of 10 percent in the temperature coefficient will introduce less than 0.05-percent error in the calculated ring load for a temperature difference of 30° F, a greater difference than is usually encountered.

The temperature coefficient of a proving ring was also measured for the temperature range +70° to −93° F and found to be −0.00023 per degree Fahrenheit.

The temperature coefficients of rings made of steels having a total alloying content exceeding 5 percent may be expected to differ significantly from the values reported.

VII. References

[1] Am. Soc. Testing Materials Standards 1944, part I, Metals, p. 954.

[2] B. L. Wilson, D. R. Tate, and G. Borkowski, Proving rings for calibrating testing machines, Circular NBS C454 (1946).

[3] B. L. Wilson, D. R. Tate, and G. Borkowski, Dead-weight machines of 111,000- and 10,100-pound capacities, Circular NBS C446 (1943).

[4] S. Timoshenko, Strength of materials, part II, ch. 2 (D. Van Nostrand Co., Inc., New York, N. Y. 1930).

[5] Den Hartog, Mechanical vibrations, second edition, p. 41–49 (McGraw-Hill Book Co., Inc., New York, N. Y., 1940).

[6] L. B. Tuckerman, discussion, Proc. Am. Soc. Testing Materials, part II, **32,** 594 (1932).

[7] J. H. Poynting and J. J. Thomson, A text-book of physics-heat, ninth edition, pp. 284–304 (Charles Griffin & Co. Ltd., London, 1928).

[8] H. M. Dadourian, Phys. Rev. [II], **XIII,** 337 (1919).

[9] G. H. Keulegan and M. R. Houseman, BS J. Research **10,** 289 (1933) RP531.

[10] J. R. Benton, Phys. Rev. **16,** 17 (1903).

Washington, April 16, 1946.

U. S. Department of Commerce
National Bureau of Standards

Research Paper RP1727
Volume 37, July 1946

Part of Journal of Research of the National Bureau of Standards

Mutarotation and Ring Structure of Mannuronic Lactone

By Horace S. Isbell and Harriet L. Frush

The numerous commercial applications of algin, a polysaccharide derived from certain marine plants, makes important the study of its principal constituent, D-mannuronic lactone. In this paper it is shown that by oxidation with bromine mannosaccharic dilactone of known structure is formed directly from mannuronic lactone without change in ring structure, and hence the latter substance, like mannosaccharic dilactone, has a bicyclic structure consisting of two butylene oxide rings. The initial rapid mutarotation reaction of the substance is shown to consist of a conversion of the beta furanose modification to an equilibrium mixture containing the alpha furanose, and a detectable amount of the aldehyde modification. There is a small but measurable displacement of equilibrium with change in temperature. The mutarotation is exceptionally sensitive to basic catalysts and for this reason the point of minimum rate lies in the acid region at pH 3.1.

I. Introduction

The uronic acids, although few in number, constitute an important group of naturally occurring carbohydrate derivatives whose chemistry has not been adequately developed. Of the 16 possible isomeric hexuronic acids, only 3 have been found in nature. D-Glucuronic acid occurs in animal tissues, and frequently plays an important role in detoxifying processes. D-Galacturonic acid occurs in nearly all land plants as the chief constituent of pectic substances. An isomeric substance, D-mannuronic acid, is the principal constituent of algin. This polysaccharide is derived from certain marine algae [1],[1] especially from *Macrocystis pyrifera*, the giant kelp of the Pacific coast, as well as from other species existing on the Atlantic coast and elsewhere. Crystalline man-

[1] Figures in brackets indicate the literature references at the end of this paper.

Contents

	Page
I. Introduction	43
II. Ring structure of mannuronic lactone	44
1. Stereomeric factors	44
2. Application of the bromine oxidation method	44
3. Bromine oxidation measurements	45
III. Mutarotation of mannuronic lactone	46
1. Changes in optical rotation	46
2. Initial rapid mutarotation	46
(a) Application of the first-order equation	47
(b) Catalysis by hydrogen and hydroxyl ions	47
(c) Influence of temperature on the reaction rates	48
(d) Influence of temperature on the equilibrium state	48
IV. Summary	49
V. References	49

nuronic lactone [2] and two crystalline modifications of D-mannuronic acid [3] have been prepared from alginic acid. The lactone of mannuronic acid exhibits a rapid mutarotation, indicating the establishment of an equilibrium between at least two modifications. It has been assumed that this crystalline substance has a bicyclic structure, consisting of a lactone ring and a sugar ring, but no attempt has been made to assign a definite structure to the sugar entity.

II. Ring Structure of Mannuronic Lactone

1. Stereomeric Factors

A careful inspection of the structural models for mannuronic lactone reveals that it can readily form a bicyclic structure having two six-membered rings or two five-membered rings. The stereomeric relationship of the groups, however, is such that a compound having both a five- and a six-membered ring is highly improbable and may be eliminated from consideration. Thus the aldose function of a mannuronic gamma lactone can exist only in the open-chain form or in the furanoid form, whereas the aldose function of a mannuronic delta lactone can exist only in the open-chain form or in the pyranoid form. Ordinarily, gamma lactones are much more stable to hydrolysis than delta lactones, but there are exceptions to this general rule. For instance, Haworth, Jackson, Owen, and Smith [4] have pointed out that the presence of an anhydro ring in a sugar structure may affect in marked degree the relative stability of the pyranose and furanose modifications. Likewise Smith [5] has found that the dilactone of glucosaccharic acid, presumably having the 1,4-3,6-bicyclic structure, is hydrolyzed rapidly by water, and has suggested that the sensitivity to hydrolysis is due in part to the strain caused by the interlocking rings. Inasmuch as mannuronic lactone is relatively stable to hydrolysis, it might be expected to have the gamma lactone structure, but obviously this structure cannot be assigned merely from the stability of the compound to hydrolysis.

2. Application of the Bromine Oxidation Method

In previous publications from this Bureau [6] it has been shown that the ring forms of the sugars are oxidized by bromine water directly to lactones without the intermediate formation of the free acids. It has been shown also [7] that the two pyranose modifications of galacturonic acid on bromine oxidation yield an optically active lactone of mucic acid, a fact which demonstrates that the pyranose ring remains intact during the oxidation.[2] Thus the bromine oxidation method is applicable to the study of the ring structure of the uronic acids.

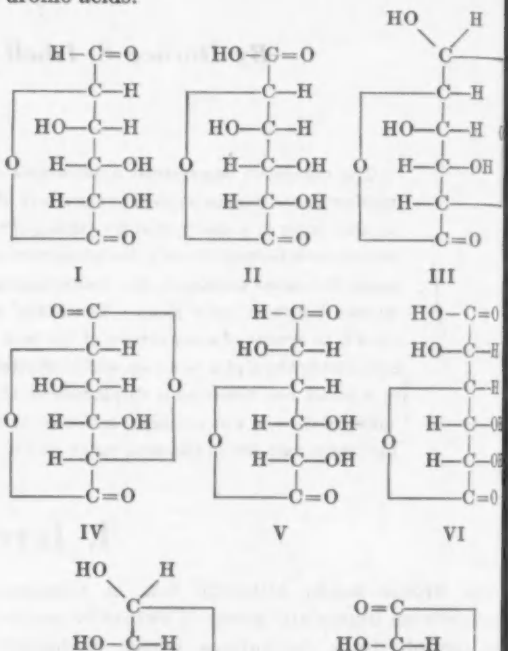

If mannuronic lactone had a delta lactone structure, oxidation of the aldehyde form I would yield the unknown delta monolactone of mannosaccharic acid II, and oxidation of the pyranose form III would yield the unknown delta dilactone

[2] If the pyranose ring were ruptured before oxidation, the two carboxyl groups of the mucic acid, a meso compound, would have equal opportunity to form a lactone, and a racemic mixture would result.

IV. If mannuronic lactone had a gamma lactone structure, the aldehyde form V would yield the unknown gamma monolactone of mannosaccharic acid VI, and the furanoid form VII would yield the known gamma dilactone VIII. The results described in this paper show that the oxidation product of mannuronic lactone is in fact the mannosaccharic gamma dilactone VIII, whose structure has been well established [8]. Hence mannuronic lactone has a furanoid structure for the sugar ring and the gamma structure for the lactone ring as represented in formula VII.

3. Bromine Oxidation Measurements

The formation of mannosaccharic dilactone from mannuronic lactone was studied by oxidation of the latter substance under conditions essentially the same as those previously used for the study of the ring structure of the sugars [9]. A 0.5-g sample of crystalline mannuronic lactone was added to a buffered solution prepared by the addition of 2 ml of bromine to an ice-cold mixture containing 2 g of barium carbonate in 25 ml of water saturated with carbon dioxide and contained in a glass-stoppered flask. The mixture was cooled in ice and kept in agitation by shaking. Time was measured beginning with the addition of the crystalline lactone to the bromine solution. After 5 minutes at 0° C a portion of the mixture was filtered. The temperature of the filtrate was raised to and kept at 20° C. From time to time the optical rotations were read in a 1-dm tube with a Bates saccharimeter. These values are reported in the second column of table 1.

TABLE 1.—*Comparison of the optical rotation of the product obtained by bromine oxidation of mannuronic lactone with the optical rotation of mannosaccharic dilactone under like conditions.*

Time	Solution obtained from—	
	Mannuronic lactone	Mannosaccharic dilactone
Minutes	°*S*	°*S*
8	+10.6	----------
15	+10.6	+10.9
45	+10.5	+10.6
180	+10.2	+10.4
1,320	+8.6	+8.8

To establish the identity of the oxidation product, the optical rotations were compared with those of an equivalent amount of mannosaccharic dilactone that had been treated in the same manner. The optical rotations, recorded in table 1, show that both solutions exhibit mutarotation, and that the values are in substantial agreement at all times. The mutarotation is undoubtedly caused by hydrolysis of the dilactone. As delta and gamma lactones differ markedly in sensitivity to hydrolysis, the agreement of the two solutions in respect to this property precludes the possibility of a delta lactone structure, and shows that the oxidation product of mannuronic lactone is indeed the known mannosaccharic dilactone having the gamma lactone structure.

The initial rotations of both solutions correspond to specific rotations somewhat lower than the recorded specific rotation of mannosaccharic dilactone. The difference presumably arises from the fact that a small part of the oxidation product and of the dilactone was converted to the barium salt.

The direction of the change in optical rotation is particularly significant. Rehorst [10] found that the specific rotation of a solution of mannosaccharic dilactone decreases from +203.1° in 47 minutes to +69.5° in 24 days, whereas that of a solution of mannosaccharic acid increases from +3.6° in 3 minutes to +48.7° in 27 days. The latter values expressed on the weight of the dilactone are +4.3° and +58.8°. Thus the specific rotation of the equilibrium mixture lies between +69.5° and +58.8°. The decrease in optical rotation of the solution from mannuronic lactone shows that mannosaccharic dilactone is present immediately after oxidation *in excess of the equilibrium proportion*, and must have been formed without the intermediate production of the free acid. It follows that there was no alteration in ring structure during oxidation and that mannuronic lactone has a bicyclic structure like that of mannosaccharic dilactone.

To confirm the conclusion that mannosaccharic dilactone is formed by bromine oxidation of mannuronic lactone without the intermediate formation of free mannosaccharic acid, 5 g of mannuronic lactone was oxidized under the conditions described above, and the product was isolated. The oxidation was stopped after 5 minutes by removal of the bromine with a mixture of 1 part of linseed oil and 2 parts of benzene. The solution was filtered, and an aliquot corresponding to four-fifths of the material was concentrated in vacuum at a temperature of 40° C to a semisolid crystalline massecuite, which was then extracted

with a total of 200 ml of acetone. The extract was filtered and evaporated in a stream of dry air. The residue, 2.32 g, corresponding to a 59-percent yield, crystallized in slender needles. After one crystallization from ethyl alcohol, $[\alpha]_D^{20}=+200.0°$ (15 minutes. Water, c=1.5). For a sample of pure mannosaccharic dilactone prepared in this laboratory, $[\alpha]_D^{20}=+201.1°$ (15 minutes. Water, c=1.5).

Inasmuch as the oxidation was conducted in the presence of barium carbonate, a basic substance, and the product was extracted with acetone without previous acidification, the formation of the free mannosaccharic acid could not have been an intermediate step in obtaining the dilactone as described above.

III. Mutarotation of Mannuronic Lactone

1. Changes in Optical Rotation

Nelson and Cretcher [2], who first prepared mannuronic lactone, reported a mutarotation from +79.9° at 3 minutes to a maximum of +93.8° in 28 minutes, followed by a slow decrease over a period of days. After 864 hours the solution had a specific rotation of +61.8° and contained 39.1 percent of acid and 60.9 percent of lactone. The authors state that "the rapid initial increase is probably due to attainment of equilibrium between the α and β forms of the aldehyde, and the subsequent decrease is due to the formation of mannuronic acid." Subsequently, Ault, Haworth, and Hirst [11] reported an optical rotation of +95°, with no mutarotation, whereas Stacey and Wilson [12] reported a value of +50°, increasing to +94° in 30 minutes. The measurements obtained in the present investigation (table 2) show an initial rotation of +57.7° and a rapid increase to a maximum of 92.2° in about half an hour. As noted by Nelson and Cretcher, the subsequent decrease in optical rotation is caused by cleavage of the lactone rather than by a change in the sugar function and consequently it will not be discussed in this paper.

TABLE 2.—*Mutarotation of mannuronic lactone in water at 20° C*

4 g per 100 ml, read in a 2-dm tube.
$^\circ S=-7.86\times10^{-0.1284}+21.02.^\circ$
$[\alpha]_D^{20}=-34.5\times10^{-0.1284}+92.2.$
$[\alpha]_D^{20}=+57.7$ (initial), +92.2 (maximum).

Time	Observed reading	m	Time	Observed reading	m
Minutes	° *S*		*Minutes*	° *S*	
0	----------	-----	4.4	18.83	0.126
0	14.78	-----	5.1	19.21	.125
1.2	15.45	0.123	6.0	19.60	.124
1.7	16.25	.130	7.1	19.97	.123
2.0	16.55	.121	8.5	20.27	.120
2.2	16.90	.129	9.7	20.53	.124
2.5	17.25	.129	60.0	21.02 (maximum)	-----
Average					0.125

° This equation is converted to a specific-rotation basis by multiplying by the ratio of the maximum specific rotation (measured on a separate sample) to the observed maximum rotation in sugar degrees. The method for deriving the equation and calculating the initial rotation is given on page 156 of reference [9].

2. Initial Rapid Mutarotation

As mannuronic lactone has a bicyclic structure with a furanose ring and a gamma lactone ring, the initial rapid mutarotation might involve the alpha and beta furanose modifications and the open-chain modification of the sugar function or hydrolysis of the lactone ring. However, it has been shown [2] that the slow mutarotation is due to the hydrolysis of the lactone ring, and hence the rapid mutarotation must be associated with changes in the sugar function. When the material is treated with Schiff's aldehyde reagent, a pink color gradually develops. The intensity of the color is greater than that obtained with galacturonic acid or with mannose. However, as the color does not appear immediately, but only after an interval of at least 5 minutes, it may be assumed that the crystalline material is not the aldehyde, but that some of the aldehyde is formed by the mutarotation reaction. The aldehyde modification of mannuronic lactone differs from mannonic gamma lactone only in that it contains a CHO group in place of the terminal CH_2OH group, and consequently it may be assumed that the specific rotation of the aldehyde form does not differ widely from the specific rotation of mannonic gamma lactone (+51). During the mutarotation, the specific rotation increases from +58 to +92. This requires the formation of a substance having an optical rotation of at least +92, a value considerably larger than that anticipated for the aldehyde. Undoubtedly, the substance is the

alpha furanose modification. Thus the reaction involves establishment of equilibrium between the alpha and beta furanose modifications and the aldehyde. As already pointed out, the presence of a gamma lactone ring precludes the existence of mannuronic lactone in the pyranoid form. As an equilibrium solution of mannose does not contain an appreciable quantity of the aldehyde form, the presence of the aldehyde in the equilibrium solution of mannuronic lactone shows that the lactone ring enhances the tendency of the sugar to exist in the aldehyde form.

(a) Application of the first-order equation

As shown by the values given in table 2, the rapid mutarotation follows the usual first-order equation:

$$m=\frac{1}{t}\log\frac{r_o-r_\infty}{r_t-r_\infty},$$

in which r_t is the rotation at time t, $r\infty$ is the maximum rotation, r_0 is the rotation at the beginning of the time period t, and m is the mutarotation constant. The observed value for the mutarotation constant of mannuronic lactone at 20° C (0.125) is much higher than the constant (0.0148) for the interconversion of the pyranose modifications of galacturonic acid [7], but it does not differ widely from that (0.16) found for the rapid mutarotation reaction of galacturonic acid hydrate, which was ascribed to a pyranose-furanose interconversion.

(b) Catalysis by hydrogen and hydroxyl ions

It has been established [13] that the mutarotation constants for sugars in solutions of varying acidity may be represented by an equation of the type:

$$m=A+B[\mathrm{H}]+C[\mathrm{OH}],$$

in which A represents the catalytic effect of the solvent, $B[\mathrm{H}]$ the catalytic effect of the hydrogen ion, and $C[\mathrm{OH}]$ the catalytic effect of the hydroxyl ion. Some values obtained for the mutarotation constant of mannuronic lactone at various acidities are given in table 3. The following equation, which represents the effect of hydrogen and hydroxyl ions on the mutarotation constant of mannuronic lactone at 1.2° C, was calculated from three simultaneous equations, using the values at pH 1.0, 3.0, and 4.9:

$$m=0.0057+0.59[\mathrm{H}]+260{,}000{,}000[\mathrm{OH}].$$

TABLE 3.—*Mutarotation constants for mannuronic lactone at 1.2°C in aqueous solutions of various acidities*

Solution	Mutarotation constant	pH (measured)
0.1 *N* HCl	0.065	1.0
0.01 *N* HCl	.0115	2.0
0.001 *N* HCl	.0066	3.0
Water	.0106	4.0
Nitrophenol buffer[a]	.0318	4.9

[a] This buffer solution consisted of 1 part of o-nitrophenol solution saturated at 20°C and 1 part of water. Sodium hydroxide was added to the extent of 0.0004 equivalent per liter.

The constant passes through a minimum (0.0066) at a hydrogen concentration of 7.4×10^{-4} (pH 3.13), at which point the catalytic effect of the solvent is approximately six times the combined catalytic effect of the hydrogen and hydroxyl ions. The mutarotation constants at 20° C for levulose and glucose are reported to show minima at pH 4.4 and 4.6, respectively [14]. It is of interest to compare the relative sensitivities of the mutarotations of mannuronic lactone, levulose, and glucose to the catalytic effect of hydrogen and hydroxyl ions. The data for mannuronic lactone is not directly comparable with that previously reported for levulose and glucose. A qualitative comparison can be made, however, by taking the minimum value of the constant for each substance as unity. This eliminates the catalytic effect of the solvent, the effect of the difference in temperature under which the measurements were made, and the large difference in minimum rates. A comparison of this character is shown in figure 1.

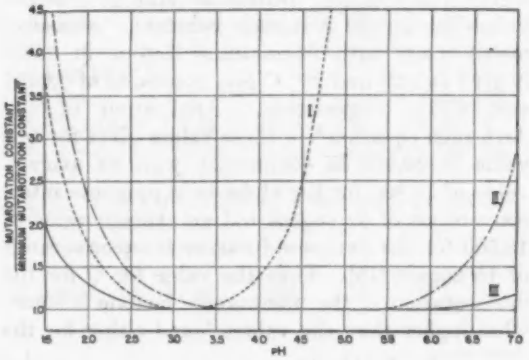

FIGURE 1.—*Variation of the mutarotation constants with acidity.*

I. Mannuronic lactone, an α-β-furanose interconversion.
II. Levulose, a pyranose-furanose interconversion. Data from reference [14].
III. Glucose, an α-β-pyranose interconversion. Data from reference [14]

The mutarotation of mannuronic lactone, an alpha-beta furanose interconversion, is more sensitive to the catalytic action of hydrogen ion than the mutarotation of glucose, an alpha-beta pyranose interconversion, and less sensitive than that of levulose, a pyranose-furanose interconversion. With respect to the hydroxyl ion, the mutarotation of mannuronic lactone is far more sensitive than the mutarotations of either glucose or levulose. In fact, the catalytic effect of the hydroxyl ion is so strong that at pH 7 the mutarotation is too rapid to be detected even at 1.2° C. The high sensitivity to the hydroxyl ion may be a characteristic property of alpha-beta furanose interconversions, but as the substance has a bicyclic structure, its mutarotation may not be typical of alpha-beta furanose interconversions in general. The long horizontal section of the glucose curve indicates that in the pH range from 2 to 7 the predominating rate-determining factor is the catalytic effect of the water, and that the specific catalytic effect of the hydrogen and hydroxyl ions is relatively small. The almost complete absence of a horizontal section in the curve for mannuronic lactone indicates that at all acidities the hydrogen and hydroxyl ions influence the reaction rate substantially.

(c) Influence of temperature on the reaction rates

Another point of distinction between reactions of the alpha-beta pyranose type and reactions of the pyranose-furanose type is that the former have higher temperature coefficients and give larger values for Q, the Arrhenius constant. Measurements made with mannuronic lactone in 0.001 N HCl at 1.2° and 20° C give constants of 0.0066 and 0.075, respectively. Application of the Arrhenius equation [3] to these values gives for Q a value of 20,600 in comparison with an average value of 16,800 for the alpha-beta pyranose interconversions of 32 sugars and an average value of 13,500 for the pyranose-furanose interconversions of 15 sugars [15]. Thus the value for Q for the mutarotation of the mannuronic lactone is somewhat higher than the values found either for the alpha-beta pyranose interconversions or for the pyranose-furanose interconversions of the sugars.

[3] $2.3026 \log \frac{k_2}{k_1} = \frac{Q}{1.9864}\left(\frac{1}{T_1} - \frac{1}{T_2}\right)$.

(d) Influence of temperature on the equilibrium rates

Reactions of the pyranose-furanose type also differ from those of the alpha-beta pyranose type in that they usually involve larger energy changes. If the energy change is small, as in the interconversion of the alpha and beta glucopyranoses, there is little displacement of the equilibrium with change in temperature. But if the energy change is high, as in the case of the pyranose-furanose interconversion of fructose, there is a considerable displacement of equilibrium with change of temperature. As shown by the data of table 4, when the temperature of a solution of mannuronic lactone of maximum rotation is suddenly lowered there is a small but measureable mutarotation that takes place at a rate substantially the same as that for a solution freshly prepared from crystalline mannuronic lactone. The optical rotation decreases, and hence the displacement of equilibrium on cooling is in favor of a less dextrorotatory substance, presumably the beta furanose or the aldehyde modification. As the change in the equilibrium with change in temperature appears to be small, it seems probable that the heat of reaction is also small.

TABLE 4.—*Thermal mutarotation of a solution of mannuronic lactone in 0.001 N HCl after cooling from 20° to 1.0° C*

[10 g of mannuronic lactone per 100 ml of solution read in a 2-dm tube]

Time after cooling	Observed reading	Mutarotation constant *
Minutes	° *S*	*m*
4.3	50.28	
8.5	50.20	0.010
15.0	50.06	.012
24.7	49.96	.010
43.4	49.81	.009
59.5	49.73	.008
103.6	49.58	.007
Constant	49.41	

* As the values given in this column are based on small changes in optical rotation, the experimental error is large, and the agreement with the mutarotation constant of the lactone in 0.001 N HCl, 0.0066, is as close as could be expected.

IV. Summary

Oxidation of mannuronic lactone with bromine water under conditions that preclude rupture of the sugar ring gives the dilactone of mannosaccharic acid that is known to have a 1,4-3,6-bicyclic structure. The production of this substance shows that mannuronic lactone is a bicyclic compound containing a 1,4-furanose ring and a 3,6-lactone ring.

The mutarotation of mannuronic lactone is characterized by two reactions, a rapid conversion of the beta furanose modification to a mixture containing the alpha furanose, and the aldehyde modification, and a slow hydrolysis of the lactone ring. The mutarotation of the sugar component in water at 20° C and at pH 4.0 follows the equation:

$$[\alpha]_D^{20} = -34.5 \times 10^{-0.125t} + 92.2.$$

$[\alpha]_D^{20} = +57.7°$ initially, and $+92.2°$ after 30 minutes (maximum). The rate of mutarotation is considerably higher than that found previously for the alpha-beta pyranose interconversion of galacturonic acid, but it does not differ widely from the rate attributed to the pyranose-furanose interconversion of this substance. The mutarotation rate does not change markedly in the range from pH 2 to pH 4, but in more strongly acid or alkaline solution, the rate rises sharply. The catalytic influence of the hydrogen and hydroxyl ions on the mutarotation constant at 1.2° C may be represented by the equation:

$$m = 0.0057 + 0.59[\mathrm{H}] + 260{,}000{,}000[\mathrm{OH}].$$

The marked sensitivity of the substance to the catalytic effect of hydroxyl ions causes the point of minimum rate of mutarotation to lie far in the acid range (pH 3.1). Mutarotation measurements at 1.2° C and 20° C in 0.001 *N* HCl give constants of 0.0066 and 0.075, respectively, corresponding to a heat of activation of 20,600 calories. There is a small but measurable thermal mutarotation when the temperature of a solution of mannuronic lactone of maximum rotation is suddenly lowered. The rate of this mutarotation is substantially the same as that of a solution freshly prepared from crystalline mannuronic lactone. The direction of the change indicates the production of either the beta furanose or the aldehyde modification.

V. References

[1] A. G. Norman, The biochemistry of cellulose, the polyuronides, lignin, etc., pp. 142–146 (Oxford University Press, 1937).

[2a] W. L. Nelson and L. H. Cretcher, J. Am. Chem. Soc. **54,** 3409 (1932).

[2b] E. Schoeffel and K. P. Link, J. Biol. Chem. **95,** 213 (1932).

[3] E. Schoeffel and K. P. Link, J. Biol. Chem. **100,** 397 (1933).

[4] W. N. Haworth, J. Jackson, and F. Smith, J. Chem. Soc. **1940,** 620; W. N. Haworth, L. N. Owen, and F. Smith, J. Chem. Soc. **1941,** 88.

[5] F. Smith, J. Chem. Soc. **1944,** 633.

[6] H. S. Isbell and C. S. Hudson, BS J. Research **8,** 327 (1932) RP418; H. S. Isbell, BS J. Research **8,** 615 (1932) RP441.

[7] H. S. Isbell and H. L. Frush, J. Research NBS **31,** 33 (1943) RP1549.

[8] O. Th. Schmidt and T. H. Kraft, Ber. deut. chem. Ges. **74,** 33 (1941); D. Heslop and F. Smith, J. Chem. Soc. **1944,** 574.

[9] H. S. Isbell and W. W. Pigman, J. Research NBS **18,** 141 (1937) RP969.

[10] K. Rehorst, Ber. deut. chem. Ges. **65,** 1476 (1932).

[11] R. G. Ault, W. N. Haworth, and E. L. Hirst, J. Chem. Soc. **1935,** 517.

[12] M. Stacey and P. I. Wilson, J. Chem. Soc. **1944,** 588.

[13] C. S. Hudson, J. Am. Chem. Soc. **29,** 1572 (1907).

[14] H. S. Isbell and W. W. Pigman, J. Research NBS **20,** 773 (1938) RP1104.

[15] F. J. Bates and associates, Polarimetry, saccharimetry, and the sugars, Circular National Bureau of Standards C440 (1942).

WASHINGTON, May 1, 1946.

U. S. Department of Commerce
National Bureau of Standards

Research Paper RP1728
Volume 37, July 1946

Part of Journal of Research of the National Bureau of Standards

Heats of Formation and Combustion of the Normal Alkylcyclopentanes and Cyclohexanes and the Increment per CH_2 Group for Several Homologous Series of Hydrocarbons[1]

By Edward J. Prosen, Walter H. Johnson, and Frederick D. Rossini

Values are presented for the heats of formation and combustion at 25° C for the normal alkylcyclopentanes and the normal alkylcyclohexanes, in the liquid state through normal butyl and in the gaseous state through normal hexadecyl, with equations to yield values for all the higher members of both series in the gaseous state.

The increment per CH_2 group is compared for the lower members of several normal alkyl homologous series, including paraffins, monoolefins (1-alkene), alkylbenzenes, alkylcyclopentanes, alkylcyclohexanes, and alkyl acetylenes (1-alkyne).

I. Introduction

A value was recently presented for the increment in energy content per CH_2 group for the members of the normal paraffin hydrocarbons above pentane [1].[2] This new value of the increment per CH_2 group, which was based on many new data on the heats of combustion and vaporization of the normal paraffin hydrocarbons [2, 3, 4, 5, 6], replaced the previous and less precise one presented in 1934 [7]. With the new value for the increment per CH_2 group, values have been calculated for the heats of formation and combustion of the higher normal monoolefins (1-alkene) [8] and the higher normal alkylbenzenes [9].

In the present paper, values are presented for the heats of formation and combustion of the normal alkylcyclopentanes and normal alkylcyclohexanes, and a comparison is made of the increment per CH_2 group for the lower members of several normal alkyl homologous series, including paraffins, monoolefins (1-alkenes), alkylbenzenes, alkylcyclopentanes, alkylcyclohexanes, and alkyl acetylenes (1-alkyne).

[1] This investigation was performed at the National Bureau of Standards jointly by the Thermochemical Laboratory and the American Petroleum Institute Research Project 44 on the "Collection, Analysis, and Calculation of Data on the Properties of Hydrocarbons."

[2] Figures in brackets indicate the literature references at the end of this paper.

Contents

	Page
I. Introduction	51
II. Heats of formation and combustion of the normal alkylcyclopentanes and cyclohexanes	52
III. Increment per CH_2 group for several homologous series of hydrocarbons	54
IV. References	56

II. Heats of Formation and Combustion of the Normal Alkylcyclopentanes and Cyclohexanes

In table 1, values are given for the heats of combustion and formation at 25° C of the normal alkylcyclopentanes, in the liquid state through normal butyl and in the gaseous state through normal hexadecyl.

TABLE 1.—*Values for the heats of combustion and formation of the alkylcyclopentanes*

Compound	Formula	Heat of combustion[a] at 25° C, $-\Delta Hc°$		Heat of formation[b] at 25° C, $\Delta Hf°$	
		Liquid	Gas	Liquid	Gas
		kcal/mole	*kcal/mole*	*kcal/mole*	*kcal/mole*
Cyclopentane	C_5H_{10}	786.54 ±0.17	793.39 ±0.17	−25.31 ±0.18	−18.46 ±0.18
Methylcyclopentane	C_6H_{12}	941.14 ±0.18	948.72 ±0.18	−33.08 ±0.20	−25.50 ±0.20
Ethylcyclopentane	C_7H_{14}	1097.50 ±0.22	1106.21 ±0.23	−39.08 ±0.24	−30.37 ±0.25
n-Propylcyclopentane	C_8H_{16}	1253.74 ±0.28	1263.56 ±0.28	−45.21 ±0.30	−35.39 ±0.30
n-Butylcyclopentane	C_9H_{18}	1410.10 ±0.34	1421.10 ±0.33	−51.22 ±0.37	−40.22 ±0.36
n-Amylcyclopentane	$C_{10}H_{20}$		1578.54 ±0.34		−45.15 ±0.37
n-Hexylcyclopentane	$C_{11}H_{22}$		1735.99 ±0.36		−50.07 ±0.39
n-Heptylcyclopentane	$C_{12}H_{24}$		1893.43 ±0.39		−55.00 ±0.42
n-Octylcyclopentane	$C_{13}H_{26}$		2050.87 ±0.42		−59.92 ±0.46
n-Nonylcyclopentane	$C_{14}H_{28}$		2208.32 ±0.46		−64.85 ±0.50
n-Decylcyclopentane	$C_{15}H_{30}$		2365.76 ±0.50		−69.78 ±0.55
n-Undecylcyclopentane	$C_{16}H_{32}$		2523.20 ±0.55		−74.70 ±0.59
n-Dodecylcyclopentane	$C_{17}H_{34}$		2680.65 ±0.60		−79.63 ±0.64
n-Tridecylcyclopentane	$C_{18}H_{36}$		2838.09 ±0.64		−84.55 ±0.70
n-Tetradecylcyclopentane	$C_{19}H_{38}$		2995.53 ±0.70		−89.48 ±0.75
n-Pentadecylcyclopentane	$C_{20}H_{40}$		3152.97 ±0.75		−94.41 ±0.80
n-Hexadecylcyclopentane	$C_{21}H_{42}$		3310.42 ±0.80		−99.33 ±0.86
Δ per CH_2	CH_2		157.443		−4.926

[a] $-\Delta Hc°_{298.16}$ represents the heat evolved in the combustion of the given hydrocarbon, in gaseous oxygen to form gaseous carbon dioxide and liquid water, at 25° C and constant pressure, with all reactants and products in their appropriate standard reference states.

[b] $\Delta Hf°_{298.16}$ represents the increment in the heat content or enthalpy of the process of forming the given hydrocarbon in the state indicated, from its elements at 25° C, with all reactants and products in their appropriate standard reference states.

Values of the heats of combustion in the gaseous state at 25° C for the normal alkylcyclopentanes from normal butyl to normal hexadecyl (given in table 1), and for all the higher members, are given by the equations:

$$C_nH_{2n}(\text{gas, normal alkylcyclopentane}) + (3n/2)O_2(\text{gas}) = nCO_2(\text{gas}) + nH_2O(\text{liquid}); \quad (1a)$$

$$-\Delta Hc°_{298.16} = 4.114 + 157.443n \pm (0.3605 - 0.05864n + 0.003428n^2)^{1/2} \text{ kcal/mole}; \; n > 8. \quad (1b)$$

Similarly, values of the heats of formation in the gaseous state at 25° C for all the normal alkylcyclopentanes above normal propyl are given by the equations:

$$n\text{C(solid, graphite)} + nH_2(\text{gas}) = C_nH_{2n}(\text{gas, normal alkylcyclopentane}); \quad (2a)$$

$$\Delta Hf°_{298.16} = 4.114 - 4.926n \pm (0.3605 - 0.05864n + 0.003637n^2)^{1/2} \text{ kcal/mole}; \; n > 8. \quad (2b)$$

In table 2, values are given for the heats of combustion and formation at 25° C of the normal alkylcyclohexanes, in the liquid state through normal butyl and in the gaseous state through normal hexadecyl.

Values of the heats of combustion in the gaseous state at 25° C for all the normal alkylcyclohexanes above normal propyl are given by the equations:

$$C_nH_{2n}(\text{gas, normal alkylcyclohexane}) + (3n/2)O_2(\text{gas}) = nCO_2(\text{gas}) + nH_2O(\text{liquid}) \quad (3a)$$

$$-\Delta Hc°_{298.16} = -1.690 + 157.443n \pm (0.4216 - 0.06358n + 0.003428n^2)^{1/2} \text{ kcal/mole}; \; n > 9 \quad (3b)$$

Similarly, values of the heats of formation in the gaseous state at 25° C for all the normal alkylcyclohexanes above normal propyl are given by the equations:

TABLE 2.—*Values for the heats of combustion and formation of the alkylcyclohexanes*

Compound	Formula	Heat of combustion[a] at 25° C, $-\Delta Hc°$		Heat of formation[b] at 25° C, $\Delta Hf°$	
		Liquid	Gas	Liquid	Gas
		kcal/mole	*kcal/mole*	*kcal/mole*	*kcal/mole*
Cyclohexane	C_6H_{12}	936.88 ±0.17	944.79 ±0.17	−37.34 ±0.19	−29.43 ±0.19
Methylcyclohexane	C_7H_{14}	1091.13 ±0.23	1099.59 ±0.23	−45.45 ±0.25	−36.99 ±0.25
Ethylcyclohexane	C_8H_{16}	1248.23 ±0.35	1257.90 ±0.35	−50.72 ±0.37	−41.05 ±0.37
n-Propylcyclohexane	C_9H_{18}	1404.34 ±0.27	1415.12 ±0.27	−56.98 ±0.30	−46.20 ±0.30
n-Butylcyclohexane	$C_{10}H_{20}$	1560.78 ±0.29	1572.74 ±0.30	−62.91 ±0.32	−50.95 ±0.33
n-Amylcyclohexane	$C_{11}H_{22}$		1730.18 ±0.37		−55.88 ±0.40
n-Hexylcyclohexane	$C_{12}H_{24}$		1887.63 ±0.39		−60.80 ±0.43
n-Heptylcyclohexane	$C_{13}H_{26}$		2045.07 ±0.42		−65.73 ±0.46
n-Octylcyclohexane	$C_{14}H_{28}$		2202.51 ±0.45		−70.65 ±0.49
n-Nonylcyclohexane	$C_{15}H_{30}$		2359.96 ±0.49		−75.58 ±0.54
n-Decylcyclohexane	$C_{16}H_{32}$		2517.40 ±0.53		−80.51 ±0.58
n-Undecylcyclohexane	$C_{17}H_{34}$		2674.84 ±0.58		−85.43 ±0.63
n-Dodecylcyclohexane	$C_{18}H_{36}$		2832.28 ±0.62		−90.36 ±0.68
n-Tridecylcyclohexane	$C_{19}H_{38}$		2989.73 ±0.67		−95.28 ±0.73
n-Tetradecylcyclohexane	$C_{20}H_{40}$		3147.17 ±0.72		−100.21 ±0.78
n-Pentadecylcyclohexane	$C_{21}H_{42}$		3304.61 ±0.77		−105.14 ±0.83
n-Hexadecylcyclohexane	$C_{22}H_{44}$		3462.06 ±0.83		−110.06 ±0.88
Δ per CH_2	CH_2		157.443		−4.926

[a] $-\Delta Hc°_{298.16}$ represents the heat evolved in the combustion of the given hydrocarbon, in gaseous oxygen to form gaseous carbon dioxide and liquid water, at 25° C and constant pressure, with all reactants and products in their appropriate standard reference states.
[b] $-\Delta Hf°_{298.16}$ represents the increment in the heat content or enthalpy of the process of forming the given hydrocarbon in the state indicated, from its elements, at 25° C, with all reactants and products in their appropriate standard reference states.

$$n\text{C(solid, graphite)}+n\text{H}_2\text{(gas)}=\text{C}_n\text{H}_{2n}\text{(gas, normal alkylcyclohexane)}; \quad (4a)$$

$$\Delta Hf_{298.16}=-1.690-4.926n\pm(0.4216-0.06358n+0.003637n^2)^{1/2}\ \text{kcal/mole};\ n>9. \quad (4b)$$

In the foregoing equations, n is the total number of carbon atoms per molecule.

The values of heats of formation and heats of combustion given in tables 1 and 2 and by equations 1, 2, 3, and 4 were derived from the following data:

Heats of combustion in the liquid state at 25° C of the first four members of the series of normal aklylcyclopentanes and the first five members of the series of normal alkylcyclohexanes [10].

Heats of vaporization of the first five members of each of the seris of normal alkylcyclopentanes and normal alkylcyclohexanes [4, 5].

Increment per CH_2 group for the gaseous normal paraffin hydrocarbons above pentane [1].

Comparison of previous experimental data with the selected "best" values from this report is shown in table 3, in which the values from earlier investigations have been converted, insofar as significant, to the present unit of energy and atomic weights.

TABLE 3.—*Comparison of previous experimental data with the values of this report for the heats of combustion of the alkylcyclopentanes and alkylcyclohexanes*

Compound	Investigators	Year	Reference	Heat of combustion	
				Difference from value of this report	Estimated uncertainty of the difference
				kcal/mole[a]	*kcal/mole*[b]
Cyclopentane (liquid).	Huffman	1943	[17]	+0.12	±0.33
Methyl cyclopentane (liquid).	Zubow	1898	[13]	−2.62	±.94
	Moore, Renquist, and Parks.	1940	[14]	−0.46	±.44
Ethyl cyclopentane (liquid).	Moore, Renquist, and Parks.	1940	[14]	−.65	±.43
Cyclohexane (liquid)	Zubow	1898	[13]	−.07	±.94
	Richards and Barry.	1915	[15]	+3.76	±1.89
	Roth and Von Auwers.	1915	[16]	+1.77	±1.89
	Moore, Renquist, and Parks.	1940	[14]	−0.16	±0.35
	Huffman	1943	[17]	−.26	±.32
Methylcyclohexane (liquid).	Zubow	1898	[13]	+1.31	±1.09
	Moore, Renquist, and Parks.	1940	[14]	−0.33	±0.51

[a] Insofar as significant, the previous value was converted to the present unit of energy and atomic weight. A negative sign in this column indicates that the earlier value is less than that of the present report; a positive sign, higher.
[b] The uncertainties have been assigned by the present authors where estimates of the uncertainties were not given by the previous authors.

III. Increment per CH_2 Group for Several Homologous Series of Hydrocarbons

Figure 1 gives a plot of the deviations from linearity with number of carbon atoms in the normal alkyl radical of the values of the heats of formation of several homologous series of hydrocarbons, expressed as the value of δ in the following relation:

$$\Delta Hf^{\circ}_{298.16}\,[\text{gas, Y}-(CH_2)_m-\text{H}] = A'+Bm+\delta \text{ kcal/mole.} \qquad (5)$$

Here $(CH_2)_m-H$ is a normal alkyl radical (methyl, ethyl, normal propyl, normal butyl, etc.) attached to any end group Y (methyl, vinyl, phenyl, cyclopentyl, cyclohexyl); A' is a constant peculiar to the end group, Y; B is a constant for all normal alkyl series, independent of Y; and δ is a term which has a small finite value for the lower members, being largest for $m=0$, and becomes zero for the higher members, beginning near $m=4$.

The new data yield more accurate values of the deviations for the paraffin and monoolefin series than those previously reported [7, 11], and give, for the first time, values of the deviations for the alkylbenzenes, alkylcyclopentanes, and alkylcyclohexanes. The new data also disclose for the first time a small, but significant, alternation in magnitude of the deviations with even or odd numbers of carbon atoms in normal alkyl radical. This effect is particularly noticeable in going from $m=1$ through $m=2$ to $m=3$. Although the uncertainties are relatively large, this alternation is believed to be definitely established because each of the five series exhibits the effect.

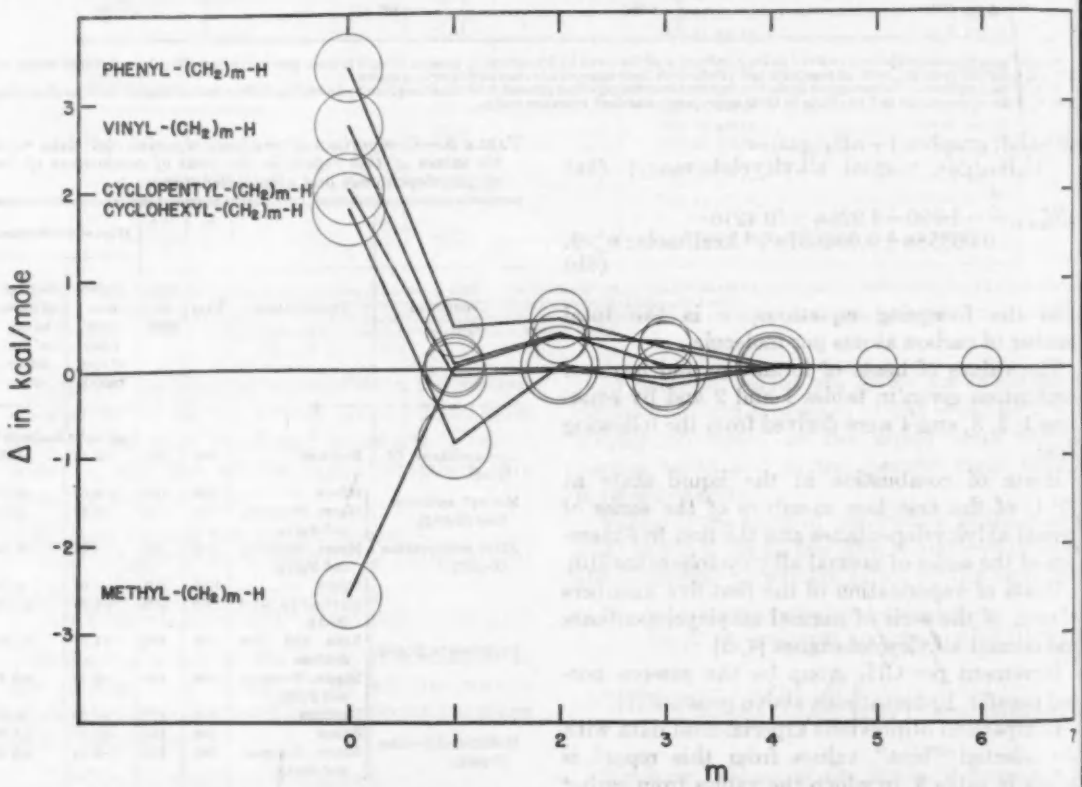

FIGURE 1.—*Plot of the deviations from linearity with number of carbon atoms, m, in the normal alkyl radical of the heats of formation of the lower members of several homologous series of hydrocarbons, expressed as the value of δ in the following relation:*

$$\Delta Hf^{\circ}_{298.16}\left[\text{gas, Y}-(CH_2)_m-\text{H}\right] = A'+Bm+\delta \text{ kcal/mole.}$$

TABLE 4.—*Values of the deviations from linearity with number of carbon atoms, m, in the normal alkyl radical of the heats of formation of the lower members of several homologous series of hydrocarbons*

Series	Structure	Values of A', B, and δ in the equation for the heat of formation in the gaseous state at 25° C $\Delta Hf° = A' + Bm + \delta$, kcal/mole							
		A'	B	δ, in kcal/mole					
				m=0	m=1	m=2	m=3	m=4	m=5
		kcal/mole	kcal/mole per CH_2 group						
Normal paraffins	Methyl−$(CH_2)_m$−H	−15.334	−4.926	−2.55 ±0.37	+0.02 ±0.33	+0.37 ±0.30	+0.30 ±0.28	+0.04 ±0.23	0.00 ±0.23
Monoolefins (1-alkene)	Vinyl−$(CH_2)_m$−H	9.740	−4.926	+2.76 ±0.37	+.07 ±0.33	+.30 ±0.33	+.04 ±0.48	.00 ±0.47	.00 ±0.47
Normal alkylbenzenes	Phenyl−$(CH_2)_m$−H	16.404	−4.926	+3.42 ±0.38	+.47 ±0.34	+.57 ±0.33	+.24 ±0.30	.00 ±0.35	.00 ±0.35
Normal alkylcyclopentanes	Cyclopentyl−$(CH_2)_m$−H	−20.516	−4.926	+2.05 ±0.40	−.06 ±0.37	−.01 ±0.36	−.10 ±0.37	.00 ±0.39	.00 ±0.39
Normal alkylcyclohexanes	Cyclohexyl−$(CH_2)_m$−H	−31.246	−4.926	+1.82 ±0.41	−.82 ±0.40	+.05 ±0.45	−.18 ±0.37	.00 ±0.37	.00 ±0.37

Table 4 gives, for each of the five series, the numerical values of the constants A' and B and of the term δ in equation 5, for the lower members of the series. The uncertainty assigned to the value of δ in each case includes the uncertainty associated with the extrapolation of the linear part of relations, equation 5, to lower values of m.

The values of δ in equation 5, for $m=0$, are characteristic of the end group in each series, and can be seen to vary regularly with changes in the number of hydrogen atoms and number and kind of carbon atoms bonded to the main or attaching carbon atom of the end group. The values of δ for $m=0$ for several end groups (including ethyl, isopropyl, *tert*-butyl, isopropenyl, and ethynyl, in addition to those given in table 4 and fig. 1) are shown in table 5 in relation to the number of carbon-hydrogen bonds and the number and kind of carbon-carbon bonds associated with the main or attaching carbon atom of the end group, not including the attaching bond. The value of δ for $m=0$ for an ethyl end group was obtained by noting that this is the same as the value of δ for $m=1$ for a methyl end group. The value of δ for $m=0$ for an isopropyl end group was calculated from the values previously reported [1] for propane, 2-methylpropane, 2-methylbutane, 2-methylpentane, 2-methylhexane, and 2-methylheptane. The value δ for $m=0$ for a tertiary butyl end group was calculated from the values of heats of formation previously reported [1] for isobutane, 2,2-dimethylpropane, 2,2-dimethylbutane, 2,2-dimethylpentane, and 2,2-dimethylhexane. The value of δ for $m=0$ for an isopropenyl end group was calculated from the values of heats of formation previously reported [8] for propene, 2-methylpropene, 2-methyl-1-butene, and 2-methyl-1-pentene. The value of δ for $m=0$ for an ethynyl end group was obtained from unpublished values for the heats of formation of the normal acetylenes (1-alkynes) [12].

TABLE 5.—*Relation between the value of the deviation from linearity for $m=0$ and the number and kind of bonds associated with the main or attaching carbon atom of the end group*

End group	Value of δ for m=0	Bonds associated with the main or attaching carbon atom of the given end group (not including the attaching bond)				
		C−H	C−C (paraffin)	C=C (phenyl)	C=C (olefin)	C≡C (acetylene)
	kcal/mole					
Methyl	−2.55 ±0.37	3				
Ethyl	0.02 ±0.33	2	1			
Cyclohexyl	1.82 ±0.41	1	2			
Cyclopentyl	2.05 ±0.40	1	2			
Isopropyl	2.05 ±0.50	1	2			
tert-Butyl	2.55 ±0.50		3			
Vinyl	2.76 ±0.37	1			1	
Phenyl	3.42 ±0.38			2		
Isopropenyl	3.68 ±0.40		1		1	
Ethynyl	4.94 ±0.55					1

IV. References

[1] E. J. Prosen and F. D. Rossini, J. Research NBS **34,** 263 (1945) RP1642.

[2] R. S. Jessup, J. Research NBS **18,** 115 (1937) RP966.

[3] E. J. Prosen and F. D. Rossini, J. Research NBS **33,** 255 (1944) RP1607.

[4] N. S. Osborne and D. C. Ginnings, National Bureau of Standards. Unpublished.

[5] D. D. Wagman, W. J. Taylor, J. M. Pignocco, and F. D. Rossini, National Bureau of Standards. Unpublished.

[6] American Petroleum Institute Research Project 44 at the National Bureau of Standards. Selected Values of Properties of Hydrocarbons. Tables 1q, 2q, 3q. Standard Heat, Entropy, and Free Energy of Vaporization. (May 31, 1944).

[7] F. D. Rossini, J. Research NBS **13,** 21 (1934) RP692.

[8] E. J. Prosen and F. D. Rossini, J. Research NBS **36,** (1946) RP1702.

[9] E. J. Prosen, W. H. Johnson, and F. D. Rossini, J. Research NBS **36,** 455 (1946) RP1714.

[10] W. H. Johnson, E. J. Prosen, and F. D. Rossini, J. Research NBS **36,** 463 (1946) RP1715.

[11] F. D. Rossini and J. W. Knowlton, J. Research NBS **19,** 339 (1937) RP1028.

[12] E. J. Prosen and F. D. Rossini. National Bureau of Standards. Unpublished.

[13] P. W. Zubow, J. Russ. Phys.-Chem. Soc. **30,** 926 (1898); **33,** 708 (1901); **35,** 815 (1903); See also, W. Świętosłowski, J. Am. Chem. Soc. **42,** 1092 (1920).

[14] G. E. Moore, M. L. Renquist, and G. S. Parks, J. Am. Chem. Soc. **62,** 1505 (1940).

[15] T. W. Richards and F. Barry, J. Am. Chem. Soc. **37,** 993 (1915).

[16] W. A. Roth and K. von Auwers, Liebigs Ann. Chem. **407,** 145 (1915).

[17] H. M. Huffman, Private communication (1943).

WASHINGTON, February 19, 1946.

U. S. Department of Commerce
National Bureau of Standards

Research Paper RP1729
Volume 37, July 1946

Part of Journal of Research of the National Bureau of Standards

Preliminary Description and Analysis of the First Spectrum of Uranium

By C. C. Kiess, Curtis J. Humphreys, and Donald D. Laun

Observations of the spectra emitted by uranium under arc and spark excitation have afforded a separation of the lines of neutral atoms from those emitted by ions. A list of more than 9,000 lines with accurate wavelengths, wave numbers, and estimated intensities, for the region 2900 A to 11000 A, has been compiled as descriptive of the spectrum of the neutral atom. About 2,000 of these lines have been classified as combinations between 18 low and metastable odd energy levels with about 280 high even levels. Well-resolved Zeeman patterns give g-values for several low levels that identify them as components of ^{5}L, ^{5}K, ^{7}M, and ^{7}K terms arising in the electron configurations f^3ds^2 and f^3d^2s. The spectrum of uranium is interpreted as that of a rare-earth element analogous to neodymium, uranium being the third member of a second group of rare earths beginning with thorium. From the fact that uranium is easily ionized in electric arcs and magnetic fields, and also that the short-wave limit of the observed spectrum does not extend below 2900 A, it is concluded that the ionization potential of neutral uranium atoms is approximately 4 volts.

I. Introduction

In the more than 30 years that have elapsed since the appearance, in 1912, of volume 6 of Kayser's "Handbuch der Spectroscopie", only a few additions have been made to our knowledge of the spectra emitted by uranium atoms. At that time Professor Kayser's [1][1] description of the uranium spectrum was expressed in the words: "Es gehört zu den linienreichsten Spectren der Elemente, gleichzeitig zu den am wenigsten charakteristischen. . . . Der Unterschied zwischen Bogen und Funken ist ausserordentlich gering, wenn überhaupt vorhanden; . . . ." In 1916 Meissner [2] published a list of 17 infrared uranium lines, and in 1920 Kiess and Meggers [3] published a list of more than 700 lines in the range

[1] Figures in brackets indicate the literature references at the end of this paper.

Contents

	Page
I. Introduction	57
II. Experimental procedure	58
III. Results	59
IV. References	72

from 5500 A, in the visible spectrum, to beyond 9500 A, in the infrared. But these extensions of the spectrum, and the improvements in wavelengths and intensities reported for uranium lines in the MIT Wavelength Tables [4], did not much alter Kayser's appraisal, as stated above.

In order to set up a system of energy levels for neutral and ionized uranium atoms, it is desirable to have a complete description of the spectrum emitted by each species of atom. Such a description includes not only precise wavelengths and well-estimated intensities for the lines, but also other characteristics, such as reversibility, diffuseness, Zeeman effect, etc. All the published descriptions of uranium spectra agree in reporting a continuous background on which the line spectra are superimposed. The effect of this continuum, in which the fainter and diffuse lines are completely lost, is to attenuate the intensity differences between the measurable lines. Despite this unfavorable circumstance, however, an enormous number of lines, in excess of 5,000, have been cataloged for uranium for both arc and spark excitation. No other significant descriptive data appear to have been published. The pressure shifts measured by W. J. Humphreys [5], and the reversals observed by McLennan, Cohen, and Liggett [6], apparently refer to lines emitted by other than uranium atoms.

Late in 1942 the Spectroscopy Section of the National Bureau of Standards was requested to undertake an investigation of the uranium spectrum and to determine, if possible, the system of energy levels responsible for their production. Available for the investigation were several spectrographs and such auxiliary equipment as interferometers, electromagnet, underwater spark, etc. Highly purified uranium metal was also available for use as electrode material. Accordingly, a program of work was mapped out to observe the spectra as emitted by arcs and condensed spark discharges in air at normal and at reduced pressures, and by discharges in hollow cathodes, in underwater sparks, and in magnetic fields.

II. Experimental Procedure

Five spectrographs in all were employed in making the Bureau of Standards observations. For the region between 2100 A and 2800 A, in the ultraviolet, a large quartz-prism spectrograph by Hilger was used. The dispersion of this instrument, described elsewhere [7], varies from 0.4 to 1.0 A per millimeter in the region for which it was used. A spectrograph in which the dispersive piece was a grating, ruled 30,000 lines per inch by R. W. Wood [8], was used in the first order to record the spectra from 2000 A to 3000 A, in the ultraviolet, and from 4200 A to 8500 A in the visible and infrared, with a dispersion of approximately 2 A per millimeter. In the second order, dispersion of 1 A per millimeter, it was used to record the spectra between 2600 A and 4300 A. A second grating with 15,000 lines per inch, also ruled by Wood, was used in the first order for recording the red and infrared portions of the spectra between 7000 A and 10000 A, the dispersion being 5 A per millimeter. The grating ruled by J. A. Anderson with 7,500 lines per inch was used to photograph the region from 9000 A to beyond 11000 A, in the first order. These three gratings are concave gratings of approximately 21-foot radius of curvature and are mounted in parallel light, according to the method of Wadsworth, as described by Meggers and Burns [9]. A fourth concave grating, ruled by Wood with 15,000 lines per inch, and set up in an Eagle mounting, was used in the fourth order for the region 4100 A to 5000 A, the dispersion being 1.2 A per millimeter.

The electrodes used in the arcs and sparks were rods of uranium metal of highest purity. The arcs were operated on currents of 5 to 7 amperes supplied by a 220-volt circuit. The condensed sparks were obtained from condensers that were charged from the 50,000-volt side of an induction coil whose primary carried a current of 10 amperes from a 110-volt a-c circuit. Each condenser unit was rated at 0.002 microfarad, so that when three or five were connected in parallel the capacitance of the discharge circuit was 0.006 or 0.010 microfarad. No self-inductance was used in this circuit.

The first observations made with arcs and sparks in air revealed the dark background reported by the earlier investigators. This background was found to emanate not only from the white-hot tips of the electrodes but also, and in greater intensity, from the incandescent particles

of uranium oxide that are formed in the outer envelopes surrounding the excited atoms. Various devices were tried to minimize, if not eliminate, the background effect. None was entirely successful, but satisfactory results were obtained either with the source shielded so that light from only a narrow zone between the electrodes could pass to the slit of the spectrograph, or with the source in a partially evacuated enclosure. The procedure finally adopted in making the spectrograms was to expose the photographic plates in succession to the shielded, or enclosed, uranium arc, to the uranium spark in air, to a similar spark enclosed in air at reduced pressure, and to the iron arc in air for the reference standards. The different exposures were recorded so that each exposure to a uranium source stood in juxtaposition to an iron exposure.

Inspection of the spectrograms showed that the number of lines recorded on them for any region was at least twice as great as hitherto reported. Yet the fact that arc and spark spectra were adjacent to each other on the plates made it possible to separate them according to the stage of ionization of their emitters on the basis of estimated intensities alone. Nevertheless, it was deemed desirable to carry out experiments on the reversal of the spectrum to single out the lines characteristic of neutral atoms and those most likely to originate in their lowest energy states. For this phase of the investigation the underwater spark was adopted, as described by Meggers and Laporte [10]. Although the continuum from the source, a condensed spark discharge between uranium electrodes submerged in flowing distilled water, was recorded on the spectrograms from the ultraviolet to the near infrared, yet no absorptions attributable to uranium atoms were observed. Instead, a few of the stronger emission lines of singly ionized uranium atoms appeared, superimposed on the continuous background.

The Zeeman-effect observations were made with a large, water-cooled Weiss magnet, equipped with both iron and ferro-cobalt pole pieces. With currents of 160 amperes applied to the coils, fields ranging in strength from 28,000 to 35,000 oersteds were obtained for pole gaps between 8 and 5 millimeters. In the earlier observations the source was a condensed spark discharge between electrodes cut from wire about a millimeter in diameter and accurately centered in the pole gap of the magnet. This source favored the excitation of lines from uranium ions rather than those from neutral atoms and was replaced by an a-c arc in which a current of 1 ampere was carried under an electromotive force of 2,200 volts. Subsequently, this source was replaced by a Back [11] lamp in which an interrupted arc was operated on 1 ampere at 220 volts, the air pressure within the arc enclosure being reduced to one-eighth or one-tenth atmosphere. This source proved to be the best for excitation of lines of the neutral atom and was used in a series of observations covering the range from 3000 A to beyond 9000 A. In order to calibrate the fields, exposures were also made with electrodes of copper, silver, magnesium, and other elements, to secure resolved magnetic patterns of known separations.

Between the pole gap of the magnet and the condensing lens of the spectrograph was placed a large quartz Wollaston prism, which separated the two polarizations in the Zeèman pattern vertically on the spectrograph slit. Owing to the stigmatic properties of a grating mounted in parallel light, it was thus possible to photograph simultaneously the two polarizations. Between them an occulting bar over the slit reserved an unexposed strip on the photographic plates for recording the spectrum without the magnetic field. The no-field exposures served effectively to mark the centers of the magnetic patterns, a desideratum of utmost importance in a complex spectrum where overlapping of the components in the patterns of close lines is of frequent occurrence.

III. Results

The spectrograms from which were derived the results presented below were measured and reduced according to well-known procedures. All the wavelength measurements are referred to iron lines adopted as international secondary standards or for which wavelengths determined by interference measurements are available. The wavelengths adopted for the uranium lines are the means of two or more determinations from measurements on separate spectrograms. The intensities assigned to the lines are estimates on an expanded scale ranging from 0 or 1 for the faintest

lines measured to 500 or more for the strongest. Most of the lines are sharp, with no tendency toward diffuseness nor any indication of self-reversal.

In the final tabulation of the results of the measurements a list has been compiled of more than 9,000 wavelengths that are believed to be characteristic of the spectrum emitted by neutral uranium atoms. The list covers the range 2900 A in the ultraviolet to 11000 A in the infrared, the basis of selection for the lines being their relative intensities in the spectra of arc and spark. That this method of selection presented no great difficulty may be seen in figure 1, which shows a portion of the violet region. For some lines, however, the ionic origin is definitely established by the number of p-components that they exhibit in well-resolved Zeeman patterns. For U I, which is built up on levels of odd multiplicity, this number is odd, whereas for U II it is even.

The Zeeman effects observed for most of the lines are either triplets or unresolved patterns. However, well-resolved patterns were recorded for a small number of lines. It was these that gave the clue to the analysis of the spectrum by telling uniquely the inner quantum numbers and g-values of the levels involved in the production of the lines. But to interpret these g-values and inner quantum numbers, it was first necessary to extend existing tables of theoretical Zeeman effects to cover terms of higher L-value. In table 1 are given a few lines with their Zeeman patterns, of which some are illustrated in figure 2.

TABLE 1.—*Zeeman effects of some* U I *lines*

Wavelength	Observed Zeeman effect
8381.86	(**0.00**, 0.26, 0.53, 0.80, 1.07, 1.30) . . . 1.71, 2.01, **2.29**
8223.08	(**0.00**, 0.20, 0.40, 0.60, 0.81, 1.04) . . . 0.00, 0.20, **0.40**
7101.61	(**0.00**, .012, 0.23, 0.34) . . . 0.80, 0.93, **1.03**
6820.76	(**0.00**, 0.23, 0.47, 0.71, 0.97, 1.17) . . . 1.38, 1.63, 1.87, **2.12**
6395.42	(**0.00**, 0.15, 0.32, 0.48, 0.63, 0.81, 0.94) . . . 1.55, 1.74, **1.86**
5997.31	(**0.00**, 0.33, 0.68, 1.04, 1.32, 1.69, 2.06) . . . 2.00, 2.32, 2.66, **3.01**
5971.50	(**0.00**. 0.15, 0.29, 0.45, 0.58, 0.73) . . . 1.18, 1.34, 1.50, **1.64**

With the key to the structure of the spectrum thus in hand, a search through the tabulated wave numbers of the lines brought to light numerous recurring constant differences, of which some proved to be significant. Although laborious, this method of search proved fruitful in leading to the groups of odd and even energy levels presented in tables 2 and 3. The odd levels have been assigned their designations on the basis of g-values derived from the resolved Zeeman-effect observations. Such terms can arise only from electron configurations containing f-electrons. There are various possible groupings of the six uranium valence electrons into such configurations, but the ^{7}M term can arise only in the configuration f^5. Inasmuch as the low ^{5}L and ^{5}K terms are of the same parity as ^{7}M and are unaccompanied by corresponding terms of the septet system, it is necessary to conclude that they owe their origin to the configuration f^5ds^2 rather than to some other configuration.

TABLE 2.—*Low odd levels of* U I

Electron configuration	Term symbol	Term value	g-values	
			LS	Observed
f^5ds^2	$^5L_6$	0.0	0.714	0.75
f^5ds^2	$^5K_5$	620.3	.667	.73
	$A_5^?=^5L_4$?	3800.8		
	$A_5^?$	3868.4		
f^5ds^2	$^5K_4$	4275.7	.905	.93
	$^5I_5$	4453.4	.600	.66
f^5d^2s	$^7K_5$	5762.0	.767	.82
	$^5H_5$	5991.3	.900	.86
f^5d^2s	$^7M_4$	6249.0	.571	.62
f^5d^2s	$^7K_4$	7005.5	.976	.97
	$B_5^?$	7103.9		
	$B_5^?=^5K_5$?	7326.1		
	$A_4^?=^5L_4$?	7645.6		
	$C_7^?=^7M_5$?	8118.6		
	$D_5^?=^7K_5$?	10347.3		
	$B_5^?=^5K_5$?	10685.7		
	$A_5^?$	11545.4		
	$A_5^?$	13127.9		

This conclusion is further supported by the interpretation of the spectrum Th II due to singly ionized thorium atoms. This spectrum has been analyzed independently by two groups of investigators [12], who are in agreement in finding that although the lowest energy states belong to the ds^2, d^2s, and d^3 configurations, yet an energetically prominent set of low states is also present due to the configurations fs^2 and fds. In passing from thorium to uranium, we might expect, on the assumption that the binding of f-type electrons is preferred, the configuration f^5ds to give the lowest states of the ion, and f^5ds^2 and f^5d^2s the lowest and metastable states of the neutral uranium atom.

[9] In a paper just received here (Physica 11, 419; 1946) Schuurmans in reporting the lowest levels of U II assigns them to the configurations f^5s^2, f^5ds, and f^5d^2. The lowest level of U II belongs to the ^{7}F° term of the f^5s^2 configuration from which the ^{5}L° term of U I is derived by adding to it a d electron to form the configuration f^5ds^2. Schuurman's report also confirms the levels $^5K_6^?$ and $^7M_4^?$ and their electron configurations as given in table 2 above.

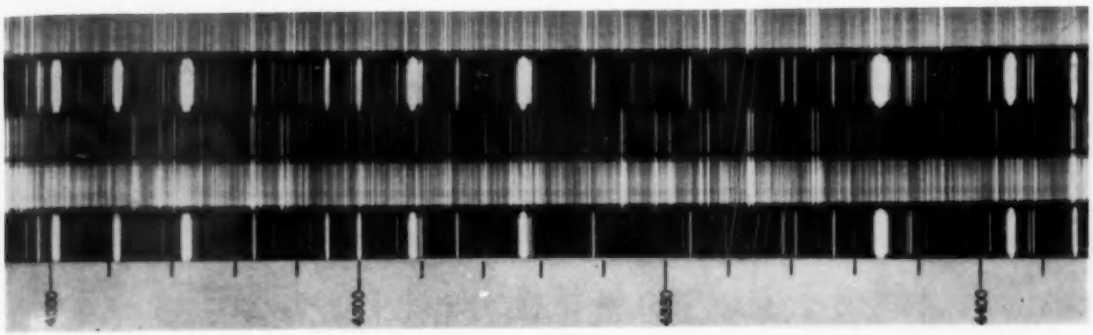

FIGURE 1.—*Top to bottom:* U *arc in vacuum;* Fe *arc in air;* U *spark in vacuum;* U *spark in air;* Fe *arc in air.*

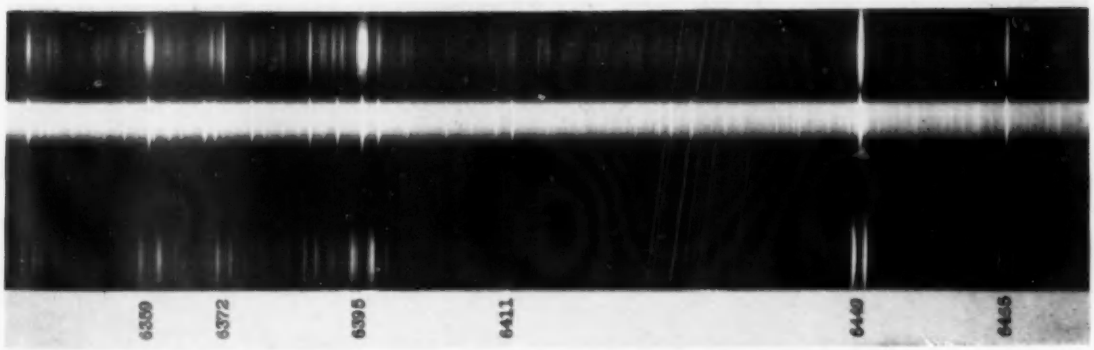

FIGURE 2.—*Zeeman effect of uranium; p-components; no-field; n-components.*

UNIV. OF MICH.

The configuration f^3ds^2 yields 158 terms, comprising 386 energy levels distributed among the quintet, triplet, and singlet systems. The f^3d^2s configuration gives rise to 1,122 terms, with a total of 3,256 levels belonging to the septet, quintet, triplet, and singlet systems. On excitation of the atom, these configurations change into f^3dps, f^3ps^2, and f^3d^2p, depending on which electron is shifted from the low-energy configurations. Each of these excited states yields an enormous number of levels, of even parity, of which more than 275 have now been found. It is obvious why the observed spectrum is so complex.

The even levels of table 3, in combination with the odd levels of table 2, account for most of the stronger lines of the spectrum, as recorded in table 4. For only a small number of the levels have g-values been found, but their inner quantum numbers can be uniquely determined from their combinatory properties. The present state of the analysis does not permit assignment of the even levels to their proper electron configurations. In table 3 the symbol for the even levels is made up of the first three figures of the level value, followed by the inner quantum number as a subscript. This follows the scheme adopted by Laporte and Mack [13] for tungsten.

TABLE 3.—*Even levels of* U I

Term symbol	Term value	Term symbol	Term value
179_2	17968. 7	210_4	21062. 3
185_2	18530. 8	215_4	21545. 1
196_2	19668. 4	220_4	22038. 0
203_2	20391. 5	223_4	22365. 0
219_3	21940. 6	224_4	22383. 4
227_3	22774. 1	225_5	22584. 5
234_3	23464. 1	231_5	23186. 9
251_3	25160. 7	234_5	23430. 1
268_3	26855. 4	235_5	23560. 6
294_3	29413. 7	238_5	23825. 4
295_2	29430. 3	247_4	24757. 2
296_2	29644. 6	249_4	24940. 5
302_2	30222. 4	252_4	25224. 1
340_2	34065. 4	256_4	25653. 3
161_4	16121. 9	265_4	26516. 8
174_4	17468. 2	271_4	27184. 1
178_4	17893. 8	283_4	28430. 5
181_4	18186. 0	284_4	28454. 0
185_4	18526. 9	285_4	28543. 4
191_4	19127. 2	292_4	29250. 5
192_4	19192. 4	297_4	29719. 9
195_4	19552. 5	303_4	30303. 7
197_4	19740. 7	304_4	30499. 1
201_4	20148. 0	309_4	30979. 7
205_4	20569. 2	312_4	31221. 3

TABLE 3.—*Even levels of* U I—Continued

Term symbol	Term value	Term symbol	Term value
313_4	31243. 5	173_6	17361. 9
316_4	31633. 9	182_6	18253. 9
321_4	32141. 2	187_6	18759. 2
116_5	11614. 0	197_6	19783. 4
122_5	12227. 8	202_6	20218. 8
134_5	13463. 4	204_6	20420. 5
157_5	15720. 7	206_6	20661. 5
169_5	16929. 8	209_6	20943. 4
179_5	17908. 2	212_6	21265. 1
184_5	18406. 5	215_6	21584. 7
189_5	18932. 8	217_6	21766. 5
194_5	19471. 9	218_6	21768. 0
196_5	19647. 5	220_6	22056. 3
201_5	20114. 3	224_6	22464. 3
203_5	20311. 5	225_6	22582. 7
206_5	20621. 2	227_6	22754. 1
208_5	20851. 6	228_6	22862. 4
210_5	21078. 7	235_6	23572. 0
213_5	21330. 0	237_6	23715. 3
216_5	21637. 0	240_6	24026. 2
223_5	22377. 7	244_6	24433. 2
233_5	23325. 2	246_6	24671. 4
234_5	23432. 8	252_6	25235. 7
235_5	23486. 7	253_6	25349. 0
239_5	23932. 8	254_6	25462. 6
244_5	24448. 0	257_6	25791. 6
245_5	24535. 3	258_6	25825. 6
249_5	24906. 8	259_6	25938. 2
250_5	25017. 1	261_6	26103. 7
251_5	25178. 1	262_6	26225. 5
252_5	25255. 4	265_6	26550. 4
253_5	25319. 2	266_6	26631. 4
258_5	25805. 8	267_6	26715. 5
263_5	26305. 0	268_6	26758. 8
265_5	26566. 9	269_6	26791. 6
269_5	26920. 7	270_6	27072. 4
273_5	27381. 7	274_6	27499. 4
276_5	27682. 2	275_6	27605. 7
277_5	27778. 0	276_6	27615. 8
278_5	27791. 1	277_6	27744. 0
281_5	28188. 3	278_6	27941. 2
284_5	28444. 5	279_6	28022. 9
285_5	28503. 5	280_6	28053. 1
286_5	28562. 7	281_6	28098. 9
287_5	28650. 3	284_6	28470. 2
292_5	29232. 6	288_6	28860. 9
301_5	30143. 1	289_6	28874. 9
309_5	30936. 6	290_6	29033. 6
310_5	30993. 0	291_6	29109. 8
311_5	31129. 5	292_6	29126. 1
313_5	31339. 8	294_6	29400. 9
314_5	31467. 6	295_6	29558. 8
315_5	31488. 2	298_6	29865. 5
317_5	31744. 2	299_6	29986. 4
319_5	31946. 0	300_6	30294. 3
323_5	32317. 8	301_6	30335. 0
146_6	14643. 9	302_6	30451. 4
156_6	15638. 4	303_6	30490. 3
165_6	16505. 8	304_6	30500. 1
170_6	17070. 5	305_6	30586. 7

TABLE 3.—*Even levels of* U I—Continued

Term symbol	Term value	Term symbol	Term value
306_6	30636.7	318_7	31968.1
307_6	30875.6	319_7	31974.4
308_6	30894.5	320_7	32016.7
311_6	31135.0	321_7	32098.2
315_6	31551.5	326_7	32641.8
324_6	32490.6	327_7	32774.2
325_6	32495.7	335_7	33570.6
334_6	33412.2	340_7	34059.9
336_6	33639.6	194_8	19489.0
156_7	15631.9	205_8	20528.9
169_7	16900.4	223_8	22383.1
197_7	19826.7	227_8	22789.8
198_7	19885.4	231_8	23110.8
204_7	20464.5	239_8	23926.7
207_7	20766.5	244_8	24451.7
223_7	22368.4	245_8	24581.2
226_7	22633.2	253_8	25388.9
229_7	22918.6	257_8	25789.0
230_7	23057.7	259_8	25918.1
231_7	23197.0	261_8	26192.4
235_7	23543.5	263_8	26313.3
237_7	23779.2	264_8	26454.1
238_7	23848.6	265_8	26492.1
240_7	24066.6	266_8	26597.0
241_7	24185.8	269_8	26979.3
243_7	24333.8	270_8	26989.1
245_7	24560.4	271_8	27086.4
256_7	25672.5	272_8	27150.5
261_7	26208.8	274_8	27477.6
262_7	26274.8	278_8	27818.5
263_7	26391.3	289_8	28993.7
266_7	26608.5	290_8	29037.2
273_7	27324.5	294_8	29413.2
278_7	27887.0	296_8	29612.7
279_7	27965.9	300_8	30027.2
280_7	28048.2	307_8	30737.1
281_7	28118.8	309_8	30986.3
282_7	28152.7	312_8	31279.1
283_7	28285.8	314_8	31445.3
284_7	28451.1	319_8	31923.1
285_7	28566.4	324_8	32477.8
287_7	28798.9	341_8	34105.4
288_7	28895.6	238_9	23843.7
291_7	29107.1	245_9	24517.3
297_7	29790.7	256_9	25626.6
298_7	29797.2	279_9	27969.7
299_7	29837.6	293_9	29339.3
300_7	29958.1	295_9	29550.3
302_7	30279.1	312_9	31270.3
306_7	30642.8	321_9	32108.4
310_7	31024.8		
311_7	31166.2		
312_7	31276.0		
313_7	31301.1		
314_7	31358.6		

TABLE 4.—*Classified lines of* U I

λ_{air}A	Intensity	ν_{vac}cm^{-1}	Term combination
11384.2	2	8781.71	$C_7^\dagger$–[illegible]
11167.8	3	8951.83	$C_7^\dagger$–[illegible]
10647.6	3	9389.23	$^7M_4^\dagger$–[illegible]
10555.02	20	9471.57	$^7M_4^\dagger$–[illegible]
10259.42	3	9744.47	$B_7^\dagger$–[illegible]
10073.54	2	9924.28	$^7K_4^\dagger$–[illegible]
9932.76	3	10064.94	$^7K_4^\dagger$–[illegible]
9917.04	2	10080.89	$B_6^\dagger$–[illegible]
9868.30	3	10130.68	$^5H_4^\dagger$–[illegible]
9818.86	5	10181.69	$D_7^\dagger$–[illegible]
9653.20	4	10356.42	$^7K_4^\dagger$–[illegible]
9645.82	5	10364.35	$B_7^\dagger$–[illegible]
9642.00	2	10368.45	$^5K_4^\dagger$–[illegible]
9595.06	4	10419.18	$D_7^\dagger$–[illegible]
9395.37	5	10640.63	$C_7^\dagger$–[illegible]
9385.89	5	10651.37	$^7M_4^\dagger$–[illegible]
9329.43	6	10715.83	$A_6^\dagger$–[illegible]
9305.18	4	10743.76	$^7K_4^\dagger$–[illegible]
9257.66	10	10798.91	$A_6^\dagger$–[illegible]
9148.48	4	10927.78	$B_7^\dagger$–[illegible]
9139.57	10	10938.44	$^5H_4^\dagger$–[illegible]
9093.68	25	10993.64	$^5K_4^\dagger$–[illegible]
8996.08	2	11112.91	$^7M_4^\dagger$–[illegible]
8951.94	20	11167.70	$^7K_4^\dagger$–[illegible]
8887.76	3	11248.35	$^7K_4^\dagger$–[illegible]
8828.49	2	11323.86	$A_6^\dagger$–[illegible]
8792.34	3	11370.42	$C_7^\dagger$–[illegible]
8777.69	10	11389.40	$A_6^\dagger$–[illegible]
8753.68	25	11420.64	$D_7^\dagger$–[illegible]
8728.75	8	11453.25	$A_6^\dagger$–[illegible]
8710.76	40	11476.91	$^5H_4^\dagger$–[illegible]
8618.47	8	11599.81	$^7K_4^\dagger$–[illegible]
8607.96	600	11613.97	$^5L_4^\dagger$–[illegible]
8574.59	30	11659.17	$^7M_4^\dagger$–[illegible]
8570.52	120	11664.70	$C_7^\dagger$–[illegible]
8567.71	40	11668.53	$^5I_4^\dagger$–[illegible]
8557.32	30	11682.70	$B_6^\dagger$–[illegible]
8540.19	100	11706.13	$^7K_4^\dagger$–[illegible]
8496.09	100	11766.89	$C_7^\dagger$–[illegible]
8450.02	400	11831.04	$A_7^\dagger$–[illegible]
8445.37	400	11837.56	$A_7^\dagger$–[illegible]
8441.20	80	11843.41	$A_7^\dagger$–[illegible]
8399.25	15	11902.56	$^5H_4^\dagger$–[illegible]
8389.16	40	11916.87	$^5H_4^\dagger$–[illegible]
8381.86	120	11927.25	$^7K_4^\dagger$–[illegible]
8346.75	80	11977.43	$^5H_4^\dagger$–[illegible]
8316.39	6	12021.15	$D_7^\dagger$–[illegible]
8270.05	15	12088.51	$B_6^\dagger$–[illegible]
8262.05	150	12100.21	$C_7^\dagger$–[illegible]
8259.44	10	12104.04	$B_6^\dagger$–[illegible]
8240.51	20	12131.84	$^7K_4^\dagger$–[illegible]
8230.83	40	12146.11	$^7K_4^\dagger$–[illegible]
8223.09	200	12157.54	$^7M_4^\dagger$–[illegible]
8175.84	20	12227.81	$^5L_4^\dagger$–[illegible]
8174.30	250	12230.11	$^5K_4^\dagger$–[illegible]
8153.71	20	12260.99	$A_6^\dagger$–[illegible]
8137.21	30	12285.85	$D_7^\dagger$–[illegible]
8126.59	15	12301.91	$C_7^\dagger$–[illegible]
8055.61	30	12410.30	$C_7^\dagger$–[illegible]
8034.79	40	12442.46	$D_7^\dagger$–[illegible]

TABLE 4.—*Classified lines of* U I—Continued

λ_{air}A	Intensity	ν_{vac}cm^{-1}	Term combination
8019.38	20	12466.38	$^{7}K_{3}^{\circ}-194_{5}$
8012.96	20	12476.36	$^{5}I_{4}^{\circ}-169_{5}$
7998.60	20	12498.76	$A_{3}^{\circ}-256_{9}$
7991.30	40	12510.17	$^{7}M_{3}^{\circ}-187_{6}$
7975.08	40	12535.62	$^{5}H_{4}^{\circ}-185_{4}$
7970.46	100	12542.88	$C_{2}^{\circ}-206_{5}$
7959.97	20	12559.41	$B_{2}^{\circ}-198_{7}$
7918.79	50	12624.73	$^{5}K_{3}^{\circ}-169_{7}$
7907.96	20	12642.02	$^{7}K_{3}^{\circ}-196_{5}$
7904.28	30	12647.90	$C_{2}^{\circ}-207_{7}$
7900.39	40	12654.13	$^{5}K_{3}^{\circ}-169_{5}$
7895.99	15	12661.18	$A_{3}^{\circ}-257_{5}$
7881.91	400	12683.80	$^{7}M_{3}^{\circ}-189_{5}$
7868.73	100	12705.05	$A_{2}^{\circ}-165_{6}$
7823.89	20	12777.86	$^{7}K_{3}^{\circ}-197_{6}$
7816.29	40	12790.28	$A_{3}^{\circ}-259_{5}$
7784.13	500	12843.13	$^{5}K_{3}^{\circ}-134_{5}$
7761.84	50	12880.01	$^{7}K_{3}^{\circ}-198_{7}$
7759.88	30	12883.26	$A_{3}^{\circ}-205_{8}$
7754.18	40	12892.73	$B_{2}^{\circ}-202_{6}$
7748.18	40	12902.71	$A_{3}^{\circ}-244_{5}$
7724.99	8	12941.45	$^{5}H_{4}^{\circ}-189_{5}$
7691.89	20	12997.14	$^{7}K_{3}^{\circ}-187_{6}$
7652.21	6	13064.53	$A_{3}^{\circ}-261_{8}$
7639.52	200	13086.22	$^{5}K_{4}^{\circ}-173_{6}$
7634.74	50	13094.43	$B_{2}^{\circ}-204_{6}$
7631.72	250	13099.61	$A_{2}^{\circ}-169_{7}$
7619.34	300	13120.89	$A_{3}^{\circ}-207_{7}$
7609.16	100	13138.44	$B_{2}^{\circ}-204_{7}$
7597.86	12	13157.99	$B_{3}^{\circ}-238_{9}$
7595.04	25	13162.87	$B_{3}^{\circ}-238_{7}$
7590.52	25	13170.71	$^{7}K_{3}^{\circ}-189_{5}$
7575.86	20	13196.20	$D_{2}^{\circ}-235_{7}$
7573.03	30	13201.13	$^{5}H_{4}^{\circ}-192_{4}$
7572.06	20	13202.82	$B_{2}^{\circ}-205_{8}$
7566.03	30	13213.34	$^{7}K_{3}^{\circ}-202_{6}$
7550.21	30	13241.02	$B_{3}^{\circ}-239_{9}$
7533.91	250	13269.68	$A_{2}^{\circ}-170_{9}$
7501.97	10	13326.17	$A_{3}^{\circ}-264_{5}$
7480.54	8	13364.35	$A_{4}^{\circ}-265_{8}$
7443.79	20	13430.33	$^{7}K_{3}^{\circ}-192_{4}$
7442.92	10	13431.90	$D_{2}^{\circ}-237_{7}$
7438.22	20	13440.38	$B_{2}^{\circ}-207_{7}$
7425.50	150	13463.41	$^{5}L_{4}^{\circ}-134_{5}$
7396.98	40	13515.33	$^{5}I_{4}^{\circ}-179_{9}$
7371.95	12	13561.21	$^{5}H_{4}^{\circ}-195_{4}$
7341.58	10	13617.31	$B_{2}^{\circ}-209_{6}$
7227.86	8	13831.55	$B_{3}^{\circ}-245_{9}$
7210.28	20	13865.28	$^{7}M_{3}^{\circ}-201_{5}$
7205.42	12	13874.63	$B_{3}^{\circ}-245_{7}$
7172.09	10	13939.11	$B_{2}^{\circ}-212_{6}$
7164.87	25	13953.15	$^{5}I_{4}^{\circ}-184_{5}$
7147.87	20	13986.34	$D_{2}^{\circ}-243_{7}$
7130.05	40	14021.28	$^{7}K_{3}^{\circ}-197_{6}$
7128.89	200	14023.57	$^{5}K_{3}^{\circ}-146_{5}$
7109.13	10	14062.55	$^{7}M_{3}^{\circ}-203_{5}$
7101.61	30	14077.44	$^{5}I_{4}^{\circ}-185_{5}$
7090.10	10	14100.28	$A_{3}^{\circ}-179_{9}$
7074.78	80	14130.83	$^{5}K_{3}^{\circ}-184_{5}$
7033.84	20	14213.08	$D_{2}^{\circ}-245_{7}$

TABLE 4.—*Classified lines of* U I—Continued

λ_{air}A	Intensity	ν_{vac}cm^{-1}	Term combination
7015.70	12	14249.83	$C_{2}^{\circ}-223_{7}$
6955.93	6	14372.27	$^{7}M_{3}^{\circ}-206_{5}$
6942.43	6	14400.23	$^{5}H_{4}^{\circ}-203_{5}$
6922.71	6	14441.24	$B_{3}^{\circ}-215_{4}$
6917.05	20	14453.06	$A_{2}^{\circ}-182_{6}$
6915.27	15	14456.77	$^{7}K_{3}^{\circ}-202_{6}$
6902.51	20	14483.50	$^{5}K_{3}^{\circ}-187_{6}$
6887.64	10	14514.55	$C_{2}^{\circ}-226_{7}$
6857.21	6	14579.18	$^{7}K_{3}^{\circ}-215_{6}$
6846.22	30	14602.58	$^{7}M_{3}^{\circ}-208_{5}$
6832.71	20	14631.45	$^{7}K_{3}^{\circ}-216_{5}$
6830.84	10	14635.45	$C_{2}^{\circ}-227_{6}$
6826.91	400	14643.88	$^{5}L_{4}^{\circ}-146_{6}$
6820.76	80	14657.09	$^{5}K_{3}^{\circ}-189_{5}$
6818.29	50	14662.39	$A_{3}^{\circ}-185_{8}$
6812.98	15	14673.82	$^{5}I_{4}^{\circ}-191_{4}$
6810.02	8	14680.19	$A_{3}^{\circ}-262_{6}$
6805.21	12	14690.58	$A_{3}^{\circ}-278_{8}$
6799.42	10	14703.09	$B_{3}^{\circ}-253_{6}$
6790.30	30	14722.85	$A_{3}^{\circ}-223_{7}$
6783.50	4	14737.59	$A_{3}^{\circ}-223_{8}$
6782.85	20	14739.01	$^{5}I_{4}^{\circ}-192_{4}$
6780.62	20	14743.85	$C_{2}^{\circ}-228_{8}$
6772.72	15	14761.05	$^{7}K_{3}^{\circ}-217_{6}$
6754.93	25	14799.94	$C_{2}^{\circ}-229_{7}$
6751.63	15	14807.17	$^{7}K_{3}^{\circ}-205_{4}$
6741.36	50	14829.73	$^{7}M_{3}^{\circ}-210_{5}$
6738.16	12	14836.75	$B_{3}^{\circ}-219_{9}$
6727.96	25	14859.26	$^{7}K_{3}^{\circ}-206_{5}$
6692.01	15	14939.08	$C_{2}^{\circ}-230_{7}$
6691.20	20	14940.88	$B_{3}^{\circ}-256_{9}$
6683.38	40	14958.38	$A_{2}^{\circ}-187_{6}$
6670.37	8	14987.54	$A_{3}^{\circ}-226_{7}$
6668.30	10	14992.18	$C_{2}^{\circ}-231_{8}$
6662.53	12	15005.18	$A_{3}^{\circ}-265_{8}$
6657.68	15	15016.11	$^{7}M_{3}^{\circ}-212_{6}$
6656.81	25	15018.08	$^{5}K_{3}^{\circ}-156_{6}$
6656.64	10	15018.46	$^{5}I_{4}^{\circ}-194_{5}$
6646.05	8	15042.38	$B_{2}^{\circ}-223_{7}$
6642.35	8	15050.77	$^{7}K_{3}^{\circ}-220_{6}$
6633.41	8	15071.06	$^{5}H_{4}^{\circ}-210_{4}$
6630.18	12	15078.40	$C_{2}^{\circ}-231_{7}$
6629.04	10	15080.98	$^{7}M_{3}^{\circ}-213_{5}$
6625.29	20	15089.53	$^{7}K_{3}^{\circ}-208_{5}$
6621.07	20	15099.14	$^{5}I_{4}^{\circ}-195_{4}$
6620.52	50	15100.39	$^{5}K_{3}^{\circ}-157_{5}$
6619.26	6	15103.27	$B_{3}^{\circ}-257_{8}$
6603.98	30	15138.21	$B_{2}^{\circ}-224_{6}$
6601.39	12	15144.16	$A_{3}^{\circ}-227_{8}$
6585.20	15	15181.39	$^{7}K_{3}^{\circ}-209_{6}$
6578.78	15	15196.21	$^{5}K_{3}^{\circ}-194_{5}$
6570.63	4	15215.05	$^{5}I_{4}^{\circ}-196_{5}$
6552.75	25	15256.58	$B_{2}^{\circ}-225_{6}$
6551.80	10	15258.78	$A_{3}^{\circ}-191_{4}$
6550.75	8	15261.22	$B_{3}^{\circ}-223_{4}$
6545.71	15	15272.98	$A_{3}^{\circ}-229_{7}$
6542.98	30	15279.35	$B_{3}^{\circ}-224_{4}$
6539.57	6	15287.32	$^{5}I_{4}^{\circ}-197_{4}$
6531.15	8	15307.03	$B_{2}^{\circ}-226_{7}$
6527.03	30	15316.68	$^{7}K_{3}^{\circ}-210_{6}$

TABLE 4.—*Classified lines of* U I—Continued

λ_{air}A	Intensity	ν_{vac}cm^{-1}	Term combination
6518.94	80	15335.70	$^{7}M\frac{1}{2}-215_{5}$
6517.67	6	15338.69	$^{5}H\frac{1}{2}-213_{3}$
6503.62	30	15371.81	$^{5}K\frac{1}{2}-196_{5}$
6503.45	8	15372.22	$^{7}K\frac{1}{2}-223_{5}$
6502.15	4	15375.29	$A\frac{1}{2}-269_{5}$
6496.80	12	15387.96	$^{7}M\frac{1}{2}-216_{5}$
6486.63	8	15412.08	$A\frac{1}{2}-230_{7}$
6481.22	12	15424.94	$C\frac{1}{2}-235_{7}$
6479.94	20	15228.00	$B\frac{1}{2}-227_{6}$
6469.36	8	15453.23	$C\frac{1}{2}-235_{6}$
6467.02	6	15458.82	$^{7}K\frac{1}{2}-224_{6}$
6464.97	150	15463.72	$B\frac{1}{2}-227_{6}$
6458.94	8	15478.15	$D\frac{1}{2}-258_{6}$
6449.16	300	15501.63	$^{5}K\frac{1}{2}-161_{4}$
6448.56	12	15503.07	$^{7}K\frac{1}{2}-212_{6}$
6442.55	15	15517.53	$^{7}M\frac{1}{2}-217_{6}$
6441.95	10	15518.98	$^{7}M\frac{1}{2}-218_{6}$
6428.69	15	15550.99	$^{5}K\frac{1}{2}-197_{7}$
6427.48	20	15553.91	$^{5}H\frac{1}{2}-215_{4}$
6411.58	25	15592.47	$B\frac{1}{2}-229_{7}$
6409.84	15	15596.71	$C\frac{1}{2}-237_{6}$
6404.44	20	15609.87	$^{5}K\frac{1}{2}-198_{7}$
6397.14	60	15627.67	$^{7}K\frac{1}{2}-226_{7}$
6395.42	200	15631.88	$^{5}L\frac{1}{2}-156_{7}$
6392.74	80	15638.43	$^{5}L\frac{1}{2}-156_{6}$
6389.77	80	15645.69	$^{5}H\frac{1}{2}-216_{5}$
6383.56	30	15660.93	$^{5}I\frac{1}{2}-201_{3}$
6379.76	4	15670.25	$B\frac{1}{2}-227_{5}$
6374.12	15	15684.11	$A\frac{1}{2}-195_{4}$
6372.43	200	15688.27	$A\frac{1}{2}-194_{5}$
6369.84	50	15694.64	$^{5}I\frac{1}{2}-201_{4}$
6359.28	100	15720.71	$^{5}L\frac{1}{2}-157_{5}$
6354.89	10	15731.57	$B\frac{1}{2}-230_{7}$
6348.01	4	15748.62	$^{7}K\frac{1}{2}-227_{6}$
6327.38	4	15799.97	$A\frac{1}{2}-196_{5}$
6324.44	20	15807.31	$^{7}M\frac{1}{2}-220_{6}$
6324.11	3	15808.14	$C\frac{1}{2}-239_{5}$
6318.32	5	15822.62	$^{7}K\frac{1}{2}-215_{6}$
6309.36	4	15845.10	$D\frac{1}{2}-261_{5}$
6301.13	3	15865.79	$A\frac{1}{2}-289_{5}$
6298.53	40	15872.34	$A\frac{1}{2}-197_{4}$
6293.32	60	15885.47	$^{5}K\frac{1}{2}-165_{4}$
6284.57	8	15907.60	$C\frac{1}{2}-240_{6}$
6270.55	20	15943.16	$^{5}K\frac{1}{2}-202_{6}$
6268.66	50	15947.97	$C\frac{1}{2}-240_{7}$
6246.53	20	16004.47	$^{7}K\frac{1}{2}-217_{6}$
6238.19	8	16025.87	$A\frac{1}{2}-197_{7}$
6234.30	40	16035.87	$^{5}K\frac{1}{2}-203_{5}$
6231.22	4	16043.79	$D\frac{1}{2}-263_{7}$
6227.96	5	16052.18	$^{7}K\frac{1}{2}-230_{7}$
6222.14	25	16067.20	$C\frac{1}{2}-241_{7}$
6215.37	100	16084.71	$A\frac{1}{2}-198_{7}$
6206.86	5	16106.76	$D\frac{1}{2}-264_{6}$
6203.37	20	16115.82	$^{5}I\frac{1}{2}-205_{4}$
6201.97	25	16119.46	$^{7}M\frac{1}{2}-223_{7}$
6198.39	15	16128.76	$^{7}M\frac{1}{2}-223_{5}$
6196.52	20	16133.64	$A\frac{1}{2}-237_{7}$
6175.38	200	16188.86	$^{5}K\frac{1}{2}-204_{7}$
6174.37	60	16191.52	$^{7}K\frac{1}{2}-231_{7}$
6171.85	250	16198.12	$A\frac{1}{2}-238_{6}$

TABLE 4.—*Classified lines of* U I—Continued

λ_{air}A	Intensity	ν_{vac}cm^{-1}	Term combinati
6166.80	4	16211.39	$A\frac{1}{2}-2$
6165.35	20	16215.21	$C\frac{1}{2}-2$
6164.50	80	16217.43	$B\frac{1}{2}-2$
6153.66	50	16246.00	$B\frac{1}{2}-2$
6152.25	60	16249.73	$D\frac{1}{2}-2$
6147.93	12	16261.15	$D\frac{1}{2}-2$
6142.32	20	16276.00	$^{7}K\frac{1}{2}-2$
6140.37	8	16281.17	$A\frac{1}{2}-2$
6138.79	4	16285.36	$A\frac{1}{2}-2$
6135.72	8	16293.51	$B\frac{1}{2}-2$
6129.72	100	16309.47	$^{5}K\frac{1}{2}-1$
6127.77	20	16314.64	$C\frac{1}{2}-2$
6120.64	12	16333.65	$^{7}M\frac{1}{2}-2$
6110.67	6	16360.30	$B\frac{1}{2}-2$
6107.74	8	16368.16	$D\frac{1}{2}-2$
6101.77	40	16384.16	$^{7}M\frac{1}{2}-2$
6101.15	20	16385.83	$^{5}K\frac{1}{2}-2$
6099.90	15	16389.20	$B\frac{1}{2}-2$
6098.81	5	16392.12	$^{5}H\frac{1}{2}-2$
6089.19	12	16418.01	$A\frac{1}{2}-2$
6088.12	6	16420.90	$A\frac{1}{2}-2$
6087.54	4	16422.45	$A\frac{1}{2}-2$
6080.37	30	16441.83	$C\frac{1}{2}-2$
6077.29	200	16450.15	$^{5}K\frac{1}{2}-1$
6074.86	10	16456.74	$B\frac{1}{2}-2$
6062.30	80	16490.84	$^{5}K\frac{1}{2}-2$
6057.07	30	16505.07	$^{7}M\frac{1}{2}-2$
6056.80	40	16505.81	$^{5}L\frac{1}{2}-1$
6050.67	20	16522.54	$B\frac{1}{2}-2$
6050.48	15	16523.06	$A\frac{1}{2}-2$
6039.60	40	16552.81	$C\frac{1}{2}-2$
6019.19	40	16608.94	$^{5}I\frac{1}{2}-2$
6017.57	30	16613.41	$^{7}M\frac{1}{2}-2$
6016.73	20	16615.73	$^{7}K\frac{1}{2}-2$
6010.86	20	16631.95	$D\frac{1}{2}-2$
6006.91	10	16642.89	$A\frac{1}{2}-2$
5999.41	40	16663.70	$A\frac{1}{2}-2$
5997.96	30	16667.73	$^{5}K\frac{1}{2}-2$
5997.31	150	16669.54	$^{7}M\frac{1}{2}-2$
5986.10	150	16700.75	$A\frac{1}{2}-2$
5982.87	8	16709.77	$^{7}K\frac{1}{2}-2$
5978.70	10	16721.42	$B\frac{1}{2}-2$
5976.32	200	16728.07	$A\frac{1}{2}-2$
5971.50	250	16741.58	$^{5}K\frac{1}{2}-1$
5955.86	60	16782.74	$^{5}H\frac{1}{2}-2$
5949.66	20	16803.05	$^{5}K\frac{1}{2}-2$
5948.57	40	16806.12	$A\frac{1}{2}-2$
5947.69	15	16808.62	$^{7}M\frac{1}{2}-2$
5942.77	25	16822.52	$^{7}K\frac{1}{2}-2$
5933.82	60	16847.90	$^{5}K\frac{1}{2}-1$
5929.33	25	16860.67	$A\frac{1}{2}-2$
5925.46	20	16871.66	$A\frac{1}{2}-2$
5915.40	600	16900.36	$^{5}L\frac{1}{2}-1$
5905.13	4	16929.75	$^{5}L\frac{1}{2}-1$
5898.78	80	16947.96	$^{7}M\frac{1}{2}-2$
5892.62	40	16965.69	$A\frac{1}{2}-2$
5878.07	3	17007.69	$B\frac{1}{2}-2$
5862.02	12	17054.27	$^{5}K\frac{1}{2}-2$
5856.45	20	17070.47	$^{5}L\frac{1}{2}-1$
5849.17	8	17091.71	$^{5}I\frac{1}{2}-2$

TABLE 4.—*Classified lines of* U I—Continued

λ_{air}A	Intensity	ν_{vac}cm^{-1}	Term combination
5836.03	80	17130.19	D$\frac{1}{2}$—274$_3$
5835.19	8	17132.67	B$\frac{1}{2}$—278$_3$
5831.82	10	17142.57	A$\frac{1}{2}$—209$_3$
5819.01	8	17180.30	^{7}K$\frac{1}{2}$—241$_7$
5817.92	8	17183.50	^{5}I$\frac{1}{2}$—216$_3$
5814.42	25	17193.87	A$\frac{1}{2}$—210$_4$
5813.83	20	17195.61	^{5}H$\frac{1}{2}$—231$_4$
5802.11	60	17230.34	C$\frac{1}{2}$—253$_3$
5800.78	8	17234.28	B$\frac{1}{2}$—245$_7$
5787.60	6	17273.55	^{5}K$\frac{1}{2}$—178$_4$
5784.11	8	17283.96	B$\frac{1}{2}$—279$_3$
5782.81	10	17287.86	^{5}K$\frac{1}{2}$—179$_3$
5780.59	100	17294.49	^{7}M$\frac{1}{2}$—235$_7$
5771.05	30	17323.08	^{7}M$\frac{1}{2}$—235$_3$
5767.43	15	17333.95	^{5}H$\frac{1}{2}$—233$_3$
5763.63	15	17345.38	B$\frac{1}{2}$—246$_3$
5758.35	25	17361.27	^{5}K$\frac{1}{2}$—216$_3$
5758.14	40	17361.94	^{5}L$\frac{1}{2}$—173$_3$
5737.27	25	17425.08	^{7}K$\frac{1}{2}$—231$_4$
5736.38	30	17427.78	^{7}K$\frac{1}{2}$—244$_3$
5732.74	5	17438.86	^{5}H$\frac{1}{2}$—234$_4$
5731.87	10	17441.49	^{5}H$\frac{1}{2}$—234$_3$
5731.49	8	17442.64	^{7}K$\frac{1}{2}$—244$_5$
5716.87	20	17487.25	^{5}I$\frac{1}{2}$—219$_3$
5715.69	10	17490.86	^{5}K$\frac{1}{2}$—217$_3$
5714.20	6	17495.41	^{5}H$\frac{1}{2}$—235$_3$
5702.85	10	17530.24	^{7}M$\frac{1}{2}$—237$_7$
5699.87	20	17539.41	D$\frac{1}{2}$—278$_7$
5695.18	6	17553.85	C$\frac{1}{2}$—256$_7$
5694.85	4	17554.88	^{7}K$\frac{1}{2}$—245$_7$
5691.35	15	17565.65	^{5}K$\frac{1}{2}$—181$_4$
5690.18	3	17569.29	^{5}H$\frac{1}{2}$—235$_4$
5685.19	12	17584.68	^{5}I$\frac{1}{2}$—220$_4$
5680.37	8	17599.61	^{7}M$\frac{1}{2}$—238$_7$
5674.25	8	17618.60	D$\frac{1}{2}$—279$_7$
5669.42	25	17633.60	^{5}K$\frac{1}{2}$—182$_3$
5658.26	15	17668.39	^{7}K$\frac{1}{2}$—234$_4$
5646.49	4	17705.23	A$\frac{1}{2}$—292$_4$
5645.92	40	17706.99	C$\frac{1}{2}$—258$_3$
5640.30	40	17724.63	^{7}K$\frac{1}{2}$—235$_3$
5634.38	80	17743.26	A$\frac{1}{2}$—253$_3$
5625.43	5	17771.49	D$\frac{1}{2}$—281$_7$
5622.54	30	17780.63	^{5}K$\frac{1}{2}$—220$_3$
5621.51	100	17783.89	A$\frac{1}{2}$—215$_3$
5620.78	200	17786.21	^{5}K$\frac{1}{2}$—184$_3$
5616.88	10	17798.53	^{7}K$\frac{1}{2}$—235$_4$
5616.58	80	17799.51	C$\frac{1}{2}$—259$_3$
5614.74	40	17805.34	D$\frac{1}{2}$—282$_7$
5613.26	30	17810.04	^{7}K$\frac{1}{2}$—235$_3$
5610.89	150	17817.56	^{7}M$\frac{1}{2}$—240$_7$
5591.10	30	17880.61	B$\frac{1}{2}$—285$_7$
5584.62	40	17901.36	^{7}K$\frac{1}{2}$—249$_3$
5577.46	8	17924.34	^{5}I$\frac{1}{2}$—223$_3$
5573.59	60	17936.80	^{7}M$\frac{1}{2}$—241$_7$
5573.07	60	17938.47	D$\frac{1}{2}$—283$_7$
5572.09	15	17941.63	^{5}H$\frac{1}{2}$—239$_3$
5568.48	40	17953.24	^{7}K$\frac{1}{2}$—237$_3$
5564.17	300	17967.16	A$\frac{1}{2}$—218$_3$
5559.88	20	17981.03	A$\frac{1}{2}$—256$_3$
5546.97	6	18022.87	B$\frac{1}{2}$—253$_3$

TABLE 4.—*Classified lines of* U I—Continued

λ_{air}A	Intensity	ν_{vac}cm^{-1}	Term combination
5545.75	4	18026.83	A$\frac{1}{2}$—256$_7$
5534.72	50	18062.76	B$\frac{1}{2}$—253$_3$
5531.26	100	18074.05	C$\frac{1}{2}$—261$_3$
5527.98	80	18084.80	^{7}M$\frac{1}{2}$—243$_7$
5526.33	30	18090.18	C$\frac{1}{2}$—261$_7$
5522.20	5	18103.70	D$\frac{1}{2}$—284$_7$
5517.16	10	18120.25	B$\frac{1}{2}$—252$_4$
5511.49	250	18138.88	^{5}K$\frac{1}{2}$—187$_3$
5507.77	10	18151.14	A$\frac{1}{2}$—312$_3$
5502.18	60	18169.57	A$\frac{1}{2}$—220$_4$
5501.82	25	18170.78	^{7}K$\frac{1}{2}$—239$_3$
5500.69	120	18174.51	A$\frac{1}{2}$—297$_4$
5497.75	15	18184.23	^{7}M$\frac{1}{2}$—244$_3$
5496.43	150	18188.59	^{5}K$\frac{1}{2}$—224$_3$
5494.59	25	18194.68	C$\frac{1}{2}$—263$_3$
5487.24	6	18219.04	D$\frac{1}{2}$—285$_7$
5477.99	6	18249.82	^{7}K$\frac{1}{2}$—252$_3$
5467.11	8	18286.14	^{7}M$\frac{1}{2}$—245$_3$
5459.27	15	18312.41	^{5}K$\frac{1}{2}$—189$_3$
5458.88	8	18313.69	^{7}K$\frac{1}{2}$—253$_3$
5452.41	40	18335.44	C$\frac{1}{2}$—264$_3$
5445.87	10	18357.44	^{5}K$\frac{1}{2}$—226$_7$
5441.09	6	18373.59	C$\frac{1}{2}$—265$_3$
5431.35	50	18406.54	^{5}L$\frac{1}{2}$—184$_3$
5426.68	20	18422.38	^{7}M$\frac{1}{2}$—246$_3$
5418.10	6	18451.53	D$\frac{1}{2}$—287$_7$
5414.76	30	18462.92	B$\frac{1}{2}$—257$_3$
5410.24	80	18478.34	^{5}K$\frac{1}{2}$—227$_3$
5406.87	100	18489.86	C$\frac{1}{2}$—266$_7$
5404.90	8	18496.60	A$\frac{1}{2}$—223$_4$
5401.90	30	18506.87	^{5}K$\frac{1}{2}$—191$_4$
5399.54	10	18514.98	A$\frac{1}{2}$—224$_4$
5390.28	10	18546.77	A$\frac{1}{2}$—261$_3$
5389.46	6	18549.60	B$\frac{1}{2}$—256$_4$
5385.54	100	18563.10	A$\frac{1}{2}$—261$_7$
5384.22	50	18567.64	A$\frac{1}{2}$—223$_7$
5382.94	100	18572.07	^{5}K$\frac{1}{2}$—192$_4$
5379.96	6	18582.34	A$\frac{1}{2}$—223$_3$
5378.68	6	18586.78	^{5}K$\frac{1}{2}$—228$_3$
5377.16	12	18592.03	B$\frac{1}{2}$—259$_3$
5375.76	80	18596.86	C$\frac{1}{2}$—267$_3$
5375.50	40	18597.76	A$\frac{1}{2}$—301$_3$
5371.35	15	18612.13	B$\frac{1}{2}$—259$_3$
5359.43	20	18653.54	B$\frac{1}{2}$—293$_3$
5356.58	20	18663.46	A$\frac{1}{2}$—224$_3$
5355.58	30	18666.92	^{7}K$\frac{1}{2}$—256$_7$
5355.37	15	18667.66	A$\frac{1}{2}$—263$_3$
5354.36	12	18671.18	^{7}K$\frac{1}{2}$—244$_3$
5348.99	12	18689.95	D$\frac{1}{2}$—290$_3$
5341.50	120	18716.14	A$\frac{1}{2}$—225$_4$
5338.26	10	18727.51	B$\frac{1}{2}$—294$_3$
5336.54	120	18733.55	^{5}I$\frac{1}{2}$—231$_4$
5329.26	150	18759.14	^{5}L$\frac{1}{2}$—187$_3$
5327.32	40	18765.96	^{5}H$\frac{1}{2}$—247$_4$
5324.03	20	18777.57	B$\frac{1}{2}$—261$_3$
5322.78	60	18781.98	^{5}K$\frac{1}{2}$—230$_7$
5319.01	15	18795.28	A$\frac{1}{2}$—312$_3$
5315.27	150	18808.51	A$\frac{1}{2}$—264$_3$
5308.54	300	18832.34	A$\frac{1}{2}$—226$_7$
5304.57	40	18846.44	A$\frac{1}{2}$—265$_3$

TABLE 4.—*Classified lines of* U I—Continued

λ_{air} A	Intensity	ν_{vac} cm^{-1}	Term combination
5303.09	20	18851.70	$^5K_{\frac{3}{2}}-194_5$
5300.57	120	18860.68	$C_{\frac{7}{2}}-269_8$
5299.44	100	18864.69	$B_{\frac{5}{2}}-295_9$
5297.44	150	18871.81	$^5I_{\frac{7}{2}}-233_5$
5286.93	60	18909.30	$^7K_{\frac{3}{2}}-246_9$
5283.58	50	18921.32	$^5K_{\frac{3}{2}}-231_7$
5281.99	15	18927.00	$B_{\frac{3}{2}}-296_8$
5280.54	50	18932.22	$^5K_{\frac{3}{2}}-195_4$
5280.38	300	18932.78	$^5L_{\frac{3}{2}}-189_5$
5275.93	80	18948.76	$B_{\frac{7}{2}}-262_7$
5275.19	12	18951.40	$A_{\frac{3}{2}}-266_8$
5274.68	10	18953.24	$A_{\frac{7}{2}}-227_6$
5272.01	100	18962.85	$A_{\frac{3}{2}}-266_7$
5270.62	100	18967.82	$C_{\frac{7}{2}}-271_8$
5267.42	30	18979.37	$^5I_{\frac{7}{2}}-234_5$
5267.10	5	18980.50	$A_{\frac{3}{2}}-321_9$
5265.38	50	18986.72	$^7M_{\frac{3}{2}}-252_6$
5265.25	60	18987.18	$B_{\frac{7}{2}}-263_9$
5264.76	8	18988.94	$A_{\frac{5}{2}}-227_5$
5259.90	80	19006.48	$^7M_{\frac{3}{2}}-252_5$
5258.73	4	19010.73	$^5I_{\frac{7}{2}}-234_3$
5254.13	4	19027.37	$^5K_{\frac{3}{2}}-196_5$
5244.70	20	19061.56	$A_{\frac{5}{2}}-228_6$
5242.33	12	19070.19	$^7M_{\frac{3}{2}}-253_5$
5234.16	120	19099.95	$^7M_{\frac{3}{2}}-253_9$
5232.81	30	19104.88	$B_{\frac{3}{2}}-297_7$
5232.18	10	19107.18	$^5I_{\frac{7}{2}}-235_4$
5231.02	20	19111.43	$B_{\frac{3}{2}}-298_9$
5229.30	25	19117.69	$A_{\frac{5}{2}}-229_7$
5226.51	15	19127.93	$B_{\frac{7}{2}}-264_9$
5221.90	80	19144.82	$^7K_{\frac{3}{2}}-249_5$
5218.56	12	19157.06	$^5K_{\frac{3}{2}}-234_5$
5216.92	80	19163.06	$^5K_{\frac{3}{2}}-197_6$
5215.18	40	19169.46	$^5H_{\frac{3}{2}}-251_3$
5212.74	10	19178.46	$^7K_{\frac{3}{2}}-249_4$
5210.48	8	19186.76	$^5H_{\frac{3}{2}}-251_5$
5203.20	10	19213.62	$^7M_{\frac{3}{2}}-254_6$
5201.47	20	19220.01	$^7K_{\frac{3}{2}}-262_8$
5198.00	12	19232.83	$^5H_{\frac{3}{2}}-252_4$
5192.01	25	19255.03	$^7K_{\frac{3}{2}}-250_3$
5191.51	40	19256.88	$A_{\frac{7}{2}}-230_7$
5189.54	6	19264.20	$^5H_{\frac{3}{2}}-252_5$
5189.21	30	19265.40	$D_{\frac{7}{2}}-296_9$
5188.57	25	19267.78	$^5K_{\frac{3}{2}}-235_7$
5180.89	50	19296.35	$^5K_{\frac{3}{2}}-235_6$
5180.03	12	19299.53	$^7K_{\frac{3}{2}}-263_5$
5177.22	8	19310.04	$A_{\frac{7}{2}}-231_8$
5170.90	12	19333.63	$A_{\frac{3}{2}}-269_9$
5168.79	20	19341.50	$B_{\frac{3}{2}}-300_8$
5168.25	10	19343.52	$A_{\frac{3}{2}}-270_9$
5166.74	20	19349.17	$A_{\frac{3}{2}}-308_9$
5164.14	200	19358.93	$C_{\frac{7}{2}}-274_8$
5160.67	15	19371.96	$^5I_{\frac{7}{2}}-238_4$
5156.03	25	19389.37	$B_{\frac{7}{2}}-267_6$
5155.50	8	19391.37	$A_{\frac{3}{2}}-309_8$
5154.22	15	19396.20	$A_{\frac{7}{2}}-231_7$
5148.95	15	19416.04	$^7K_{\frac{3}{2}}-251_5$
5146.98	40	19423.46	$^7M_{\frac{3}{2}}-256_7$
5144.52	60	19432.78	$B_{\frac{7}{2}}-268_9$
5144.11	10	19434.31	$A_{\frac{3}{2}}-309_4$

TABLE 4.—*Classified lines of* U I—Continued

λ_{air} A	Intensity	ν_{vac} cm^{-1}	Term combinati
5142.72	10	19439.56	$^5K_{\frac{3}{2}}-22$
5142.40	60	19440.78	$A_{\frac{3}{2}}-27$
5139.98	35	19449.94	$D_{\frac{7}{2}}-29$
5136.74	6	19462.18	$^7K_{\frac{3}{2}}-23$
5134.19	8	19471.85	$^5L_{\frac{3}{2}}-19$
5132.20	40	19479.42	$^5I_{\frac{7}{2}}-23$
5130.16	8	19487.14	$C_{\frac{7}{2}}-27$
5129.34	15	19490.28	$D_{\frac{7}{2}}-29$
5128.36	15	19493.98	$^5K_{\frac{3}{2}}-20$
5125.86	12	19503.51	$^5K_{\frac{3}{2}}-23$
5125.49	25	19504.89	$A_{\frac{3}{2}}-27$
5119.51	25	19527.71	$^5K_{\frac{3}{2}}-20$
5110.69	30	19561.39	$^7K_{\frac{3}{2}}-25$
5107.68	40	19572.94	$^5K_{\frac{3}{2}}-25$
5106.74	30	19576.54	$^7M_{\frac{3}{2}}-32$
5104.03	8	19586.93	$^7K_{\frac{3}{2}}-23$
5101.74	10	19595.71	$A_{\frac{3}{2}}-28$
5101.01	40	19598.51	$^5K_{\frac{3}{2}}-25$
5097.88	6	19610.54	$D_{\frac{7}{2}}-30$
5093.89	20	19625.91	$^7K_{\frac{3}{2}}-26$
5088.29	120	19647.52	$^5L_{\frac{3}{2}}-19$
5086.83	15	19653.15	$B_{\frac{7}{2}}-29$
5084.52	10	19662.06	$^5H_{\frac{3}{2}}-25$
5080.99	3	19675.75	$A_{\frac{3}{2}}-32$
5076.99	10	19691.23	$^5K_{\frac{3}{2}}-20$
5076.77	50	19692.10	$A_{\frac{3}{2}}-23$
5074.78	50	19699.83	$C_{\frac{7}{2}}-27$
5063.77	150	19742.66	$A_{\frac{3}{2}}-23$
5061.76	10	19750.49	$^5K_{\frac{3}{2}}-24$
5061.50	30	19751.48	$B_{\frac{3}{2}}-29$
5061.03	25	19753.34	$^7K_{\frac{3}{2}}-25$
5059.25	10	19760.30	$B_{\frac{7}{2}}-27$
5057.18	40	19768.35	$C_{\frac{7}{2}}-27$
5056.46	30	19771.18	$A_{\frac{3}{2}}-23$
5053.35	60	19783.35	$^5L_{\frac{3}{2}}-19$
5051.43	25	19790.88	$^5K_{\frac{3}{2}}-24$
5049.06	30	19800.18	$^5K_{\frac{3}{2}}-24$
5045.39	5	19814.56	$^5H_{\frac{3}{2}}-23$
5042.31	15	19826.66	$^5L_{\frac{3}{2}}-19$
5035.20	4	19854.65	$^7M_{\frac{3}{2}}-26$
5027.38	400	19885.54	$^5L_{\frac{3}{2}}-19$
5022.64	10	19904.30	$C_{\frac{7}{2}}-27$
5021.18	20	19910.09	$^5K_{\frac{3}{2}}-24$
5019.89	15	19915.20	$^7K_{\frac{3}{2}}-26$
5016.25	5	19929.66	$C_{\frac{7}{2}}-28$
5012.92	25	19942.90	$A_{\frac{3}{2}}-31$
5011.42	120	19948.90	$^5K_{\frac{3}{2}}-25$
5009.39	15	19956.94	$A_{\frac{3}{2}}-23$
5008.68	30	19959.79	$^7M_{\frac{3}{2}}-29$
5004.01	50	19978.42	$A_{\frac{3}{2}}-32$
4999.95	20	19994.66	$^5I_{\frac{7}{2}}-24$
4998.56	8	20000.20	$C_{\frac{7}{2}}-28$
4998.41	8	20000.78	$^5K_{\frac{3}{2}}-26$
4990.12	30	20034.04	$C_{\frac{7}{2}}-28$
4988.32	10	20041.24	$^5K_{\frac{3}{2}}-26$
4986.69	5	20047.82	$A_{\frac{7}{2}}-23$
4985.82	8	20051.32	$B_{\frac{3}{2}}-30$
4984.62	15	20056.14	$^7M_{\frac{3}{2}}-29$
4984.12	15	20058.12	$^5K_{\frac{3}{2}}-24$
4981.95	25	20066.88	$^7K_{\frac{3}{2}}-27$

TABLE 4.—*Classified lines of* U I—Continued

λ_{air}A	Intensity	ν_{vac}cm^{-1}	Term combination
4978.22	8	20081.91	$^5I_4^1 - 245_5$
4972.72	10	20104.12	$D_7^2 - 302_6$
4970.20	20	20114.32	$^5L_4^1 - 201_5$
4967.33	120	20125.93	$A_7^2 - 239_5$
4963.31	15	20142.26	$^7M_4^1 - 263_7$
4961.10	20	20151.20	$B_7^2 - 274_5$
4959.55	25	20157.53	$^5K_4^1 - 244_6$
4955.90	10	20172.34	$^5K_4^1 - 244_5$
4955.78	120	20172.83	$A_4^2 - 278_5$
4954.96	50	20176.18	$^7K_4^1 - 259_6$
4949.41	5	20198.80	$A_7^2 - 317_5$
4944.52	80	20218.80	$^5L_4^1 - 202_5$
4941.47	10	20231.25	$^5K_4^1 - 208_5$
4934.56	10	20259.60	$^5K_4^1 - 245_5$
4933.06	50	20265.75	$A_7^2 - 240_7$
4928.44	100	20284.74	$^5K_4^1 - 245_7$
4921.38	30	20313.84	$^5H_4^1 - 263_5$
4919.13	25	20323.13	$^5K_4^1 - 209_6$
4918.90	15	20324.07	$A_4^2 - 279_5$
4916.88	40	20332.45	$C_7^2 - 284_7$
4910.35	120	20359.49	$^7M_4^1 - 266_7$
4906.29	10	20376.33	$^7K_4^1 - 273_5$
4904.21	15	20384.98	$A_7^2 - 241_7$
4901.64	8	20395.68	$^5K_4^1 - 246_5$
4896.39	5	20417.55	$B_7^2 - 277_6$
4895.68	15	20420.51	$^5L_4^1 - 204_6$
4889.16	8	20447.74	$C_7^2 - 285_7$
4885.15	120	20464.51	$^5L_4^1 - 204_7$
4879.76	10	20487.10	$^5I_4^1 - 249_4$
4878.50	30	20492.39	$B_7^2 - 278_5$
4878.16	5	20493.84	$^7K_4^1 - 274_6$
4874.35	20	20509.83	$^7M_4^1 - 268_6$
4868.87	25	20532.95	$A_7^2 - 243_7$
4866.59	6	20542.56	$^7M_4^1 - 269_6$
4866.48	4	20543.00	$^7K_4^1 - 263_5$
4856.65	50	20584.57	$B_4^2 - 312_5$
4852.96	20	20600.26	$^7K_4^1 - 275_5$
4850.59	8	20610.30	$^7K_4^1 - 276_5$
4848.00	30	20621.33	$^5L_4^1 - 206_5$
4845.67	15	20631.23	$^5K_4^1 - 249_5$
4842.48	80	20644.82	$^5K_4^1 - 212_6$
4841.04	12	20650.97	$A_7^2 - 244_5$
4835.91	8	20672.88	$B_4^2 - 314_7$
4834.18	12	20680.27	$C_7^2 - 287_7$
4827.86	4	20707.34	$^5I_4^1 - 251_5$
4816.84	4	20754.72	$^7K_4^1 - 265_4$
4816.47	5	20756.30	$C_7^2 - 289_5$
4815.71	80	20759.57	$B_4^2 - 314_5$
4814.11	12	20766.50	$^5L_4^1 - 207_7$
4812.72	10	20772.47	$^7K_4^1 - 277_5$
4810.90	100	20780.36	$A_7^2 - 245_5$
4808.03	5	20792.73	$B_7^2 - 281_7$
4805.22	3	20804.88	$^7K_4^1 - 265_5$
4800.23	10	20826.54	$B_7^2 - 282_7$
4794.50	10	20851.44	$^5L_4^1 - 208_5$
4791.57	6	20864.18	$^5H_4^1 - 268_5$
4790.38	5	20869.36	$^7K_4^1 - 266_6$
4790.06	80	20870.73	$A_7^2 - 246_5$
4789.03	6	20875.22	$C_7^2 - 289_5$
4787.60	8	20881.49	$^7K_4^1 - 278_7$

TABLE 4.—*Classified lines of* U I—Continued

λ_{air}A	Intensity	ν_{vac}cm^{-1}	Term combination
4782.81	8	20902.38	$^5K_4^1 - 251_5$
4779.09	8	20918.66	$C_7^2 - 290_5$
4777.67	80	20924.86	$^5K_4^1 - 215_4$
4773.43	60	20943.45	$^5L_4^1 - 209_5$
4768.66	60	20964.39	$^5K_4^1 - 215_5$
4761.34	15	20996.65	$^7K_4^1 - 268_5$
4756.81	120	21016.64	$^5K_4^1 - 216_5$
4750.72	8	21043.56	$^5K_4^1 - 253_5$
4744.30	12	21072.04	$A_4^2 - 249_4$
4744.04	12	21073.22	$^5K_4^1 - 253_5$
4743.53	50	21075.48	$^7M_4^1 - 273_7$
4739.50	4	21093.40	$^7K_4^1 - 281_5$
4738.44	30	21098.10	$D_7^2 - 314_5$
4732.43	5	21124.92	$B_7^2 - 284_7$
4730.68	25	21132.70	$^7M_4^1 - 273_5$
4727.66	20	21146.21	$^5K_4^1 - 217_6$
4727.34	25	21147.63	$^5K_4^1 - 218_5$
4715.68	120	21199.93	$^5I_4^1 - 256_4$
4706.74	8	21240.18	$B_7^2 - 285_7$
4701.23	50	21265.10	$^5L_4^1 - 212_5$
4697.87	8	21280.32	$^7K_4^1 - 283_7$
4696.06	12	21288.53	$B_4^2 - 319_7$
4695.23	25	21292.27	$A_4^2 - 251_5$
4694.71	15	21294.64	$C_7^2 - 294_5$
4691.26	10	21310.30	$^7K_4^1 - 270_5$
4686.92	30	21330.00	$^5L_4^1 - 213_5$
4682.00	40	21352.43	$^5I_4^1 - 258_5$
4681.06	6	21356.74	$^7M_4^1 - 275_5$
4666.66	8	21422.65	$B_4^2 - 321_5$
4663.75	120	21435.98	$^5K_4^1 - 220_5$
4662.83	10	21440.22	$C_7^2 - 295_5$
4661.65	30	21445.64	$^7K_4^1 - 284_7$
4651.13	12	21494.14	$C_7^2 - 296_5$
4643.61	50	21528.98	$^7M_4^1 - 277_5$
4639.36	6	21548.69	$B_7^2 - 289_6$
4633.51	8	21575.90	$D_7^2 - 319_5$
4631.62	100	21584.67	$^5L_4^1 - 215_5$
4630.90	8	21588.03	$A_7^2 - 253_5$
4623.91	5	21620.69	$D_7^2 - 318_7$
4620.44	60	21636.94	$^5L_4^1 - 216_5$
4620.23	300	21637.88	$^7M_4^1 - 278_7$
4618.75	8	21644.85	$^7K_4^1 - 287_5$
4612.93	8	21672.16	$C_7^2 - 297_7$
4608.35	6	21693.66	$A_4^2 - 293_6$
4605.42	4	21707.50	$B_7^2 - 290_6$
4603.43	12	21716.87	$^7M_4^1 - 279_7$
4599.07	4	21737.46	$^7K_4^1 - 274_6$
4594.85	8	21757.44	$^5K_4^1 - 223_5$
4593.65	5	21763.12	$^5K_4^1 - 224_4$
4592.93	15	21766.53	$^5L_4^1 - 217_6$
4592.63	5	21767.95	$^5L_4^1 - 218_6$
4588.65	15	21786.83	$^5H_4^1 - 277_5$
4577.59	4	21839.47	$C_7^2 - 300_7$
4576.64	80	21843.97	$^5K_4^1 - 224_5$
4575.03	8	21851.68	$^5I_4^1 - 263_5$
4574.27	6	21855.32	$^7K_4^1 - 288_5$
4571.68	8	21867.69	$C_7^2 - 299_6$
4571.24	10	21869.81	$^7M_4^1 - 281_7$
4563.95	40	21904.72	$A_4^2 - 295_5$
4558.05	25	21933.09	$^5K_4^1 - 261_7$

TABLE 4.—*Classified lines of* U I—Continued

λ_{air}A	Intensity	ν_{vac}cm^{-1}	Term combination
4554.59	4	21949.73	$^5K_3^1-262_3$
4551.98	80	21962.31	$^5K_3^2-225_3$
4551.58	15	21964.27	$^5K_3^1-225_4$
4550.98	12	21967.15	$A_3^1-296_3$
4546.62	8	21988.24	$A_3^1-257_3$
4546.10	6	21990.76	$A_3^1-257_6$
4544.36	15	21999.17	$^5K_3^2-262_7$
4539.08	12	22024.75	$A_3^1-258_6$
4536.60	20	22036.76	$^7M_3^1-283_7$
4532.58	12	22056.31	$^5L_3^1-220_3$
4531.14	10	22063.33	$^5I_3^1-265_4$
4526.25	6	22087.18	$B_3^1-294_3$
4525.98	8	22088.51	$B_3^1-327_7$
4517.40	3	22130.42	$D_3^1-324_6$
4516.73	80	22133.72	$^5K_3^1-227_6$
4514.11	10	22146.56	$B_3^1-292_4$
4504.87	6	22192.01	$A_3^1-299_7$
4504.16	5	22195.50	$^7M_3^1-284_3$
4499.92	5	22216.39	$C_3^1-301_6$
4494.71	60	22242.18	$^5K_3^1-228_6$
4484.81	5	22291.27	$^5K_3^2-265_3$
4481.07	10	22309.87	$B_3^1-294_2$
4476.46	40	22332.82	$^5K_3^1-266_7$
4469.32	100	22368.51	$^5L_3^1-223_7$
4468.70	4	22371.60	$C_3^1-303_6$
4466.71	4	22381.59	$C_3^1-304_6$
4461.44	8	22408.00	$A_3^1-261_7$
4458.10	5	22424.79	$A_3^1-262_6$
4455.23	5	22439.23	$^5H_3^1-283_4$
4449.66	5	22467.34	$^5I_3^1-269_3$
4449.52	8	22468.07	$C_3^1-305_6$
4448.90	8	22471.18	$B_3^1-298_7$
4448.33	40	22474.05	$A_3^1-262_7$
4446.53	12	22483.18	$^5K_3^1-268_6$
4440.74	60	22512.49	$A_3^1-263_6$
4438.43	6	22524.17	$C_3^1-306_7$
4435.16	6	22540.77	$B_3^1-296_3$
4430.08	30	22566.64	$^5K_3^1-231_4$
4426.94	80	22582.67	$^5L_3^1-225_3$
4425.41	12	22590.47	$A_3^1-263_7$
4421.22	3	22611.84	$^7M_3^1-288_6$
4420.40	20	22616.05	$B_3^1-297_4$
4418.47	25	22625.93	$^7M_3^1-289_3$
4414.75	8	22645.01	$^5K_3^1-269_3$
4414.08	8	22648.46	$A_3^1-265_4$
4413.14	15	22653.29	$A_3^1-264_3$
4412.03	2	22658.98	$^5H_3^1-287_3$
4405.74	20	22691.34	$A_3^1-265_3$
4403.07	4	22705.09	$^5K_3^1-233_3$
4398.10	4	22730.72	$^5I_3^1-271_4$
4394.45	3	22749.59	$A_3^1-265_3$
4393.60	200	22754.01	$^5L_3^1-227_6$
4387.70	6	22784.61	$^7M_3^1-290_3$
4385.48	6	22796.16	$A_3^1-266_3$
4385.38	10	22796.66	$^5K_3^1-270_3$
4383.27	50	22807.62	$A_3^1-266_7$
4382.84	8	22809.86	$^5K_3^2-234_4$
4382.34	40	22812.47	$^5K_3^2-234_3$
4378.90	3	22830.40	$A_3^1-266_6$
4373.60	5	22858.08	$^7M_3^1-291_7$

TABLE 4.—*Classified lines of* U I—Continued

λ_{air}A	Intensity	ν_{vac}cm^{-1}	Term combination
4373.08	4	22860.80	$^7M_3^1-$
4372.76	80	22862.44	$^5L_3^1-$
4372.01	10	22866.36	$^5K_3^1-$
4371.76	100	22867.66	C_3^1-
4369.96	20	22877.11	$^7M_3^1-$
4368.47	6	22884.88	B_3^1-
4362.80	20	22914.64	A_3^1-
4362.05	300	22918.58	$^5L_3^1-$
4357.92	25	22940.30	$^5K_3^1-$
4355.75	80	22951.74	$^5A_3^1-$
4352.59	4	22968.37	B_3^1-
4349.71	4	22983.62	$^7M_3^1-$
4349.07	5	22986.97	A_3^1-
4343.53	3	23016.30	C_3^1-
4337.63	15	23047.61	C_3^1-
4337.40	25	23048.83	$^5K_3^1-$
4335.73	60	23057.71	$^5L_3^1-$
4329.42	6	23091.31	A_3^1-
4328.73	60	23095.00	$^5K_3^1-$
4328.01	5	23098.82	$^7K_3^1-$
4325.38	4	23112.88	$^7K_3^1-$
4323.05	3	23125.35	B_3^1-
4318.09	15	23151.89	$^7M_3^1-$
4317.07	30	23157.37	C_3^1-
4316.48	50	23160.53	C_3^1-
4315.82	5	23164.09	B_3^1-
4313.13	100	23178.50	A_3^1-
4312.39	8	23182.50	C_3^1-
4311.31	4	23188.29	A_3^1-
4309.68	25	23197.06	$^5L_3^1-$
4309.17	30	23199.82	B_3^1-
4308.20	8	23205.06	$^5K_3^1-$
4304.81	4	23223.32	D_3^1-
4303.80	6	23228.79	$^5I_3^1-$
4301.72	15	23240.02	C_3^1-
4297.92	10	23260.56	B_3^1-
4295.88	5	23271.59	A_3^1-
4293.30	30	23285.59	$^5-$
4288.84	200	23309.80	$^7M_3^1-$
4288.70	10	23310.54	B_3^1-
4287.75	6	23315.70	A_3^1-
4287.56	10	23316.76	B_3^1-
4286.00	6	23325.22	$^5L_3^1-$
4285.74	8	23326.67	C_3^1-
4285.23	20	23329.44	$^7K_3^1-$
4283.17	3	23340.63	A_3^1-
4276.10	5	23379.25	A_3^1-
4273.19	6	23395.17	B_3^1-
4271.24	15	23405.85	$^5K_3^1-$
4271.12	3	23406.50	$^5K_3^1-$
4270.25	4	23411.27	B_3^1-
4266.32	40	23432.82	$^5L_3^1-$
4265.18	6	23439.08	$^5H_3^1-$
4259.88	6	23468.23	$^5K_3^1-$
4259.46	12	23470.56	$^7K_3^1-$
4256.91	10	23484.64	$^7K_3^1-$
4256.54	3	23486.69	$^5L_3^1-$
4255.10	5	23494.62	$^7K_3^1-$
4253.71	8	23502.29	$^5K_3^1-$
4249.83	4	23523.74	$^5-$

TABLE 4.—*Classified lines of* U I—Continued

λ_{air}A	Intensity	ν_{vac}cm^{-1}	Term combination
4246.58	2	23541.73	$^{7}M\frac{1}{2}-297_{7}$
4246.26	100	23543.52	$^{5}L\frac{4}{2}-235_{7}$
4241.11	15	23572.12	$^{5}L\frac{3}{2}-235_{6}$
4233.13	25	23616.55	$^{7}M\frac{3}{2}-298_{6}$
4231.67	60	23624.71	$A\frac{3}{2}-312_{9}$
4230.51	6	23631.18	$^{7}K\frac{1}{2}-306_{3}$
4226.54	3	23653.37	$^{6}H\frac{1}{2}-296_{3}$
4226.17	3	23655.46	$A\frac{3}{2}-313_{7}$
4225.32	3	23660.21	$B\frac{3}{2}-309_{3}$
4224.36	10	23665.57	$^{5}K\frac{3}{2}-278_{6}$
4222.36	150	23676.76	$A\frac{5}{2}-274_{3}$
4219.96	25	23690.25	$^{5}K\frac{3}{2}-279_{7}$
4218.46	8	23698.70	$B\frac{5}{2}-310_{7}$
4216.61	6	23709.07	$^{7}M\frac{3}{2}-300_{7}$
4215.99	8	23712.57	$D\frac{9}{2}-340_{7}$
4215.88	4	23713.16	$A\frac{3}{2}-314_{7}$
4215.50	5	23715.32	$^{5}L\frac{4}{2}-237_{6}$
4211.60	30	23737.31	$^{7}M\frac{3}{2}-299_{3}$
4209.83	3	23747.28	$^{5}K\frac{3}{2}-279_{6}$
4207.92	5	23758.02	$D\frac{9}{2}-341_{3}$
4204.16	12	23779.26	$^{5}L\frac{4}{2}-237_{7}$
4199.63	10	23804.95	$A\frac{5}{2}-275_{3}$
4198.22	40	23812.93	$^{5}K\frac{3}{2}-244_{3}$
4196.40	8	23823.24	$^{5}K\frac{1}{2}-281_{6}$
4195.62	4	23827.71	$^{5}K\frac{3}{2}-244_{3}$
4193.42	5	23840.17	$B\frac{5}{2}-311_{7}$
4192.91	10	23843.09	$^{5}K\frac{3}{2}-281_{7}$
4191.94	30	23848.63	$^{5}L\frac{4}{2}-238_{7}$
4191.77	3	23849.60	$C\frac{7}{2}-318_{7}$
4186.96	30	23876.97	$^{5}K\frac{3}{2}-282_{7}$
4183.26	20	23898.08	$C\frac{7}{2}-320_{7}$
4180.31	30	23914.97	$^{5}K\frac{1}{2}-245_{3}$
4177.49	4	23931.12	$^{7}K\frac{1}{2}-309_{3}$
4177.19	3	23932.82	$^{5}L\frac{4}{2}-239_{3}$
4175.40	5	23943.09	$A\frac{5}{2}-277_{6}$
4173.68	12	23952.97	$B\frac{5}{2}-312_{3}$
4169.85	5	23974.92	$B\frac{3}{2}-313_{7}$
4169.06	50	23979.52	$C\frac{7}{2}-321_{7}$
4167.04	20	23991.14	$^{5}I\frac{1}{2}-284_{3}$
4163.75	25	24010.08	$^{5}K\frac{1}{2}-283_{7}$
4162.43	60	24017.68	$A\frac{5}{2}-278_{3}$
4160.95	40	24026.20	$^{5}L\frac{4}{2}-240_{3}$
4160.28	4	24030.10	$^{7}M\frac{1}{2}-302_{7}$
4157.64	8	24045.34	$^{7}M\frac{3}{2}-300_{3}$
4156.82	6	24050.06	$^{5}I\frac{1}{2}-285_{3}$
4156.66	100	24051.04	$^{5}K\frac{1}{2}-246_{3}$
4153.97	150	24066.58	$^{5}L\frac{4}{2}-240_{7}$
4147.62	3	24103.46	$^{7}K\frac{1}{2}-298_{3}$
4145.23	4	24117.34	$B\frac{3}{2}-312_{4}$
4144.93	3	24119.09	$B\frac{5}{2}-314_{3}$
4141.86	25	24136.94	$^{5}K\frac{3}{2}-247_{6}$
4139.30	15	24151.88	$^{6}H\frac{1}{2}-301_{3}$
4137.03	5	24165.13	$A\frac{5}{2}-279_{7}$
4136.44	10	24168.59	$^{5}K\frac{1}{2}-284_{3}$
4133.50	30	24185.78	$^{5}L\frac{4}{2}-241_{7}$
4132.02	5	24194.47	$^{5}K\frac{3}{2}-284_{3}$
4130.66	8	24202.40	$^{7}M\frac{1}{2}-302_{3}$
4127.34	8	24221.90	$A\frac{5}{2}-279_{3}$
4125.78	3	24231.05	$^{6}H\frac{1}{2}-302_{3}$
4124.03	3	24241.32	$^{7}M\frac{3}{2}-303_{3}$

TABLE 4.—*Classified lines of* U I—Continued

λ_{air}A	Intensity	ν_{vac}cm^{-1}	Term combination
4123.00	5	24247.38	$A\frac{7}{2}-280_{7}$
4119.09	4	24270.41	$^{7}K\frac{1}{2}-312_{7}$
4117.91	4	24277.34	$A\frac{3}{2}-319_{3}$
4116.35	6	24286.54	$^{5}K\frac{3}{2}-249_{3}$
4115.65	8	24290.67	$^{5}K\frac{3}{2}-285_{7}$
4111.02	15	24318.01	$A\frac{7}{2}-281_{7}$
4110.66	4	24320.18	$^{5}K\frac{1}{2}-249_{4}$
4109.22	3	24328.68	$A\frac{5}{2}-319_{7}$
4108.36	30	24333.77	$^{5}L\frac{4}{2}-243_{7}$
4105.32	10	24351.80	$A\frac{7}{2}-282_{7}$
4101.91	50	24372.03	$C\frac{7}{2}-324_{3}$
4099.27	6	24387.75	$^{7}M\frac{3}{2}-306_{3}$
4097.75	15	24396.79	$^{5}K\frac{3}{2}-250_{3}$
4091.64	50	24433.24	$^{5}L\frac{4}{2}-244_{3}$
4089.16	8	24448.02	$^{5}L\frac{3}{2}-244_{3}$
4086.68	6	24462.86	$A\frac{3}{2}-321_{3}$
4083.04	6	24484.64	$A\frac{7}{2}-283_{9}$
4076.63	12	24523.18	$^{5}K\frac{3}{2}-287_{7}$
4075.48	4	24530.07	$B\frac{3}{2}-316_{7}$
4074.62	15	24535.26	$^{5}L\frac{3}{2}-245_{3}$
4073.55	15	24541.73	$^{7}K\frac{1}{2}-303_{4}$
4072.84	10	24546.02	$^{7}K\frac{1}{2}-315_{3}$
4070.89	20	24557.72	$^{5}K\frac{1}{2}-251_{5}$
4068.38	4	24572.91	$^{7}K\frac{1}{2}-301_{3}$
4066.29	20	24585.51	$A\frac{3}{2}-284_{4}$
4064.38	6	24597.06	$B\frac{7}{2}-319_{3}$
4064.03	6	24599.20	$^{5}K\frac{3}{2}-289_{6}$
4061.35	25	24615.41	$^{5}K\frac{3}{2}-252_{6}$
4060.61	4	24619.90	$^{5}K\frac{1}{2}-288_{7}$
4059.51	3	24626.59	$^{7}M\frac{3}{2}-307_{6}$
4058.11	30	24635.10	$^{5}K\frac{1}{2}-252_{5}$
4055.94	12	24648.28	$B\frac{7}{2}-319_{7}$
4055.58	10	24650.42	$A\frac{7}{2}-284_{7}$
4051.56	3	24674.92	$A\frac{3}{2}-285_{4}$
4049.20	15	24689.29	$^{7}K\frac{1}{2}-302_{6}$
4049.00	3	24690.53	$B\frac{7}{2}-320_{7}$
4047.62	80	24698.92	$^{5}K\frac{1}{2}-253_{6}$
4042.76	150	24728.64	$^{5}K\frac{3}{2}-253_{6}$
4037.97	8	24757.94	$^{5}K\frac{3}{2}-290_{3}$
4036.73	3	24765.54	$A\frac{7}{2}-285_{7}$
4035.67	4	24772.06	$B\frac{7}{2}-321_{7}$
4035.06	2	24775.80	$^{7}M\frac{1}{2}-310_{7}$
4034.50	30	24779.26	$^{5}I\frac{3}{2}-292_{6}$
4031.60	5	24797.08	$^{5}I\frac{1}{2}-292_{4}$
4025.58	3	24834.14	$^{5}K\frac{1}{2}-291_{6}$
4022.93	3	24850.49	$^{5}K\frac{1}{2}-292_{6}$
4013.84	15	24906.80	$^{5}L\frac{4}{2}-249_{6}$
4008.43	8	24940.40	$^{7}K\frac{3}{2}-319_{3}$
4005.21	80	24960.44	$^{5}I\frac{1}{2}-294_{3}$
4004.90	4	24962.38	$^{7}K\frac{3}{2}-318_{7}$
4002.58	15	24976.82	$^{5}I\frac{3}{2}-295_{3}$
4000.73	8	24988.39	$^{6}H\frac{1}{2}-309_{6}$
3999.18	40	24998.08	$A\frac{5}{2}-287_{7}$
3997.09	30	25011.18	$^{7}K\frac{3}{2}-320_{7}$
3996.13	8	25017.18	$^{5}L\frac{4}{2}-250_{3}$
3994.57	4	25026.96	$^{7}M\frac{3}{2}-312_{7}$
3989.29	8	25060.05	$A\frac{7}{2}-288_{6}$
3983.77	10	25094.77	$A\frac{7}{2}-288_{7}$
3980.80	30	25113.51	$^{7}K\frac{1}{2}-307_{6}$
3978.40	20	25128.64	$A\frac{3}{2}-327_{7}$

TABLE 4.—*Classified lines of* U I—Continued

λ_{air} A	Intensity	ν_{vac} cm^{-1}	Term combination
3977.80	4	25132.42	$^{7}K_{3}^{\frac{1}{2}}-308_{3}$
3974.75	4	25151.75	$B_{7}^{\frac{1}{2}}-324_{3}$
3972.73	3	25164.54	$B_{7}^{\frac{1}{2}}-324_{6}$
3971.67	5	25171.26	$^{5}K_{3}^{\frac{1}{2}}-257_{6}$
3970.59	15	25178.08	$^{5}L_{3}^{\frac{1}{2}}-251_{5}$
3969.42	25	25185.52	$^{5}K_{3}^{\frac{1}{2}}-258_{5}$
3968.52	3	25191.24	$^{5}I_{3}^{\frac{1}{2}}-296_{3}$
3968.26	8	25192.87	$A_{7}^{\frac{1}{2}}-289_{3}$
3966.31	5	25205.23	$^{5}K_{3}^{\frac{1}{2}}-258_{5}$
3964.22	12	25218.51	$^{7}M_{3}^{\frac{1}{2}}-314_{5}$
3961.98	12	25232.78	$A_{7}^{\frac{1}{2}}-290_{4}$
3961.52	40	25235.75	$^{5}L_{3}^{\frac{1}{2}}-252_{4}$
3961.42	25	25236.38	$A_{7}^{\frac{1}{2}}-290_{5}$
3958.93	3	25252.26	$^{5}H_{3}^{\frac{1}{2}}-313_{4}$
3954.10	6	25283.05	$^{5}K_{3}^{\frac{1}{2}}-295_{6}$
3952.45	12	25293.64	$C_{7}^{\frac{1}{2}}-334_{6}$
3951.05	4	25302.57	$^{7}M_{3}^{\frac{1}{2}}-315_{6}$
3950.48	12	25306.27	$A_{7}^{\frac{1}{2}}-291_{7}$
3950.05	3	25308.97	$A_{7}^{\frac{1}{2}}-291_{6}$
3948.99	12	25315.79	$B_{7}^{\frac{1}{2}}-326_{7}$
3948.65	5	25317.95	$^{5}K_{3}^{\frac{1}{2}}-259_{6}$
3948.45	35	25319.27	$^{5}L_{3}^{\frac{1}{2}}-253_{5}$
3947.50	3	25325.32	$A_{7}^{\frac{1}{2}}-292_{6}$
3943.82	200	25348.98	$^{5}L_{3}^{\frac{1}{2}}-253_{6}$
3940.09	4	25373.00	$^{7}K_{3}^{\frac{1}{2}}-311_{6}$
3938.68	3	25382.08	$A_{3}^{\frac{1}{2}}-292_{4}$
3928.45	8	25448.16	$B_{7}^{\frac{1}{2}}-327_{7}$
3926.73	30	25459.33	$^{7}K_{3}^{\frac{1}{2}}-312_{4}$
3926.22	50	25462.62	$^{5}L_{3}^{\frac{1}{2}}-254_{6}$
3924.10	4	25476.34	$^{5}H_{4}^{\frac{1}{2}}-314_{5}$
3923.02	12	25483.36	$^{5}K_{3}^{\frac{1}{2}}-261_{6}$
3921.19	6	25495.24	$^{7}M_{3}^{\frac{1}{2}}-317_{5}$
3918.15	5	25515.03	$^{5}K_{3}^{\frac{1}{2}}-297_{7}$
3917.25	6	25520.94	$C_{7}^{\frac{1}{2}}-336_{6}$
3913.51	6	25545.32	$A_{3}^{\frac{1}{2}}-294_{3}$
3910.96	10	25561.94	$^{5}K_{3}^{\frac{1}{2}}-299_{7}$
3905.12	5	25600.16	$A_{7}^{\frac{1}{2}}-294_{6}$
3904.35	6	25605.23	$^{5}K_{3}^{\frac{1}{2}}-262_{3}$
3903.26	8	25612.37	$A_{7}^{\frac{1}{2}}-294_{3}$
3898.66	4	25642.58	$^{5}H_{4}^{\frac{1}{2}}-316_{4}$
3894.12	120	25672.49	$^{5}L_{3}^{\frac{1}{2}}-256_{7}$
3892.26	3	25684.80	$^{5}K_{3}^{\frac{1}{2}}-263_{3}$
3891.50	6	25689.75	$^{5}I_{3}^{\frac{1}{2}}-301_{5}$
3889.11	10	25705.59	$^{7}K_{3}^{\frac{1}{2}}-314_{5}$
3887.10	4	25718.88	$^{7}M_{3}^{\frac{1}{2}}-318_{7}$
3886.14	4	25725.18	$^{7}M_{3}^{\frac{1}{2}}-319_{7}$
3885.99	8	25726.18	$^{7}K_{3}^{\frac{1}{2}}-315_{5}$
3881.15	4	25758.31	$A_{7}^{\frac{1}{2}}-295_{5}$
3879.53	30	25769.02	$^{5}I_{3}^{\frac{1}{2}}-302_{3}$
3876.45	5	25789.50	$^{7}K_{3}^{\frac{1}{2}}-315_{6}$
3876.13	60	25791.63	$^{5}L_{3}^{\frac{1}{2}}-257_{4}$
3873.08	15	25811.98	$A_{7}^{\frac{1}{2}}-296_{3}$
3871.04	120	25825.59	$^{5}L_{3}^{\frac{1}{2}}-258_{6}$
3867.50	15	25849.18	$^{7}M_{3}^{\frac{1}{2}}-321_{7}$
3867.17	30	25851.41	$A_{3}^{\frac{1}{2}}-297_{4}$
3864.10	30	25871.93	$^{7}K_{3}^{\frac{1}{2}}-316_{4}$
3855.43	20	25930.12	$^{5}K_{3}^{\frac{1}{2}}-265_{6}$
3854.22	100	25938.25	$^{5}L_{3}^{\frac{1}{2}}-259_{6}$
3852.97	5	25946.65	$^{5}K_{3}^{\frac{1}{2}}-265_{5}$
3851.72	20	25955.07	$^{5}H_{4}^{\frac{1}{2}}-319_{5}$

TABLE 4.—*Classified lines of* U I—Continued

λ_{air} A	Intensity	ν_{vac} cm^{-1}	Term combi
3847.05	8	25986.59	$C_{7}^{\frac{1}{2}}$
3846.55	25	25989.96	$A_{7}^{\frac{1}{2}}$
3845.59	3	25996.49	$A_{7}^{\frac{1}{2}}$
3843.42	8	26011.12	$^{5}K_{3}^{\frac{1}{2}}$
3842.32	3	26018.59	$^{5}K_{3}^{\frac{1}{2}}$
3839.62	120	26036.86	$A_{7}^{\frac{1}{2}}$
3838.31	4	26045.80	$^{5}I_{3}^{\frac{1}{2}}$
3835.51	5	26064.77	$A_{7}^{\frac{1}{2}}$
3834.92	8	26068.82	$^{7}M_{3}^{\frac{1}{2}}$
3832.37	6	26086.13	$B_{7}^{\frac{1}{2}}$
3831.06	5	26095.03	$^{5}K_{3}^{\frac{1}{2}}$
3829.79	25	26103.69	$^{5}L_{3}^{\frac{1}{2}}$
3821.95	30	26157.26	$A_{7}^{\frac{1}{2}}$
3819.89	8	26171.38	$^{5}K_{3}^{\frac{1}{2}}$
3819.25	6	26175.74	$^{5}K_{3}^{\frac{1}{2}}$
3818.02	6	26184.21	$^{7}K_{3}^{\frac{1}{2}}$
3812.00	150	26225.57	$^{5}L_{3}^{\frac{1}{2}}$
3811.88	4	26226.33	$A_{7}^{\frac{1}{2}}$
3809.66	4	26241.61	$^{7}M_{3}^{\frac{1}{2}}$
3808.93	40	26246.66	$^{7}M_{3}^{\frac{1}{2}}$
3801.15	25	26300.38	$^{5}K_{3}^{\frac{1}{2}}$
3800.47	6	26305.09	$^{5}L_{3}^{\frac{1}{2}}$
3797.38	8	26326.53	$^{5}H_{3}^{\frac{1}{2}}$
3791.53	4	26367.10	$^{5}K_{3}^{\frac{1}{2}}$
3789.81	3	26379.07	$^{7}K_{3}^{\frac{1}{2}}$
3788.06	4	26391.26	$^{5}L_{3}^{\frac{1}{2}}$
3781.75	15	26435.31	$A_{3}^{\frac{1}{2}}$
3779.35	5	26452.10	$^{5}K_{3}^{\frac{1}{2}}$
3778.26	8	26459.75	$A_{3}^{\frac{1}{2}}$
3775.61	12	26478.27	$A_{7}^{\frac{1}{2}}$
3774.91	15	26483.22	$^{5}I_{3}^{\frac{1}{2}}$
3773.44	40	26493.53	$A_{7}^{\frac{1}{2}}$
3768.76	8	26526.42	$^{5}I_{3}^{\frac{1}{2}}$
3766.89	40	26539.60	$^{5}I_{3}^{\frac{1}{2}}$
3765.35	40	26550.43	$^{5}L_{3}^{\frac{1}{2}}$
3763.45	30	26563.83	$^{5}K_{3}^{\frac{1}{2}}$
3763.27	40	26565.11	$^{7}K_{3}^{\frac{1}{2}}$
3763.01	12	26566.94	$^{5}L_{3}^{\frac{1}{2}}$
3758.36	20	26599.85	$^{5}K_{3}^{\frac{1}{2}}$
3753.93	20	26631.21	$^{5}L_{3}^{\frac{1}{2}}$
3751.18	35	26650.74	$A_{7}^{\frac{1}{2}}$
3749.74	4	26660.94	$^{5}K_{3}^{\frac{1}{2}}$
3747.61	8	26676.10	$^{5}I_{3}^{\frac{1}{2}}$
3742.10	3	26715.37	$^{5}L_{3}^{\frac{1}{2}}$
3737.38	5	26749.10	$^{5}K_{3}^{\frac{1}{2}}$
3736.02	12	26758.88	$^{5}L_{3}^{\frac{1}{2}}$
3733.17	3	26779.28	$B_{7}^{\frac{1}{2}}$
3732.26	60	26785.86	$A_{7}^{\frac{1}{2}}$
3731.45	100	26791.64	$^{5}L_{3}^{\frac{1}{2}}$
3725.31	6	26835.81	$A_{7}^{\frac{1}{2}}$
3724.45	15	26842.02	$A_{7}^{\frac{1}{2}}$
3719.29	40	26879.22	$^{5}K_{3}^{\frac{1}{2}}$
3718.31	6	26886.30	$^{5}I_{3}^{\frac{1}{2}}$
3717.72	20	26890.55	$^{5}K_{3}^{\frac{1}{2}}$
3713.56	20	26920.71	$^{5}L_{3}^{\frac{1}{2}}$
3707.95	25	26961.41	$B_{7}^{\frac{1}{2}}$
3704.65	3	26985.45	$^{5}K_{3}^{\frac{1}{2}}$
3703.27	30	26995.50	$^{5}K_{3}^{\frac{1}{2}}$
3702.62	25	27000.26	$^{5}K_{3}^{\frac{1}{2}}$
3699.18	10	27025.36	$^{5}K_{3}^{\frac{1}{2}}$

TABLE 4.—*Classified lines of* U I—Continued

λ_{air} A	Intensity	ν_{vac} cm^{-1}	Term combination
3695.21	20	27054.42	$^{7}K_{3}^{\frac{1}{2}}-340_{7}$
3694.17	5	27062.01	$^{5}K_{3}^{\frac{1}{2}}-276_{5}$
3692.75	30	27072.40	$^{5}L_{3}^{\frac{1}{2}}-270_{5}$
3692.43	10	27074.79	$A_{3}^{\frac{1}{2}}-307_{6}$
3689.86	5	27093.65	$A_{3}^{\frac{1}{2}}-308_{5}$
3687.46	30	27111.26	$A_{3}^{\frac{1}{2}}-309_{4}$
3685.78	40	27123.64	$^{5}K_{3}^{\frac{1}{2}}-277_{6}$
3679.38	60	27170.82	$^{5}K_{3}^{\frac{1}{2}}-278_{5}$
3677.39	60	27185.47	$A_{3}^{\frac{1}{2}}-309_{3}$
3676.52	10	27191.91	$^{5}K_{3}^{\frac{1}{2}}-314_{5}$
3673.73	6	27212.54	$^{5}K_{3}^{\frac{1}{2}}-315_{3}$
3672.19	5	27223.97	$A_{3}^{\frac{1}{2}}-310_{7}$
3665.21	12	27275.84	$^{5}K_{3}^{\frac{1}{2}}-315_{6}$
3663.19	8	27290.84	$^{5}I_{3}^{\frac{1}{2}}-317_{5}$
3659.16	100	27320.93	$^{5}K_{3}^{\frac{1}{2}}-278_{6}$
3658.68	12	27324.51	$^{5}L_{3}^{\frac{1}{2}}-273_{7}$
3654.89	40	27352.83	$A_{3}^{\frac{1}{2}}-312_{4}$
3653.21	25	27365.41	$A_{3}^{\frac{1}{2}}-311_{7}$
3651.93	15	27375.04	$A_{3}^{\frac{1}{2}}-313_{4}$
3651.04	4	27381.68	$^{5}L_{3}^{\frac{1}{2}}-273_{5}$
3649.86	3	27390.55	$^{7}M_{3}^{\frac{1}{2}}-336_{6}$
3648.25	15	27402.64	$^{5}K_{3}^{\frac{1}{2}}-279_{3}$
3644.24	60	27432.77	$^{5}K_{3}^{\frac{1}{2}}-280_{6}$
3639.49	30	27468.58	$^{5}K_{3}^{\frac{1}{2}}-317_{5}$
3638.60	3	27475.25	$A_{3}^{\frac{1}{2}}-312_{7}$
3638.20	150	27478.35	$A_{3}^{\frac{1}{2}}-312_{3}$
3636.31	15	27492.60	$^{5}I_{3}^{\frac{1}{2}}-319_{3}$
3635.30	30	27500.27	$A_{3}^{\frac{1}{2}}-313_{7}$
3627.70	6	27557.85	$A_{3}^{\frac{1}{2}}-314_{7}$
3626.36	15	27568.05	$^{5}K_{3}^{\frac{1}{2}}-281_{5}$
3620.08	60	27615.81	$^{5}L_{3}^{\frac{1}{2}}-276_{3}$
3616.33	40	27644.47	$A_{3}^{\frac{1}{2}}-314_{3}$
3612.96	5	27670.29	$^{5}K_{3}^{\frac{1}{2}}-319_{3}$
3611.40	20	27682.26	$^{5}L_{3}^{\frac{1}{2}}-276_{5}$
3603.74	25	27741.03	$^{5}K_{3}^{\frac{1}{2}}-320_{7}$
3603.36	30	27743.96	$^{5}L_{3}^{\frac{1}{2}}-277_{6}$
3602.48	30	27750.75	$A_{3}^{\frac{1}{2}}-315_{5}$
3600.56	3	27765.55	$A_{3}^{\frac{1}{2}}-316_{4}$
3598.94	30	27778.02	$^{5}L_{3}^{\frac{1}{2}}-277_{5}$
3594.81	8	27810.01	$^{5}K_{3}^{\frac{1}{2}}-283_{4}$
3593.20	40	27822.47	$^{5}K_{3}^{\frac{1}{2}}-321_{7}$
3592.97	15	27824.23	$^{5}K_{3}^{\frac{1}{2}}-284_{5}$
3591.74	50	27833.72	$^{5}K_{3}^{\frac{1}{2}}-284_{4}$
3589.66	20	27849.84	$^{5}K_{3}^{\frac{1}{2}}-284_{3}$
3587.78	4	27864.45	$^{5}I_{3}^{\frac{1}{2}}-323_{5}$
3585.38	25	27883.15	$^{5}K_{3}^{\frac{1}{2}}-285_{5}$
3584.88	250	27887.01	$^{5}L_{3}^{\frac{1}{2}}-278_{7}$
3580.25	25	27923.08	$^{5}K_{3}^{\frac{1}{2}}-285_{4}$
3577.92	30	27941.25	$^{5}L_{3}^{\frac{1}{2}}-278_{6}$
3577.78	8	27942.31	$^{5}K_{3}^{\frac{1}{2}}-286_{5}$
3574.76	50	27965.94	$^{5}L_{3}^{\frac{1}{2}}-279_{7}$
3567.49	4	28022.92	$^{5}L_{3}^{\frac{1}{2}}-279_{6}$
3566.60	200	28029.97	$^{5}K_{3}^{\frac{1}{2}}-287_{5}$
3565.05	10	28042.15	$^{5}K_{3}^{\frac{1}{2}}-323_{5}$
3564.27	3	28048.26	$^{5}L_{3}^{\frac{1}{2}}-280_{7}$
3563.66	50	28053.05	$^{5}L_{3}^{\frac{1}{2}}-280_{6}$
3557.84	50	28098.91	$^{5}L_{3}^{\frac{1}{2}}-281_{6}$
3555.32	60	28118.85	$^{5}L_{3}^{\frac{1}{2}}-281_{7}$
3554.88	8	28122.37	$A_{3}^{\frac{1}{2}}-319_{3}$
3549.20	25	28167.36	$A_{3}^{\frac{1}{2}}-318_{7}$

TABLE 4.—*Classified lines of* U I—Continued

λ_{air} A	Intensity	ν_{vac} cm^{-1}	Term combination
3548.42	6	28173.57	$A_{3}^{\frac{1}{2}}-319_{7}$
3546.55	25	28188.41	$^{5}L_{3}^{\frac{1}{2}}-281_{5}$
3543.21	4	28214.98	$^{5}K_{3}^{\frac{1}{2}}-324_{3}$
3542.57	25	28220.04	$^{5}K_{3}^{\frac{1}{2}}-325_{3}$
3540.00	5	28240.59	$^{5}K_{3}^{\frac{1}{2}}-288_{5}$
3538.23	4	28254.66	$^{5}K_{3}^{\frac{1}{2}}-289_{3}$
3535.96	10	28272.78	$A_{3}^{\frac{1}{2}}-321_{4}$
3534.33	30	28285.84	$^{5}L_{3}^{\frac{1}{2}}-283_{7}$
3532.89	8	28297.41	$A_{3}^{\frac{1}{2}}-321_{7}$
3518.47	5	28413.33	$^{5}K_{3}^{\frac{1}{2}}-290_{6}$
3514.61	200	28444.54	$^{5}L_{3}^{\frac{1}{2}}-284_{5}$
3511.44	30	28470.23	$^{5}L_{3}^{\frac{1}{2}}-284_{4}$
3509.06	8	28489.58	$^{5}K_{3}^{\frac{1}{2}}-291_{6}$
3507.34	80	28503.50	$^{5}L_{3}^{\frac{1}{2}}-285_{5}$
3507.05	30	28505.87	$^{5}K_{3}^{\frac{1}{2}}-292_{6}$
3500.07	80	28562.71	$^{5}L_{3}^{\frac{1}{2}}-286_{5}$
3499.61	4	28566.46	$^{5}L_{3}^{\frac{1}{2}}-285_{7}$
3493.99	40	28612.42	$^{5}K_{3}^{\frac{1}{2}}-292_{5}$
3489.37	80	28650.33	$^{5}L_{3}^{\frac{1}{2}}-287_{5}$
3486.12	3	28677.02	$A_{3}^{\frac{1}{2}}-324_{5}$
3473.56	8	28780.70	$^{5}K_{3}^{\frac{1}{2}}-294_{6}$
3466.30	40	28840.99	$A_{3}^{\frac{1}{2}}-326_{7}$
3463.90	8	28860.94	$^{5}L_{3}^{\frac{1}{2}}-288_{6}$
3462.21	30	28875.01	$^{5}L_{3}^{\frac{1}{2}}-289_{6}$
3454.61	30	28938.53	$^{5}K_{3}^{\frac{1}{2}}-295_{6}$
3435.49	20	29099.60	$^{5}K_{3}^{\frac{1}{2}}-297_{4}$
3434.28	10	29109.85	$^{5}L_{3}^{\frac{1}{2}}-291_{5}$
3432.36	4	29126.15	$^{5}L_{3}^{\frac{1}{2}}-292_{6}$
3431.14	8	29136.53	$^{5}K_{3}^{\frac{1}{2}}-334_{6}$
3418.39	5	29245.18	$^{5}K_{3}^{\frac{1}{2}}-298_{6}$
3412.58	5	29295.00	$^{5}K_{3}^{\frac{1}{2}}-335_{7}$
3404.33	12	29366.00	$^{5}K_{3}^{\frac{1}{2}}-299_{6}$
3400.28	2	29400.95	$^{5}L_{3}^{\frac{1}{2}}-294_{6}$
3386.24	5	29522.83	$^{5}K_{3}^{\frac{1}{2}}-301_{5}$
3376.04	4	29612.00	$^{5}I_{3}^{\frac{1}{2}}-340_{5}$
3368.98	5	29674.05	$^{5}K_{3}^{\frac{1}{2}}-300_{5}$
3358.14	8	29769.87	$A_{3}^{\frac{1}{2}}-335_{7}$
3250.51	8	29837.69	$^{5}L_{3}^{\frac{1}{2}}-299_{7}$
3347.37	5	29865.62	$^{5}L_{3}^{\frac{1}{2}}-298_{6}$
3345.89	15	29878.88	$^{5}K_{3}^{\frac{1}{2}}-304_{4}$
3337.03	12	29958.16	$^{5}L_{3}^{\frac{1}{2}}-300_{7}$
3333.89	8	29986.42	$^{5}L_{3}^{\frac{1}{2}}-299_{6}$
3316.55	8	30143.21	$^{5}L_{3}^{\frac{1}{2}}-301_{5}$
3310.63	6	30197.08	$A_{3}^{\frac{1}{2}}-340_{3}$
3303.84	8	30259.13	$A_{3}^{\frac{1}{2}}-340_{7}$
3301.65	4	30279.21	$^{5}L_{3}^{\frac{1}{2}}-302_{7}$
3298.88	8	30304.58	$A_{3}^{\frac{1}{2}}-341_{5}$
3292.94	15	30359.30	$^{5}K_{3}^{\frac{1}{2}}-309_{4}$
3282.98	2	30451.43	$^{5}L_{3}^{\frac{1}{2}}-302_{6}$
3278.79	3	30490.29	$^{5}L_{3}^{\frac{1}{2}}-303_{6}$
3277.73	6	30500.20	$^{5}L_{3}^{\frac{1}{2}}-304_{6}$
3276.76	10	30509.19	$^{5}K_{3}^{\frac{1}{2}}-311_{5}$
3276.15	5	30514.84	$^{5}K_{3}^{\frac{1}{2}}-311_{6}$
3268.45	4	30586.72	$^{5}L_{3}^{\frac{1}{2}}-305_{6}$
3266.93	20	30600.98	$^{5}K_{3}^{\frac{1}{2}}-312_{4}$
3264.55	6	30623.30	$^{5}K_{3}^{\frac{1}{2}}-313_{4}$
3263.12	20	30636.75	$^{5}L_{3}^{\frac{1}{2}}-306_{6}$
3254.33	8	30719.49	$^{5}K_{3}^{\frac{1}{2}}-313_{5}$
3238.67	2	30868.01	$^{5}K_{3}^{\frac{1}{2}}-315_{5}$
3237.87	15	30875.62	$^{5}L_{3}^{\frac{1}{2}}-307_{6}$

TABLE 4.—*Classified lines of* U I—Continued

λ_{air}A	Intensity	ν_{vac}cm^{-1}	Term combination
3235.90	6	30894.46	$^5L_4^1-308_8$
3225.60	2	30993.09	$^5L_4^1-310_8$
3223.45	8	31013.72	$^5K_3^1-316_6$
3212.03	8	31124.03	$^5K_3^1-317_8$
3211.46	2	31129.52	$^5L_4^1-311_6$
3210.90	5	31134.96	$^5L_4^1-311_6$
3207.67	6	31166.29	$^5L_4^1-311_7$
3196.41	3	31276.12	$^5L_4^1-312_7$
3189.91	5	31339.84	$^5L_4^1-313_8$
3187.99	8	31358.73	$^5L_4^1-314_7$
3174.87	3	31488.25	$^5L_4^1-315_8$
3171.58	5	31520.94	$^5K_3^1-321_4$
3136.30	4	31875.54	$^5K_3^1-325_8$
3129.38	3	31946.01	$^5L_4^1-319_9$
3122.46	4	32016.76	$^5L_4^1-320_7$
3114.54	4	32098.19	$^5L_4^1-321_7$
3076.91	2	32490.73	$^5L_4^1-324_8$
3076.43	8	32495.83	$^5L_4^1-325_8$
3062.66	2	32641.92	$^5L_4^1-326_7$
3048.64	3	32791.96	$^5K_3^1-334_8$
3027.66	5	33019.20	$^5K_3^1-336_8$
2992.04	3	33412.29	$^5L_4^1-334_8$
2977.92	8	33570.67	$^5L_4^1-335_7$
2671.82	8	33639.60	$^5L_4^1-336_8$
2935.15	6	34059.87	$^5L_4^1-340_7$

From the spectroscopic evidence presented in this paper, it is clear that uranium is an element of the rare-earth type; that, in fact, it is the homologue of neodymium, being the third member of a series beginning with thorium. That the seventh period of elements in the periodic system should encompass a second group of rare earths similar to the group in the sixth period was foresee more than 20 years ago by Bohr [14]. Since th time opinion has differed concerning the aton number at which the binding of the *5f* electr first sets in. Some investigators, notably Vi [15], have suggested Th(90), others U(92), a still others, including Starke [16], the transurani element 93 as the first in which a *5f* electr appears. In each instance the basis of opini was evidence derived from chemical behavi nuclear activity, behavior of ions in crystals a solutions, etc. The testimony of the spectrosco however, in selecting thorium for this role unique and decisive, and it is supported by t recent spatial classifications of the elements Djounkovsky and Kavos [17] and by Talpain [1 which array thorium, protoactinium, and uraniu as the chemical homologues of cerium, prase dymium, and neodymium.

At the present time the state of the analysis U I does not permit a calculation to be made of t ionization potential of neutral uranium atoms fro series-forming terms. Nevertheless, an approx mate value of 4 volts for this important atom constant may be estimated from the fact th no lines of neutral atoms have been found belo wavelength 2900 A. This accounts for the ea with which uranium is ionized in electric arcs, a magnetic fields, and explains the appearan of lines due to ionized atoms in the red and n infrared regions and their overwhelmimg pr ponderance in the regions of shorter wavelength

IV. References

[1] H. Kayser, Handbuch der Spectroscopie, p. 734 (S. Hirzel, Leipzig, 1912).

[2] K. W. Meissner, Ann. Physik **50,** 713 (1916).

[3] C. C. Kiess and W. F. Meggers, BS Sci. Pap. **16,** 51 (1920) S372.

[4] G. R. Harrison, MIT wavelength tables (John Wiley & Sons, Inc., New York, N. Y., 1939).

[5] W. J. Humphreys, Astrophys. J. **6,** 169 (1897).

[6] J. C. McLennan, E. Cohen, M. J. Liggett, Trans. Roy. Soc. Can. **20,** 365 (1926).

[7] C. C. Kiess and E. Z. Stowell, BS J. Research **12,** 460 (1934) RP671.

[8] R. W. Wood, Nature **140,** 723 (1937).

[9] W. F. Meggers and K. Burns, BS Sci. Pap. **18,** 201 (1922) S442.

[10] W. F. Meggers and O. Laporte, Phys. Rev. **28,** (1926).

[11] E. Back, Ann. Physik. [IV] **70,** 333 (1923).

[12] J. R. McNally, G. R. Harrison, and H. B. Pa J. Opt. Soc. Am. **32,** 334 (1942); T. L. de Bru P. Schuurmans, and P. F. A. Klinkenberg, Physik **121,** 667 (1943); **122,** 23, (1944).

[13] O. Laporte and J. E. Mack, Phys. Rev. **63,** 246 (19

[14] N. Bohr, Nature **112,** 43 (1923).

[15] G. E. Villar; Ann. acad. brasil. sci. **12,** 51, (1940).

[16] K. Starke, Z. anorg. allgem. Chem. **251,** 251 (1943).

[17] G. E. Djounkovsky and S. Kavos, J. phys. radiu [8] **5,** 53 (1944).

[18] L. Talpain, J. phys. radium [8] **6,** 176 (1945).

WASHINGTON, April 30, 1946.

U. S. GOVERNMENT PRINTING OFFICE: 1946